

https://dspace.org/

Investigating the Effect of Cholesterol Depletion on IL-6 Cytokine Induced Epithelial-to-Mesenchymal Transition in Colorectal Cancer

Aronson, Ruth Shifra

2022
University of the Witwatersrand, Johannesburg
https://hdl.handle.net/10539/46126

Aronson, Ruth Shifra . (2022). Investigating the Effect of Cholesterol Depletion on IL-6 Cytokine Induced Epithelial-to-Mesenchymal Transition in Colorectal Cancer [Masters dissertation, University of the Witwatersrand, Johannesburg]. WIReDSpace. https://hdl.handle.net/10539/46126

Downloaded from a DSpace repository. https://dspace.org/



Investigating the Effect of Cholesterol Depletion on IL-6 Cytokine Induced Epithelial-to-Mesenchymal Transition in Colorectal Cancer

by

Ruth Aronson

(1173641)

Dissertation

Submitted in fulfilment of the requirements for the degree

Master of Science

in

Molecular and Cell Biology

in the Faculty of Science, University of the Witwatersrand, Johannesburg, South Africa

Supervisor: Professor Mandeep Kaur

June 2022

Declaration

I, Ruth Aronson (1173641), am a student registered for the degree of Master of Science by Dissertation in the academic year 2020-2021.

I hereby declare the following:

- I am aware that plagiarism (the use of someone else's work without their permission and/or without acknowledging the original source) is wrong.
- I confirm that the work submitted for assessment for the above degree is my own unaided work except where I have explicitly indicated otherwise.
- I have not submitted this work before for any other degree or examination at this or any other University.
- The information used in the Dissertation HAS NOT been obtained by me while employed by, or working under the aegis of, any person or organisation other than the University.
- I have followed the required conventions in referencing the thoughts and ideas of others.
- I understand that the University of the Witwatersrand may take disciplinary action against me if there is a belief that this is in not my own unaided work or that I have failed to acknowledge the source of the ideas or words in my writing.

NRF Declaration

The financial assistance of the National Research Foundation (NRF) towards this research is hereby acknowledged.

Opinions expressed and conclusions arrived at, are those of the author and are not necessarily to be contributed to the NRF.

Signature:  10 June 2022

Abstract

Colorectal cancer (CRC) is the third leading cause of cancer globally. Poor patient prognosis is attributed to late diagnosis and high metastatic potential of the disease. The process of metastasis usually favours the conversion between epithelial and mesenchymal cellular states, termed epithelial-to-mesenchymal transition (EMT). EMT has been reported to contribute to drug resistance, following treatments with chemotherapy, which allows for cancer recurrence and metastasis. Additionally, increasing evidence indicates the role of the cholesterol biosynthesis pathway in EMT progression. The lipid composition of epithelial cells compared to mesenchymal cells is distinct and cells that undergo EMT show an elevation in cholesterol levels to facilitate increased proliferation and oncogenic signalling. This study aimed to investigate the effect of cholesterol depletion in EMT induced CRC and explored how cholesterol depletion influences the susceptibility of EMT induced cells to the chemotherapy cocktail referred to as FOLFOX (5-fluorouracil and oxaliplatin). Results showed that following EMT induction by proinflammatory cytokine interleukin-6 (IL-6), in HT-29 cells, cellular cholesterol content increased by ~30%. Cholesterol depletion with compounds methyl-β-cyclodextrin (MβCD) and KS-01, in post-EMT cells, showed to reverse EMT phenotypic changes as noted by increased epithelial marker E-cadherin (by 46.9% and 55.3%, respectively), decreased mesenchymal marker vimentin (by 41.0% and 52.8%, respectively) and reduced invasive potential (by 43.0% and 47.8%, respectively). Interestingly, EMT induced cells displayed increased sensitivity to the FOLFOX chemotherapy, following cholesterol depletion, as observed by enhanced susceptibility to apoptosis (by 46.7% and 60.3%, respectively) and attenuation of multidrug resistance (by 80.6% and 71.8%, respectively). Ultimately, this study highlights cholesterol depletion to be a promising strategy for potential treatment of metastatic CRC.

Acknowledgments

First and foremost, I would like to express my gratitude to my supervisor, Professor Kaur, for her invaluable guidance and mentorship, as well as for her support and encouragement that made this project possible.

I would like to thank members of GH527 for providing a warm and fun lab environment to work in. I would also like to express my thanks for their constant advice and support during the course of this project.

I would like to thank the University of the Witwatersrand (Postgraduate Merit Award) and the National Research Foundation (NRF) for financial support during my studies.

Thank you to my parents for their unconditional love, patience, and encouragement. This project would not have been made possible if were it not for their support.

Table of Contents

Declaration ..... **ii**

Abstract ..... **iii**

Acknowledgments ..... **iv**

List of Figures ..... **viii**

List of Tables ..... **x**

List of Symbols ..... **xi**

List of Abbreviations ..... **xii**

1. Introduction **1**

1.1 Colorectal cancer 1

1.2 Colorectal cancer development and progression 1

1.3 Epithelial-to-mesenchymal transition 3

1.4 The IL-6 pathway in cancer progression and EMT 7

1.4.1 The IL-6/IL-6R pathway 7

1.4.2 The role of the IL-6/IL-6R/STAT3 pathway in EMT induction 7

1.5 Current treatments for colorectal cancer 10

1.6 FOLFOX chemotherapy against metastatic colorectal cancer 11

1.6.1 FOLFOX mechanism of action 11

1.6.2 Limitations to the FOLFOX chemotherapy 13

1.7 Cholesterol metabolism 14

1.8 Deregulated cholesterol metabolism in colorectal cancer 16

1.9 Cholesterol as a target for colorectal cancer treatment 18

1.9.1 Cholesterol biosynthesis inhibitors 18

1.9.2 Cholesterol depleting agents 19

1.10 Introduction to this study 21

2. Aim and Objectives **23**

2.1 Aims 23

2.2 Objectives 23
3. Methodology 24
3.1 Cell Culture 25
3.2 IL-6 induced EMT 25
3.3 Cell Counting 25
3.4 Cell Viability Assay 26
3.5 Cell Proliferation Assay 27
3.6 Immunofluorescent Staining 28
3.7 Reverse Transcription Quantitative Polymerase chain reaction (RT-qPCR) 30
3.8 Cholesterol Staining 34
3.8.1 Vybrant Alexa Fluor® Lipid Raft Labelling 34
3.8.2 Filipin 35
3.8.3 BODIPY 493/503 35
3.9 Transwell® Invasion Assay 36
3.10 Apoptosis Assay 37
3.11 Vybrant™ Multidrug Resistance Assay 38
3.12 Statistical Analysis 39
4. Results 40
4.1 Optimisation of FOLFOX chemotherapy suitable for HT-29 cells 40
4.2 Increasing concentrations of IL-6 represses E-cadherin protein expression 42
4.3 IL-6 exposure promotes an EMT phenotype in colorectal cancer cells 43
4.4 Cholesterol depleting agents successfully reduce cellular cholesterol following EMT induction 47
4.5 Cholesterol depletion promotes an epithelial phenotype in EMT induced cells 52
4.6 Cholesterol depletion and exposure to FOLFOX reduces the invasive potential of EMT induced cells 55
4.7 The effect of cholesterol depletion on apoptosis of EMT induced cells exposed to FOLFOX 57

4.8 The effect of cholesterol depletion on multidrug resistance of EMT induced cells exposed to FOLFOX 59

5. Discussion 61

5.1 IL-6 mediated EMT induction in colorectal cancer 61

5.2 Cholesterol: an important driver of EMT induction 64

5.3 Cholesterol depletion as a novel strategy for EMT phenotype reversal 66

5.4 Cholesterol depletion enhances the effectiveness of the FOLFOX chemotherapy 69

6. Conclusions 72

7. Future work 74

8. Limitations to the study 75

References 76

Appendix 97

List of Figures

Figure 1.1: Colorectal cancer progression via the adenoma-carcinoma 3

Figure 1.2: Epithelial-to-mesenchymal transition 5

Figure 1.3: Signalling networks that promote EMT in colorectal cancer 6

Figure 1.4: IL-6/IL-6R mediates EMT through the JAK/STAT3 pathway 9

Figure 1.5: Current strategies aimed at treating colorectal cancer 11

Figure 1.6: Metabolic pathway of FOLFOX chemotherapy 13

Figure 1.7: Cholesterol metabolism and homeostasis 15

Figure 3.1: Project workflow 24

Figure 4.1: Dose-response curves of 5-fluorouracil and oxaliplatin at 24 and 48 hours 40

Figure 4.2: HT-29 cell viability following combination treatments with 5-fluorouracil and oxaliplatin 41

Figure 4.3: E-cadherin expression following exposure of HT-29 cells to increasing concentrations of IL-6 42

Figure 4.4: Changes in HT-29 cell morphology following exposure to 50 ng/ml IL-6 43

Figure 4.5: Changes in E-cadherin and Vimentin expression levels following 50 ng/ml IL-6 exposure 44

Figure 4.6: *SNAI1* and *TWIST1* expression levels are upregulated in HT-29 cells exposed to IL-6 45

Figure 4.7: IL-6 treatment increases STAT3 phosphorylation at Tyrosine 705 46

Figure 4.8: IL-6 increases HT-29 cell proliferation 47

Figure 4.9: Vybrant Alexa Fluor® Lipid Raft Labelling of cells pre- and post-EMT induction 49

Figure 4.10: Filipin staining of free cholesterol in cells pre- and post-EMT induction 50

Figure 4.11: BODIPY staining of lipid droplets in cells pre- and post-EMT induction 51

Figure 4.12: Treatment with cholesterol depleting agents increases E-cadherin epithelial marker in EMT induced cells 53

Figure 4.13: Treatment with cholesterol depleting agents decreases vimentin mesenchymal marker in EMT induced cells 54

Figure 4.14: Treatment with cholesterol depleting agents decreases invasive potential in EMT induced cells 56

Figure 4.15: Effect of cholesterol depleting agents on susceptibility to apoptosis in EMT induced cells 58

Figure 4.16: Treatment with cholesterol depleting agents decreases drug resistance in EMT induced cells 60

Figure 5.1: The EMT/MET spectrum 64

Figure 6.1: Proposed model exploring the link between IL-6, EMT and cholesterol in cancer 73

Figure A.1: The effect of DMSO on cell viability in HT-29 cells, over 48 hours. 97

Figure A.2: The effect of increasing concentrations of folinic acid on 5-FU cytotoxicity 98

List of Tables

Table 3.1: Primary antibodies and dilutions used for immunofluorescence 29

Table 3.2: Secondary antibodies and dilutions used for immunofluorescence 29

Table 3.3: Reaction set up for RevertAid First Strand cDNA synthesis 31

Table 3.4: Reaction set up for SensiFAST™ SYBR® No-ROX qPCR reaction 32

Table 3.5: Sequences and annealing temperature of *SNAI1*, *TWIST1* and *GAPDH* primers 33

Table 3.6: 3-step qPCR cycling conditions 33

List of Symbols

Å	Angstrom
α	Alpha
β	Beta
γ	Gamma
κ	Kappa
µ	Micro
°C	Degree Celsius
x *g*	Centrifugal Force
%	Percentage
©	Copyright
®	Registered Trademark
™	Trademark

List of Abbreviations

5,10-CH_2FH_4	5,10-methylenetetrahydrofolate
5-FU	5-fluorouracil
ABC	ATP binding cassette
ACAT	Acyl coenzyme A:cholesterol acyltransferase
Acetyl-Co-A	Acetyl coenzyme A
ACF	Aberrant crypt foci
Akt	Protein kinase B
ANOVA	Analysis of variance
APC	Adenomatous polyposis coli
α-SMA	α-smooth muscle actin
ATP	Adenosine triphosphate
AUF-1	AU-rich element RNA-binding protein-1
Bcl	B-cell lymphoma
BODIPY	4,4-Difluoro-1,3,5,7,8-pentamethyl-4-bora-3a,4a-diaza-s-indacene
BSA	Bovine serum albumin
Calcein AM	Calcein acetoxymethyl ester
CD	Cyclodextrin
CDK	Cyclin dependent kinase
cDNA	Complementary DNA
CE	Cholesteryl ester
CI	Confidence interval
CO_2	Cardon dioxide
CRC	Colorectal cancer

CSC	Cancer stem cell
Ct	Threshold cycle
CT-B	Cholera toxin-B
CTLA-4	Cytotoxic T lymphocyte antigen 4
DAPI	4′,6-Diamidino-2-phenylindole
dH_2O	Distilled water
DMSO	Dimethyl sulfoxide
DNA	Deoxyribonucleic acid
DNase	Deoxyribonuclease
dTMP	Deoxythymidine monophosphate
dUMP	Deoxyuridine monophosphate
ECM	Extracellular matrix
EDTA	Ethylenediaminetetraacetic acid
EGFR	Epidermal growth factor receptor
EMT	Epithelial-to-mesenchymal transition
ER	Estrogen receptor
FAK	Focal adhesion kinase
FBS	Foetal bovine serum
FdUMP	Fluorodeoxyuridine monophosphate
FdUrd	Fluorodeoxyuridine
FOLFOX	Folinic acid, 5-Fluorouracil, Oxaliplatin
FoxQ1	Forkhead Box Q1
Fra-1	Fos-related antigen-1
FUDP	Fluorouridine monophosphate

FUTP	Fluorouridine triphosphate
GAPDH	Glyceraldehyde-3-phosphate dehydrogenase
gp130	Glycoprotein 130
GSK3β	Glycogen synthase kinase 3β
HCl	Hydrochloric acid
HDL	High density lipoprotein
HIF-1α	Hypoxia-inducing factor-1α
HMG-CoA	3-Hydroxy-3-methylglutaryl coenzyme A
HMGCR	3-Hydroxy-3-methylglutaryl coenzyme A reductase
HPβCD	2-Hydroxypropyl-β-cyclodextrin
HT-29	Human colorectal adenocarcinoma cell line
IDOL	Inducible degrader of the LDL-receptor
IDT	Integrated DNA Technologies
IL-6	Interleukin-6
IL-6R	Interleukin-6 receptor
JAK	Janus kinase
KRAS	Kirsten rat sarcoma virus
LDL	Low density lipoprotein
LDLR	Low density lipoprotein receptor
log_2FC	log_2(fold-change)
LRP	Low density lipoprotein receptor-related protein
LSD	Least significant difference
LXR	Liver X receptor
MAPK	Mitogen activated protein kinase

MβCD	Methyl-β-cyclodextrin
mCRC	Metastatic colorectal cancer
MDR	Multidrug resistance
MET	Mesenchymal-to-epithelial transition
mIL-6R	Membrane bound IL-6R
miRNA	Micro-RNA
MMP	Matrix metalloproteinases
mRNA	Messenger RNA
MTT	3-(4,5-Dimethylthiazol-2-yl)-2,5-diphenyltetrazolium bromide
NF-κB	Nuclear factor κ-light-chain-enhancer of activated B cells
NTC	No template control
OS	Overall survival
PBS	Phosphate buffered saline
PBS-T	PBS-Tween-20
PCSK9	Proprotein convertase subtilisin/kexin type-9
PD-1	Programmed death-1
PDK1	Protein dependent kinase 1
pEMT	Partial epithelial-to-mesenchymal transition
P-gp	P-glycoprotein
PI3K	Phosphatidylinositol 3-kinase
PL	Plumbagin
pSTAT3	Phosphorylated STAT3
RNA	Ribonucleic acid
ROS	Reactive oxygen species

RTK	Receptor tyrosine kinase
RT-qPCR	Reverse transcription quantitative polymerase chain reaction
SCAP	Sterol-sensing SREBP-cleavage activating protein
SDS	Sodium dodecyl sulphate
sIL-6R	Soluble form of IL-6R
SRE	Sterol regulatory element
SREBP	Sterol regulatory element-binding protein
STAT3	Signal transducer and activator of transcription 3
TBE	Tris-borate EDTA
TF	Transcription factor
TGF-β	Transforming growth factor-β
TME	Tumour microenvironment
TS	Thymidylate synthase
VEGF	Vascular endothelial growth factor
VEGFR	Vascular endothelial growth factor receptor
ZEB	Zinc finger E-box binding homeobox

1. Introduction

1.1 Colorectal cancer

Colorectal cancer (CRC) is a prominent cause of morbidity and mortality worldwide. CRC is the second leading cause of cancer death and the third most diagnosed cancer in the world. In 2020, there were an estimated 1.9 million new CRC cases and 935 000 deaths (Sung et al., 2021). Risk factors for promoting CRC growth include an unhealthy diet, smoking, alcohol consumption, obesity and an inactive lifestyle (Rawla et al., 2019). Epidemiological studies show that a high-fat, high-cholesterol diet is associated with enhanced risk of developing CRC (Giovannucci and Michaud, 2007). Age is considered an additional major risk factor for sporadic CRC onset. The risk of CRC increases between the ages of 40 and 50 years and increases substantially in subsequent decades (Rawla et al., 2019). Growing evidence has suggested the role of inflammation in CRC. People with chronic inflammatory bowel conditions such as ulcerative colitis and Crohn's disease have a higher chance of acquiring CRC (Ullman and Itzkowitz, 2011).

The rates of CRC incidence are progressively increasing globally. CRC cases are notably rising in developing countries that are adopting a "westernised" lifestyle. South Africa has the highest incidences of CRC in Sub-Saharan Africa; with an age-standardised incidence rate of 11.67 and 6.68 per 100 000, for men and women, respectively (Bebington et al., 2018). South Africa's public healthcare sector, that cares for 85% of the population, has limited ability for screening, diagnostic and treatment programs for CRC (Herbst et al., 2020). These poor resources are a likely contributing factor to disparate mortality rates in comparison to developed countries and the rise of CRC occurrence.

1.2 Colorectal cancer development and progression

The high mortality rate of CRC is attributed to late diagnosis and high metastatic potential of the disease. The 5-year survival rates for CRC are 93% at Stage I, 72-85% at Stage II, 52-64% at Stage III and drops to a staggering 8% at Stage IV metastatic CRC (mCRC) (Stintzing, 2014). Majority of CRC cases are adenocarcinomas that develop in the epithelial cells of the colon and rectal mucosa (Fleming et al., 2012). More than 90% of colorectal adenocarcinomas originate from adenomatous polyps. The hyperproliferation and cellular accumulation of colonic epithelium, termed aberrant crypt foci (ACF), promote the formation of adenomatous polyps (Manne et al., 2010). Polyps are tissue growths that form on the inner lining of the colon wall. Most polyps are benign, however, if the tumour grows >2 mm in size

there is increased risk of developing CRC (Manne et al., 2010). The development into an invasive adenocarcinoma is defined by the expansion of the tumour into the colorectal wall and where cells dissociate into blood or lymphatic vessels, resulting in metastasis to distant organs (Welch and Hurst, 2019).

The transformation of normal cells to cancerous cells is triggered through a series of complex and aberrant processes. There are three understood pathways that lead to CRC progression which are associated with distinct genetic and epigenetic modifications, namely, the adenoma–carcinoma pathway (otherwise referred to as the chromosomal instability pathway), the serrated neoplasia pathway and the microsatellite instability pathway (Dekker et al., 2019).

70-90% of all CRC incidences follow the transition from ACF to invasive CRC via the adenoma–carcinoma pathway (Dekker et al., 2019). The aberrant activation of the Wnt signalling pathway is the earliest event that drives pathway progression. Wnt signalling is involved in maintaining tissue homeostasis and deregulations in Wnt are often implicated in tumour development (MacDonald et al., 2009). The tumour suppressor gene *Adenomatous Polyposis Coli* (*APC*) of the Wnt pathway becomes inactivated, promoting the development of ACF (Dekker et al., 2019). This mutation is followed by the aberrant activation of *Kirsten rat sarcoma virus* (*KRAS)*, which regulates various cellular pathways including mitogen-activated protein kinase (MAPK) and phosphatidylinositol 3-kinase (PI3K) pathways, involved in cell growth and survival (Pino and Chung, 2010). As CRC develops, tumour suppressors *SMAD2* and *SMAD4* (mediators of the transforming growth factor-β (TGF-β) pathway) are downregulated due to allelic loss at chromosome 18q (Pino and Chung, 2010). Finally, *TP53* is a crucial tumour suppressor involved in response to DNA damage and abnormal proliferative signals. Loss of *TP53* is a defining step in the transition from CRC adenoma to CRC carcinoma and malignant transformation (Figure 1.1).

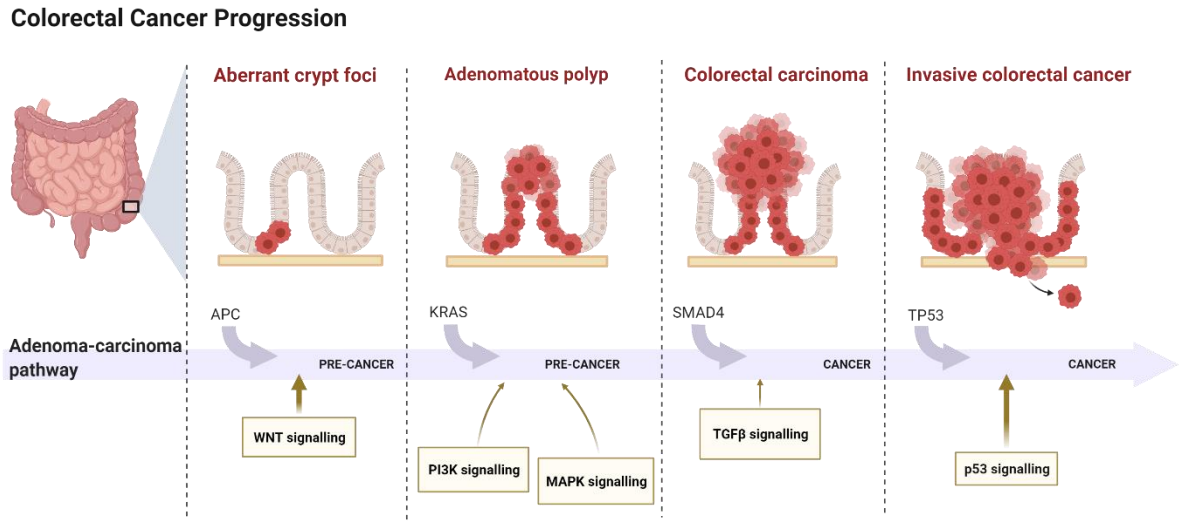


Figure 1.1: Colorectal cancer progression via the adenoma-carcinoma. *Colorectal adenocarcinomas develop from an accumulation of chromosomal instability and genetic mutations. The adenoma-carcinoma pathway is usually initiated by mutations in the APC gene leading to deregulation in the Wnt signalling pathway. Deregulated activation in KRAS further drives cell proliferation and tumour growth through the MAPK and PI3K pathways. Mutations to the TGFβ signalling pathway and inactivation of p53 tumour suppressor gene advance colorectal cancer and promote metastasis. Figure created with BioRender.com*

The characteristics of all human tumours can be succinctly described by several underlying principles namely acquired growth signal autonomy, poor response to growth-inhibitory signals, resistance to apoptosis, infinite proliferative potential, induced angiogenesis, and the invasion and metastasis to distant sites (Hanahan and Weinberg, 2000). Over 90% of cancer related mortalities are a result of metastatic disease (Mittal, 2018). Tumour metastasis involves a series of sequential, interconnected, and intricate steps, allowing for cells to disassociate from surrounding epithelial cells, disseminate and form metastases at distant sites. Metastasis is typically characterised by enhanced motility and invasion, modifications of the microenvironment and increased cell plasticity (Welch and Hurst, 2019). The formation of metastases at distant sites usually favours the cellular conversion between epithelial and mesenchymal states, by means of the process epithelial-to-mesenchymal transition (EMT) (Cao et al., 2015). CRC is a highly invasive cancer, and it is therefore worthwhile to explore EMT in further detail.

1.3 Epithelial-to-mesenchymal transition

EMT is a cell plasticity program that normally occurs during embryonic development, wound healing and tissue regeneration (Iwatsuki et al., 2010). Additionally, EMT is implicated in promoting tumour metastasis and cancer progression. The reversible EMT program allows

cells to de-differentiate, invade into the blood stream, disseminate to distant organs, where mesenchymal-to-epithelial transition (MET) allows for the efficient colonisation of cells and the formation of micro-metastases (Roche, 2018). Cancer cells undergoing EMT are involved in forming a favourable microenvironment, allowing for cancer metastasis and the resistance to apoptotic stimuli. Consequently, EMT contributes to poorer prognosis and difficulties in treatment including drug resistance (Iwatsuki et al., 2010). It is for these reasons that targeting the EMT process has become an attractive therapeutic strategy against tumour progression and invasion.

Epithelial cells are adherent, polarised cells that are anchored laterally by specialised junctions and interact with the basement membrane. The activated EMT program promotes the disruption of cell-cell contacts, loss of apical-basal polarity and detachment from the basement membrane (Mittal, 2018). Cells lose key markers that are necessary for maintaining the structural integrity of an epithelial phenotype (Figure 1.2). Additionally, cells gain mesenchymal properties that facilitate cytoskeletal remodelling necessary for migration and invasion (Mittal, 2018).

EMT cells exhibit great plasticity in the transition between epithelial and mesenchymal states. Additionally, EMT cells have shown to transition along a spectrum of intermediate states exhibiting hybrid epithelial and mesenchymal markers, termed partial EMT (Nieto et al., 2016). Partial EMT is considered most relevant in cancer progression, as cells can travel in clusters, ensuing a more aggressive disease than with complete EMT (Jolly et al., 2015). Changes between the two phenotypes are regulated by intricate networks involving the activation of three core groups of EMT transcription factors (EMT-TFs) (Roche, 2018). These EMT-TFs include SNAIL and SLUG (also known as SNAI1 and SNAI2), the zinc finger E-box binding homeobox (ZEB) family (ZEB1 and ZEB2) and the basic helix–loop–helix Twist family (TWIST1 and TWIST2) (Vu and Datta, 2017). The EMT-TFs function to suppress epithelial proteins and up regulate mesenchymal proteins. Additionally, they regulate EMT by decreasing expression of microRNAs (miRNAs) involved in stabilising an epithelial phenotype and by recruiting co-repressors and activators to enhance EMT (Stemmler et al., 2019).

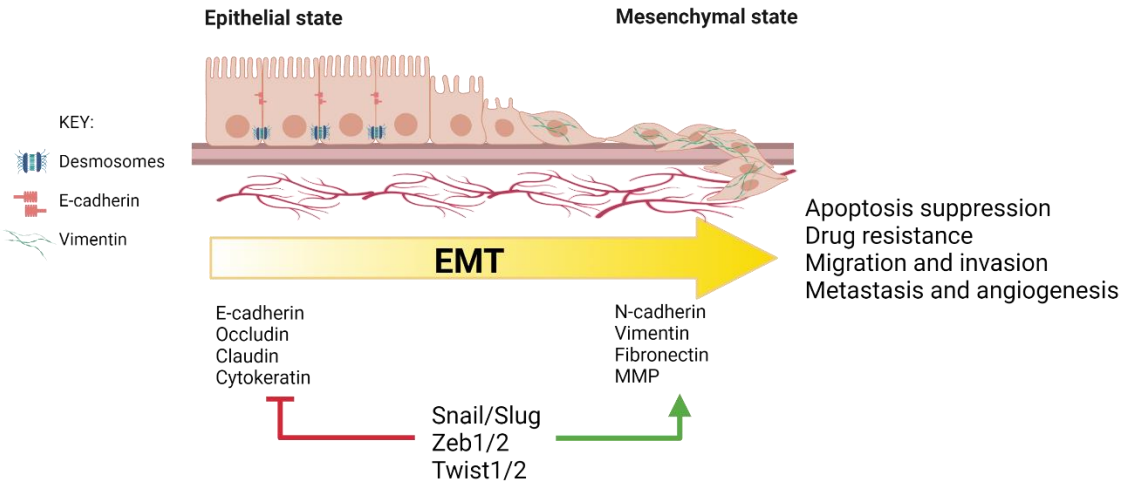


Figure 1.2: Epithelial-to-mesenchymal transition. *The process of EMT disrupts epithelial cell-cell adhesion, results in loss of apical-basal polarity and undergoes cytoskeletal remodelling, to resemble a mesenchymal phenotype. The change in cell physiology is initiated by EMT transcription factors: Snail, Twist and Zeb. Cells that have undergone EMT are characterised by the loss of epithelial surface markers such as E-cadherin, occludin, claudins and cytokeratin. EMT stimulates cells to express mesenchymal markers including N-cadherin, vimentin, fibronectin, and matrix metalloproteinases (MMPs). Figure created with BioRender.com*

The transcriptional activation of EMT-TFs are mediated by several signalling pathways including Wnt, Hedgehog, TGF-β and receptor tyrosine kinase (RTK) signalling as well as inflammatory cytokines and physical stresses like hypoxia (Figure 1.3) (Cao et al., 2015). There is considerable crosstalk between EMT inducing signals and many of these pathways are expressed in specific cells or tissue types. This indicates that cells may respond differently to specific signalling pathways, depending on their cell state and microenvironment (Gonzalez and Medici, 2014).

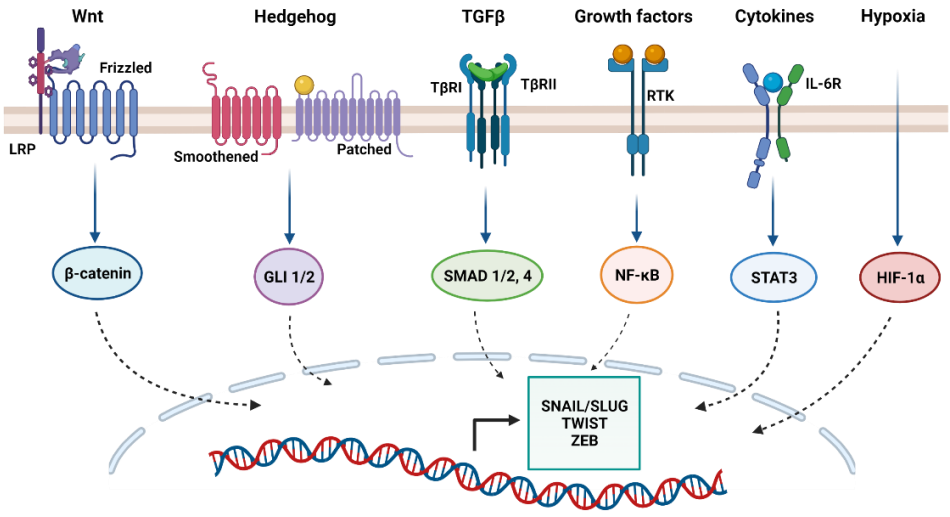


Figure 1.3: Signalling networks that promote EMT in colorectal cancer. *The major signalling pathways implicated in EMT include Wnt, Hedgehog, TGF-β and RTK signalling as well as inflammatory cytokines and physical stresses like hypoxia. Wnt signalling drives the EMT process through the inhibitory phosphorylation of glycogen synthase kinase 3β (GSK3β). Successively, β-catenin is stabilised and translocates to the nucleus to activate SNAI1 and ZEB1.The activation of hedgehog signalling results in the de-repression of transmembrane receptor Smoothened, that functions to active the GLI family of TFs to drive EMT. TGF-β associates with TGF-β receptors and induce the phosphorylation and activation of SMAD proteins, that localise in the nucleus to transcribe Snail, Twist and Zeb TF families. Growth factors promote RTK signalling via the PI3K and MAPK signalling pathways to activate EMT-TFs via NF-κB. The phosphorylation of STAT3 via proinflammatory cytokines implicated in EMT induction. Hypoxia is an important driver of EMT through the stabilisation of hypoxia-inducing factor-1α (HIF-1α) to upregulate SNAIL, ZEB1 and TWIST. Figure created with BioRender.com*

Growing evidence has suggested the ubiquitous role of inflammation in CRC. Patients with chronic inflammatory bowel conditions have a much greater risk of acquiring CRC (Long et al., 2017). Additionally, studies have suggested that the use of anti-inflammatory medications may delay or even prevent CRC development (Friis et al., 2015). Of the mentioned pathways that induce EMT, inflammation and cytokine signalling is recognised as a key inducer of CRC. Interleukin-6 (IL-6) is a well-characterised inflammatory molecule and is considered a key player in driving tumour-associated inflammation and carcinogenesis. Chronic IL-6 signalling is responsible for driving a range of tumour-promoting properties including the ability to act on the tumour itself to support cell survival, proliferation and dissemination; and by acting extrinsically, through the interaction with cells in the tumour microenvironment (TME) to facilitate angiogenesis and tumour immune escape (Dominguez et al., 2017). The role of IL-6 in promoting EMT is discussed in detail below.

1.4 The IL-6 pathway in cancer progression and EMT

1.4.1 The IL-6/IL-6R pathway

IL-6 was first discovered for its ability to aid B cell maturation and is most known for its role in both the innate and adaptive immunity. IL-6 interacts with a dimeric cytokine receptor formed by IL-6 receptor (IL-6R) and glycoprotein 130 (gp130). The IL-6R contains a short cytoplasmic domain and cannot transduce intracellular signals, therefore, signalling is performed by the ubiquitously expressed gp130 transmembrane protein. The IL-6R/gp130 activated receptor complex transmits intracellular signals, regulating a number of pathways including the Janus kinase (JAK)/signal transducer and activator of transcription 3 (STAT3) pathway, PI3K/Akt and MAPK pathways (Masjedi et al., 2018).

There are two understood pathways involved in transmitting IL-6 signalling namely, the classical and trans-signalling pathways. The classical pathway is mediated by membrane bound IL-6R (mIL-6R). mIL-6R is uniquely expressed in immune cells such as monocytes, neutrophils and activated B cells and functions to stimulate an anti-inflammatory response and to facilitate homeostasis. The trans-signalling pathway functions similarly to the classical pathway except IL-6 binds to a soluble form of IL-6R (sIL-6R). sIL-6R is formed through proteolytic cleavage of mIL-6R protein or through alternative splicing of the IL-6R transcript (Lin et al., 2020). Importantly, sIL-6R can dimerise with gp130 even in cells that do not typically express IL-6R. Owing to the fact that all cells express gp130, the IL-6 pathway may be aberrantly activated by the trans-signalling pathway, which can contribute to cancer progression, including oncogenic signalling in CRC (Garbers and Rose-John, 2018).

1.4.2 The role of the IL-6/IL-6R/STAT3 pathway in EMT induction

Intestinal inflammation is understood to be one of the most important factors driving CRC. High IL-6 serum levels in various tumours have been linked to poor clinical outcome and chemotherapy resistance (Nakamura et al., 2020). The cytokine is one of the most abundant proinflammatory molecules in the TME. Cancerous cells utilise IL-6 through autocrine production and paracrine release, from infiltrating immune cells, to drive tumorigenesis (Dominguez et al., 2017). Chronic IL-6 signalling is responsible for driving a range of tumour-promoting properties including to support cell survival, proliferation and dissemination; and acting extrinsically through the interaction with cells in the TME to facilitate angiogenesis and tumour immune escape (Dominguez et al., 2017). The activation of downstream signalling pathways of JAK/STAT3, PI3K/Akt and MAPK promotes the

expression of proteins involved in cell proliferation (Cyclin D1, c-myc), survival (B-cell lymphoma (Bcl)-2, Bcl-xL), angiogenesis and metastasis (VEGF and MMPs), and amplifying inflammatory signals (IL-6 and TGF-β) (Johnson et al., 2018).

IL-6 was first identified as an EMT inducer of carcinoma cells in a study exposing IL-6 to estrogen receptor (ER)-α positive human breast cancer cells. IL-6 exposure repressed E-cadherin epithelial marker and induced the production of mesenchymal markers vimentin, N-cadherin, TWIST and SNAIL (Sullivan et al., 2009). Thereafter, studies have isolated JAK/STAT3 as the key pathway that IL-6 utilises to induce EMT. IL-6/IL-6R receptor complex stimulates the phosphorylation of STAT3 and its subsequent nuclear translocation, where phosphorylated STAT3 (pSTAT3), promotes the expression of key EMT-TFs (Yadav et al., 2011; Kim et al., 2016). pSTAT3 (at Tyr705 residue) has been shown to bind directly to the promotor regions of EMT-TFs TWIST, SNAIL and ZEB1 to enhance transcriptional activity (Xiong et al., 2012; Zhang et al., 2015; Saitoh et al., 2016), thereby establishing a direct role of STAT3 in EMT induction.

In addition to the direct role of STAT3 in EMT induction, the TF can transcriptionally mediate several pathways that are implicated in EMT induction (Figure 1.4). A study conducted by Lui et al., 2015, showed that STAT3 transcriptionally regulates the Fos-related antigen-1 (Fra-1) protein, in response to IL-6. Fra-1 is a significant member of the Fos family and is strongly implicated in carcinogenesis, metastasis and has been suggested to be a major regulator of EMT. Activated Fra-1 by IL-6/STAT3 drives aggressive CRC by increasing the production of EMT-enhancing proteins such as SLUG, SNAIL, ZEB1, MMP-9 and MMP-2 (Liu et al., 2015). Moreover, IL-6/STAT3 trans-signalling has shown to modulate the expression of hypoxia-inducing factor-1α (HIF-1α) and increases HIF-1α stability. Stabilised HIF-1α to upregulates the expression of *SNAIL*, *ZEB1* and *TWIST*, contributing to EMT induction (Jung et al., 2005; Holmer et al., 2015).

Furthermore, the inflammatory IL-6/STAT3/NF-κB feedback loop, is understood to be crucial for tumorigenesis and cell transformation (Iliopoulos et al., 2009). The Nuclear factor κ-light-chain-enhancer of activated B cells (NF-κB) TF is another mediator of EMT and NF-κB binding sites have been identified along the promotors of *SNAIL*, *SLUG* and *TWIST1* genes (Pires et al., 2017). Hendrayani et al., 2016, identified that AU-rich element RNA-binding protein-1 (AUF-1) is involved the IL-6/STAT3/NF-kB feedback loop and is important for the transmission of IL-6 signalling (Hendrayani et al., 2016). AUF-1 is a direct

target of STAT3 and is a positive regulator expression of mesenchymal marker α-smooth muscle actin (α-SMA) as well as EMT inducer TGF-β1 and IL-6 (Hendrayani et al., 2014). Inhibition AUF-1 blocks the IL-6/STAT3/NF-κB positive feedback loop as well as attenuates TGF-β signalling, which blocks the transformation of cancer-associated fibroblasts and prevents proliferation and cell migration (Hendrayani et al., 2016; Yan et al., 2018).

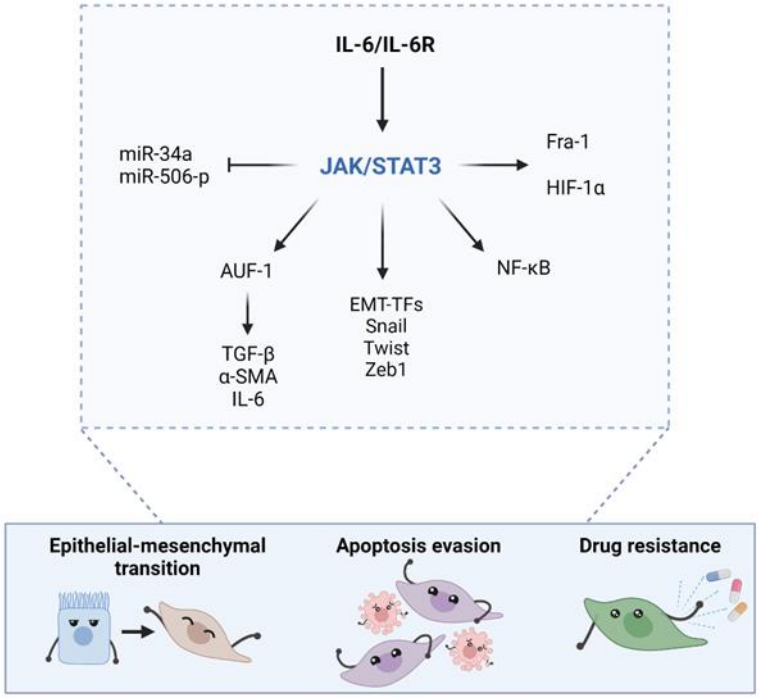


Figure 1.4: L-6/IL-6R mediates EMT through the JAK/STAT3 pathway. *Phosphorylated STAT3 functions by upregulating the expression of proteins involved in EMT induction such as Fra-1, HIF-1α, NF-κB, TGF-β, α-SMA and promotes a positive feedback loop by upregulating IL-6 expression. STAT3 inhibits the activity of miRNAs such as miR-34a and miR-506-3p which function to impede EMT. STAT3 can also directly promote EMT by binding to the promotor regions of EMT-TFs namely SNAIL, TWIST and ZEB1. Consequently, EMT induction leads to enhanced apoptosis evasion and drug resistance. Figure created with BioRender.com*

A member of the miR-34 family, miR-34a, is known to impede EMT by activating the p53 tumour suppressor (Nie et al., 2019). STAT3 inhibits miR-34a by binding to a conserved STAT3-binding region in the first intron of the *MIR34A* gene. STAT3-mediated miR34-a repression results in an upregulation of SNAI1, IL-6R and pSTAT3, further enhancing EMT and invasiveness. Rokavec et al., 2014, demonstrated that the IL-6R/STAT3/miR-34a feedback loop is in fact necessary for EMT progression and metastasis in CRC (Rokavec et al., 2014). Additionally, STAT3 indirectly downregulates Forkhead Box Q1 (FoxQ1) EMT-TF through the downregulation of miR-506-3p. STAT3 associates with the STAT3 binding region of the miRNA, inhibiting transcription. miR-506-3p is a key regulator of

FoxQ1 EMT-TF. Attenuation of FoxQ1 consequently resulted in the inhibition of EMT induction and migration in CRC cells (Wei et al., 2019). IL-6 is known to induce EMT in CRC (Rokavec et al., 2014; Liu et al., 2015; Wang et al., 2019), it is for this reason that this project utilises IL-6 cytokine to induced EMT in CRC cells.

As high as 25% individuals that are diagnosed with CRC are already at advanced stages of metastasis (Brand et al., 2018). EMT, a key characteristic of metastasis, is a major contributor of poor patient prognosis and limits the success of treatments. Therefore, there is a pressing need to improve on existing chemotherapies.

1.5 Current treatments for colorectal cancer

There are several strategies implemented for the treatment of CRC (Figure 1.5). The primary and ideal form of treatment for CRC is the surgical removal of the tumour and all metastases. Radiotherapy and chemotherapy are additional leading strategies used to control the disease and are often applied as neoadjuvant or adjuvant treatment to surgery, for the maximal reduction and stabilisation of the tumour (Xie et al., 2020).

Newer approaches such as targeted therapy and immunotherapy have been developed to improve on existing chemotherapies. Targeted therapies provide treatments that target tumour-specific mutations and oncogenic pathways, to hinder tumour growth and trigger apoptosis. While immunotherapies are designed to enhance immunorecognition against cancer cells that may express abnormal antigens. Monoclonal antibodies are often utilised by these strategies to either target and inhibit deregulated oncoproteins such as epidermal growth factor receptor (EGFR), vascular endothelial growth factor receptor (VEGFR) and B-Raf or to block the activity of immune checkpoint proteins namely programmed death-1 (PD-1) and cytotoxic T lymphocyte antigen 4 (CTLA-4), which can subsequently initiate an anti-cancer immune response (Dekker et al., 2019; Xie et al., 2020).

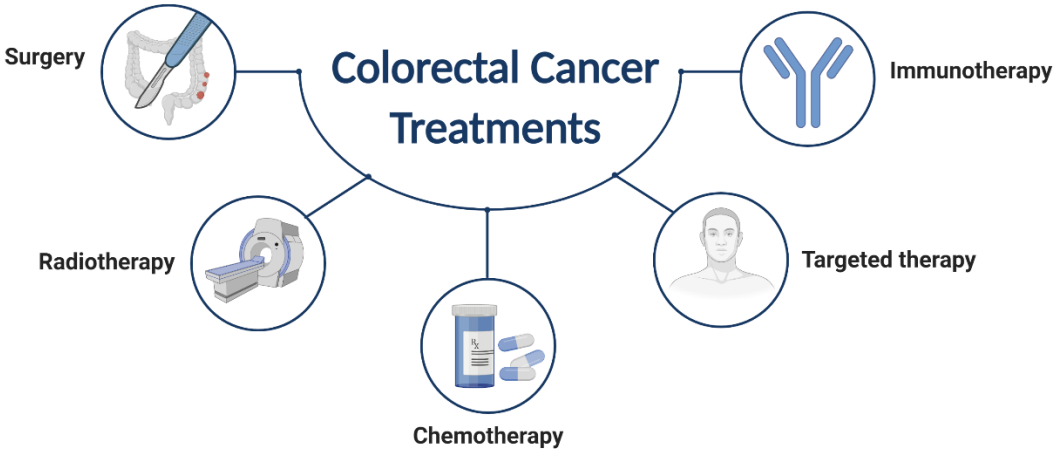


Figure 1.5: Current strategies aimed at treating colorectal cancer. *These treatments are often used in combination with each other (e.g., chemotherapy and targeted therapy) in order to increase patients' overall survival. Figure created with BioRender.com*

Studies performed in recent years have demonstrated that the use of chemotherapies, in the form of both single-agent and multiple-agent regimens, has improved CRC patients overall survival (OS) by almost 20 months (Xie et al., 2020). Administering chemotherapies has become the first line of treatment for CRC, especially mCRC. Additionally, up to 30% of patients that are diagnosed with mCRC present with an inoperable form of metastatic disease (Gustavsson et al., 2015). These patients who receive chemotherapy treatment have shown to have a median OS of greater than 2 years, compared to patients who receive supportive care alone with a median OS of 5 months (Gustavsson et al., 2015). Multiple-agent regimens consisting of a fluoropyrimidine, such as 5-fluorouracil (5-FU), and irinotecan or oxaliplatin are reported to be superior to single-agent therapies, specifically with the treatment of mCRC (Stintzing, 2014).

1.6 FOLFOX chemotherapy against metastatic colorectal cancer

1.6.1 FOLFOX mechanism of action

The fluoropyrimidine 5-FU is the most widely used drug for CRC treatment (Briffa et al., 2017). 5-FU may be used as a single agent or together with other drugs. However, the response rate of 5-FU alone is only 10-15% for the treatment of advanced CRC, therefore 5-FU is often used as a combination therapy (Johnston and Kaye, 2001). FOLFOX is one of the most common combination chemotherapies used to treat mCRC and includes an infusion of 5-FU together with folinic acid (otherwise known as leucovorin) and oxaliplatin (Folprecht et al., 2016).

5-FU is an analogue for uracil, with a fluorine atom at the C-5 of uracil. The anti-cancer metabolite functions by mis-incorporating itself and its active metabolites into DNA and RNA, and serves to inhibit tumour cell division by inhibiting thymidylate synthase (TS) (Figure 1.6) (Ghafouri-Fard et al., 2021). 5-FU is converted into a number of active metabolites including fluorouridine triphosphate (FUTP) and fluorodeoxyuridine monophosphate (FdUMP). FUTP becomes mis-incorporated into RNA, altering RNA processing and consequently, induces RNA damage (Ghafouri-Fard et al., 2021). TS converts nucleotide precursor deoxyuridine monophosphate (dUMP) into deoxythymidine monophosphate (dTMP), a vital step for DNA synthesis and repair. Following 5-FU metabolism, FdUMP metabolite binds to TS in place of dUMP, where the fluorine atom of FdUMP prevents its dissociation from the enzyme thus forming a stable inhibitory complex (Zhang et al., 2008). 5-FU is often administered together with folinic acid, that functions to improve TS inhibition (Negrei et al., 2016). Folinic acid enters the cell via the reduced folate carrier and is metabolised to 5,10-methylenetetrahydrofolate (5,10-CH_2FH_4) which binds to TS, forming a stable TS-dUMP-5,10-CH_2FH_4 ternary complex. Folinic acid has no anti-tumour activity and is included to enhance 5-FU activity, with fewer side effects (Wang et al., 2017).

Oxaliplatin has shown to be an effective anticancer agent against CRC. The platinum-based compound induces intra- and inter-strand DNA breaks by forming crosslinks between platinum and either two adjacent guanine residues or between a guanine and adenine residue. As a result, DNA replication and transcription is inhibited. Moreover, the bulky 1,2-diaminocyclohexane functional group of oxaliplatin prevents binding of the mismatch repair enzyme complex to DNA, resulting in cell-cycle arrest and apoptosis (Comella et al., 2009).

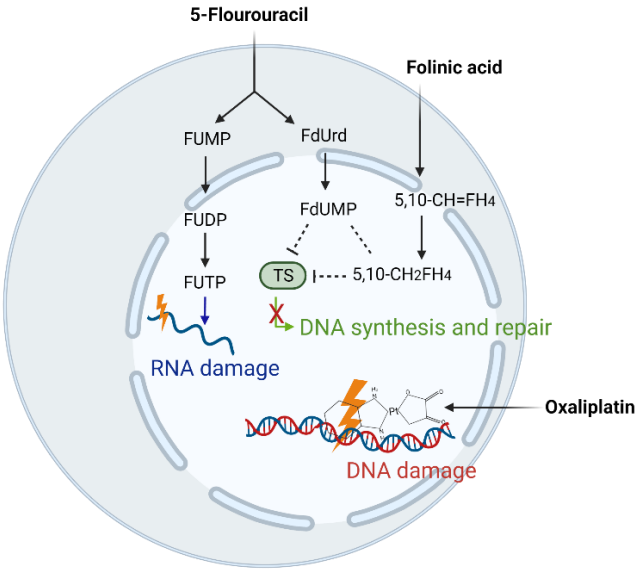


Figure 1.6: Metabolic pathway of FOLFOX chemotherapy. *The FOLFOX chemotherapy functions to induce DNA and RNA damage in CRC tumour cells. 5-FU metabolite, FUTP becomes mis-incorporated into RNA to induce RNA damage. FdUMP inhibits TS activity, preventing DNA synthesis and repair. Oxaliplatin induces DNA breaks to promote apoptosis and inhibit cell division. FOLFOX (FOL: folinic acid; F: 5-fluorouracil; OX: oxaliplatin) FUMP: fluorouridine monophosphate, FUDP: fluorouridine diphosphate, FUTP: fluorouridine triphosphate, FdUrd: fluorodeoxyuridine, FdUMP: fluorodeoxyuridine monophosphate, 5,10-CH=FH₄: 5–10 methenyltetrahydrofolate, 5-10-CH₂FH₄: 5,10-methylenetetrahydrofolate. Figure created with BioRender.com*

The FOLFOX regimen is recommended for adjuvant chemotherapy of stage III CRC following resection of the primary tumour (6 months perioperative treatment) and as a neoadjuvant treatment of mCRC, for 2-3 months (Briffa et al., 2017). Patients are administered oxaliplatin and folinic acid for 2 hours, followed by 5-FU infusion for 48 hours, following clinical practice originated from the 'De Gramont' schedule (de Gramont et al., 2000). FOLFOX treatments have enhanced OS and response rates to 40-50% in patients with mCRC (Douillard et al., 2000; Giacchetti et al., 2000)

1.6.2 Limitations to the FOLFOX chemotherapy

There are various limitations associated with chemotherapy treatments such as poor response rates, systemic toxicity, treatment resistance and low tumour specificity (Xie et al., 2020). Several severe toxicities are reported in patients treated with the FOLFOX regime such as abnormal kidney function, gastrointestinal side effects, neuropathy, cardiovascular side effects, abnormal liver enzymes and anaemia (Gresham et al., 2014). Ideally, chemotherapy for mCRC should be administered continuously until the disease improves, however, the accumulation of toxicities restricts continued use of the chemotherapy (Li et al., 2020).

Importantly, some patients do not even qualify for combination treatments of 5-FU with oxaliplatin or irinotecan because of the high toxicity profile of these drugs (Stintzing, 2014).

Furthermore, drug resistance is often reported after prolonged use of chemotherapies and remains one of the greatest obstacles in the treatment of mCRC. Multidrug resistance (MDR) is the resistance of a wide spectrum of different chemotherapeutic drugs. There are a number of mechanisms involved in MDR including the over-expression of efflux pumps such as ATP-binding cassette (ABC) transporters; reduced drug uptake; activation of detoxifying systems; DNA repair activation and evasion of apoptosis (Cho and Kim, 2020). The overexpression of ABC transporters such as P-glycoprotein (P-gp), encoded by *ABCB1*, is considered to be one of the most important processes involved in MDR and has become a source of significant interest in the research of reducing MDR. The overexpression of *ABCB1* is detected in various tumours including CRC and is associated with treatment failure. P-gp acts to expel 5-FU and oxaliplatin, preventing the drugs from reaching a sufficient concentration to induce DNA or RNA damage (Briffa et al., 2017).

Clearly, there is a pressing need to improve on existing chemotherapies. Identifying new targets and understanding related biological mechanisms is vital for the development of improved treatment strategies. Cholesterol has received increasing attention for its role in cancer progression, where cholesterol dyshomeostasis has shown to drive several cancers (Ding et al., 2019). Cholesterol metabolism and its involvement CRC cancer progression will be discussed in greater detail below.

1.7 Cholesterol metabolism

Under healthy homeostatic conditions, cholesterol is vital for cellular function and organism survival. Cholesterol acts as a precursor for the synthesis of bile acids, adrenal and gonadal steroid hormones, and vitamin D (Huang et al., 2020). Cholesterol is a vital component of the cell, to maintain integrity and fluidity of the membrane. Additionally, cholesterol accumulates in specified regions of the cell membrane, together with sphingolipids, forming micro-domains termed lipid-rafts. Lipid-rafts are central to key signalling pathways involved in apoptosis, cell cycle progression as well as tumour development and metastasis (Zalba and ten Hagen, 2017).

Cellular cholesterol levels are largely maintained by the balance between cholesterol biosynthesis, export, uptake by lipoproteins and esterification (Arnold and Kwiterovich,

2003). The liver is one of the primary sites involved in cholesterol biosynthesis. Cholesterol biosynthesis occurs through the mevalonate pathway. Three acetyl CoA molecules are condensed to yield 3-hydroxy-3-methylglutaryl (HMG-CoA). Subsequently, a series of enzymatic reactions occur for the production of cholesterol (Figure 1.7) (Arnold and Kwiterovich, 2003). Cholesterol synthesis is tightly regulated to ensure normal homeostatic conditions. HMG-CoA reductase (HMGCR), which reduces HMG-CoA to mevalonate, is the rate-limiting step and is critical for cholesterol biosynthesis. Sterol regulatory element-binding protein 2 (SREBP2) is the main transcriptional regulator of cholesterol synthesis. In the presence of high cholesterol, SREBP2 is inactive, forming an inert complex at the endoplasmic reticulum with sterol-sensing SREBP-cleavage activating protein (SCAP). When cholesterol levels fall, the amino terminal of SREBP2 is cleaved and SREBP2 is liberated from SCAP. The protein enters the nucleus and binds to the promotor region of target genes at the sterol regulatory element (SRE) sequence 5'-TCACNCCAC-3'. Target genes of SREBP2 include HMGCR and LDL receptor (LDLR) which upregulate cholesterol synthesis and uptake from the external environment (Berg et al., 2002).

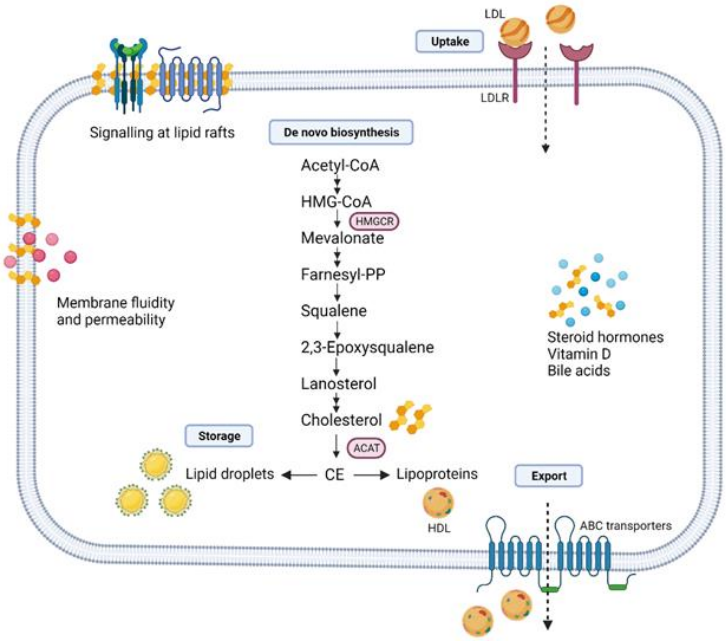


Figure 1.7: Cholesterol metabolism and homeostasis*. Cholesterol acts as a precursor for the synthesis of bile acids, steroid hormones, and vitamin D. The lipid also functions to maintain membrane fluidity, permeability and accumulates in lipid-rafts for cell signalling. Cholesterol is synthesised through a series of ~30 enzymatic reactions beginning with acetyl CoA. HMGCR is the rate-limiting step for cholesterol biosynthesis. Cholesterol is converted to cholesteryl esters (CEs) by acyl coenzyme A: cholesterol acyltransferase (ACAT), for secretion as lipoproteins or its storage in lipid droplets. Cholesterol levels are also maintained by cellular uptake of low-density lipoproteins (LDL) by LDL receptors (LDLR). Excess cholesterol is exported by ABC transporters. Figure created by BioRender.com. Figure adapted from (Luo et al., 2020).*

In addition to de novo biosynthesis of cholesterol, cells take up exogenous cholesterol supplied by the diet. Cholesterol is nonpolar and water insoluble. Therefore, cholesterol is packaged in a lipid-rich core surrounded by lipoproteins, to solubilise cholesterol in the blood. The two major transporters of cholesterol are high-density lipoprotein (HDL) and low-density lipoprotein (LDL). HDL particles are necessary for the reverse transport of cholesterol by removing excess cholesterol; cholesterol from dying cells and cells undergoing membrane turnover from peripheral tissues and transporting cholesterol back to the liver (Arnold and Kwiterovich, 2003). LDL particles functions to transport cholesterol from the liver to peripheral tissues. Cellular uptake of cholesterol is regulated by LDLR mediated endocytosis of LDL particles and subsequent hydrolysis. LDLR activity is the main player regulating cholesterol uptake. The inducible degrader of the LDL-receptor (IDOL) and proprotein convertase subtilisin/kexin type-9 (PCSK-9) are critical for LDLR regulation, targeting LDLR for degradation in the presence of excess cholesterol (Luo et al., 2020).

Excess cholesterol is either exported by ABC transporters such as ABCA1 and ABCG1 to the blood or is esterified by acyl-CoA:cholesterol acyltransferase (ACAT) to form cholesteryl esters (CEs). CEs are either secreted within lipoproteins or stored in the form of lipid droplets, which functions to decrease cellular cholesterol levels (Röhrl and Stangl, 2018). The liver X receptor (LXR) transcriptional regulator works in an opposing manner to SREBP2. Excess cholesterol and cholesterol-derived oxysterols activates the LXR pathway. The pathway acts to reduce cholesterol levels by upregulating the expression of genes involved in cholesterol efflux, transport and absorption (Zhu et al., 2012). Target genes of LXR include *ABCA1* and *ABCG1* to increase cholesterol efflux; and *IDOL* to suppress LDLR expression (Röhrl and Stangl, 2018). Loss of these homeostatic controls is one of the major hallmark features of cancer-cholesterol metabolism.

1.8 Deregulated cholesterol metabolism in colorectal cancer

Under healthy conditions, circulating and cellular cholesterol levels are tightly regulated by biosynthesis pathways, dietary cholesterol, and elimination of surplus cholesterol from peripheral tissues. In the context of carcinogenesis, cholesterol mechanisms become deregulated in order to support the increase in cell metabolic requirements such as hyperproliferation and migration (Cruz et al., 2013). Numerous malignant tumours exhibit cholesterol accumulation and overwhelming evidence indicates that cholesterol is

predominantly involved in cancer development (Ding et al., 2019). Abnormal lipid content in cancerous tissues is associated with CRC occurrence and development (Zhang et al., 2014).

Modifications to cholesterol content is mediated by a series of events that modify cholesterol biosynthesis, uptake and cholesterol efflux (Cruz et al., 2013). Increased cholesterol biosynthesis is in fact a hallmark of many cancers. Studies show that SREBP2 and its downstream target genes become significantly upregulated, in numerous cancers. Consequently, HMGCR activity is increased as well as production of LDLR, to enhance cholesterol biosynthesis and uptake (Huang et al., 2020). The *in vitro* and *in vivo* knockdown of SREBP1 or SREBP2 in CRC impeded cell proliferation and tumorigenesis, as a result of reduced cholesterol levels. While SREBP1 is mostly known for controlling fatty acid synthesis, target genes of cholesterol synthesis become downregulated by the knockdown of SREBP1 (Wen et al., 2018). Another study identified the overexpression of SREBP1 in CRC, which suggests that SREBP1 and subsequent cholesterol upregulation is involved in CRC carcinogenesis (Gao et al., 2019). Cholesterol can be made readily available in cancerous cells, through the accumulation of CEs (Huang et al., 2020). CEs prevent toxic accumulation of cellular free cholesterol and become reservoirs of cholesterol when needed by the cell. Abnormal accumulation of ACAT is detected in a number of tumours and exhibits a tumour promoting function, by converting free cholesterol into CEs (Ayyagari et al., 2020). The knockdown of ACAT1 in glioma nude-mouse xenograft model resulted in impeding tumour progression (Geng et al., 2016). LXR regulated genes, such as ABCA1 and IDOL, show reduced expression in several cancer types, consequently facilitating higher intracellular cholesterol content through decreased efflux by ABC transporters and enhanced uptake by LDLRs (Bilotta et al., 2020). Studies have shown the activation of the LXR pathway to induce cell death of glioblastoma cells by promoting IDOL-mediated LDLR degradation and cholesterol efflux by ABCA1 (Guo et al., 2011).

Increased cellular cholesterol accumulates in lipid-rafts, which is an important site for oncogenic signalling (Cruz et al., 2013). Proteins that reside at lipid rafts are involved in vital signalling pathways such as apoptosis, cell cycle progression and cell adhesion. Additionally, cholesterol serves as an activator for several pathways to support cancer stem cell like properties and tumour progression (Huang et al., 2020). Receptors of the canonical Wnt pathway namely Frizzled and LDLR-related protein (LRP), are located exclusively at lipid rafts. Wnt is a known driver of CRC and is an EMT-inducing pathway. The disruption of membrane cholesterol has shown to impede Wnt signalling and subsequently initiate

apoptosis in cancerous cells (Sezgin et al., 2017). TGF-β signalling is another EMT related pathway localised at lipid rafts. The TβRI/TβRII/TGF-β receptor-ligand complex forms at lipid rafts and is essential for mediating TGF-β dependent activation of MAPK signalling and EMT induction. The disruption of lipid rafts inhibits TGF-β signalling, impeding EMT induction and cell migration (Zuo and Chen, 2009). Interestingly, Kim et al., 2004, found that IL-6R is associated with lipid rafts and that a significant proportion of inactive and phosphorylated STAT3 accumulates in the lipid raft. Lipid raft disruption attenuated IL-6-mediated STAT3 phosphorylation (Kim et al., 2004). Clearly, cholesterol deregulation is vital for carcinogenesis by sustaining high levels of proliferation as well as by mediating EMT-related signalling pathways. It can therefore be argued that cholesterol is an important target to impede cancer progression. The next section discusses this in greater detail.

1.9 Cholesterol as a target for colorectal cancer treatment

It is recognised that several cancer types, such as prostate, breast and CRC, have higher membrane and cellular cholesterol levels compared to normal cells. These cancer cells are more susceptible to cell-death induced by cholesterol lowering (Matusewicz et al., 2015). It is for this reason that cholesterol is viewed as an attractive target for anti-cancer therapies. There are two main strategies that have been explored to reduce cholesterol levels (a) the inhibition of cholesterol biosynthesis and (b) the depletion of cholesterol from cancer cell membranes.

1.9.1 Cholesterol biosynthesis inhibitors

HMGCR inhibitors namely statins are a therapeutic class of drugs that decrease plasma cholesterol levels, that are prescribed to prevent and treat coronary heart disease. An increasing amount of evidence suggests that statins have chemo-preventative properties against cancer (Beckwitt et al., 2018). To date, statins are the most vastly used cholesterol-targeting drugs that are in clinical trials as monotherapy or combined therapy for patients with cancer (Kubatka et al., 2014). HMGCR is the rate limiting enzyme of the mevalonate pathway. Statins competitively inhibit HMGCR, to prevent HMG-CoA conversion to mevalonate, thereby reducing the substrate required for cholesterol synthesis (Brown, 2007). As mentioned previously, cholesterol is required for upholding cell membrane integrity and for critical cellular processes. The disruption of cholesterol synthesis in neoplastic cells has shown to inhibit tumour growth, metastasis and enhance apoptosis (Morandi et al., 2017). *In vitro* studies have reported that statins induce cell cycle arrest by influencing the activity of

regulatory proteins: cyclins, cyclin-dependent kinases (CDK) and CDK inhibitors. Statins may also initiate apoptosis through activating both extrinsic and intrinsic pathways. Among the many molecular pathways influenced by statins the PI3K, MAPK and NF-kB are notably affected (Matusewicz et al., 2015). Interestingly, studies have identified that various tumour types are increasingly sensitive to statin treatment that have high expression of mesenchymal markers like vimentin and reduced expression of epithelial markers such as E-cadherin. Statins have shown to preferentially target cancer cells induced to undergo EMT, which suggests that statins may be valuable for treatment of metastatic cancer (Warita et al., 2014; Yu et al., 2018).

Despite reports from studies indicating the anti-cancer properties of statins, the clinical relevance of cancer in humans and statins remains unclear. Importantly, statins selectively localise in the liver and under 5% of the selected dose reaches the circulatory system (Boudreau et al., 2010). This poor systemic availability raises concerns about the usefulness of statins as a chemo-preventative drug. The evaluation of statin therapy as a cancer treatment is inconclusive. Many studies report that statin use exerts anticancer activity on tumour growth and may be beneficial to the treatment and prevention of cancers (Campbell et al., 2006; Babcook et al., 2016). In contrast, several studies have found no association between statins and reduced risk of cancer and weak to moderate evidence for statin use as a cancer treatment (Bonovas et al., 2007; Kuoppala et al., 2008). A meta-analysis, including 18 studies and over 1.5 million patients, found no evidence suggesting that statin therapy can reduce the risk of CRC, when taken at low dosage for treatment of high cholesterol (Bonovas et al., 2007). Additionally, millions of patients treated with statins are reported to be statin-intolerant as they are unable to tolerate any form of statin therapy or cannot tolerate the full recommended dose, experiencing adverse effects such as liver damage and myopathy (Reiner, 2014). Clearly further research is necessary to establish the role of statins as an anticancer therapy.

1.9.2 Cholesterol depleting agents

In addition to metabolic inhibition by statins, reduced cholesterol levels may be achieved by using chemicals that extract or immobilise cholesterol (Mahammad and Parmryd, 2015). Cholesterol depleting agents are gaining interest as potential anticancer compounds for their ability to induce cancer cell death in several cancers, disrupting lipid rafts and subsequent signalling pathways (Gu et al., 2019).

Cyclodextrins (CDs) are a family of water-soluble, cyclic oligosaccharides. The most abundant CDs are α-, β- and γ-CDs that are composed of six, seven and eight glucopyranose units, respectively (López et al., 2011). CDs are structured with a hydrophobic interior and a hydrophilic exterior, forming a cone-like cavity. CDs and their derivatives are utilised clinically for their ability to form inclusion complexes with lipophilic functional groups of hydrophobic drugs, through a process termed "inclusion phenomenon" (Jansook et al., 2018). Consequently, CDs are used to improve drug solubility, increase permeability, and drug bioavailability. Their hydrophilic exterior and high molecular weight prevents CDs from penetrating cell membranes, leaving cells intact (Jansook et al., 2018). β-CD derivatives have the highest affinity towards cholesterol and are very effective in extracting cholesterol from cell membranes; at raft and non-raft domains (Zidovetzki and Levitan, 2007).

A single cavity of β-CDs (~8 Å) is too small to extract cholesterol (~18 Å), therefore β-CDs bind to cholesterol in a 2:1 ratio (Zidovetzki and Levitan, 2007). Methyl-β-cyclodextrin (MβCD) and 2-hydroxypropyl-β-cyclodextrin (HPβCD) are the most widely used β-CD for the extraction of membrane cholesterol (Mahammad and Parmryd, 2015). Importantly, it is estimated that ~90% of free cellular cholesterol exists in the plasma membrane of numerous cell types (Kim et al., 1991; Lange, 1991). Therefore, it is suggested that membrane cholesterol depletion by CDs may affect intracellular cholesterol levels to maintain cholesterol homeostasis and membrane integrity (Zidovetzki and Levitan, 2007).

MβCD has shown to be very efficient at depleting cellular cholesterol, MβCD can extract 80–90% of total cellular cholesterol when treated with high concentrations of 5–10 mM, for an extended period of time (>2 hours) (Zidovetzki and Levitan, 2007). The amount of cholesterol extracted is dependent on concentration of MβCD, exposure time and composition of the lipid membrane (Beseničar et al., 2008). MβCD can be cytotoxic at high concentrations, which is inhibited by the addition of cholesterol into cell culture medium (Onodera et al., 2013). Importantly, MβCD displays high selectivity against cancer cells, where cholesterol content is highly correlated with cancerous transformation. Resnick et al., 2015, demonstrated that MβCD targeted and induced apoptosis in invasive urothelial cancer cells, while MβCD did not affect the viability of normal porcine urothelial cells (Resnik et al., 2015).

MβCD is recognised to effectively reduce membrane cholesterol and disrupt the structure of lipid rafts (Gu et al., 2019). Cholesterol depletion from cell membranes can induce apoptosis

in a range of invasive cell lines and elevate caspase-3/7 activity as well as inhibit Bcl-xL in cells (Li et al., 2006; Onodera et al., 2013). Additionally, PI3K activates Akt by recruiting Akt and protein dependent kinase 1 (PDK1) to lipid rafts. MβCD inhibits Akt phosphorylation and upregulates protein degradation in breast and prostate cancer cell lines, by depleting lipid raft cholesterol which results in apoptosis (Li et al., 2006). MβCD reduced cell migration in MDA-MB-231 cells as a result of Wnt3a inhibition and an increase in IL-10 cytokine production, which suggests that cholesterol depletion also has an effect on the invasiveness of cancer cells (Guerra et al., 2016). Cholesterol depletion with β-CDs increases membrane stiffness which results in deceased cell migration, stem cell characteristics and has shown to inhibit EMT induction *in vitro* (Byfield et al., 2004; Zhao et al., 2016). Several studies report that the interference of lipid rafts inhibits the activity of key EMT-related signalling pathways which promotes the expression of epithelial markers and downregulates mesenchymal marker expression (Zuo and Chen, 2009; Guerra et al., 2016; Wu et al., 2020).

Similar to MβCD, KS-01 is a β-CD that binds to membrane cholesterol with high affinity. KS-01 is a proprietary molecule, therefore, the full name and its structure cannot be disclosed. Studies performed in Professor Kaur's laboratory identified KS-01 as an effective molecule for depleting cholesterol in cancer cells, showing reduced cytotoxicity, increased solubility, and bioavailability in comparison to MβCD. The lab identified KS-01 to successfully deplete intracellular cholesterol level in ER+ (MCF-7) and ER- (MDA-MB-231) breast cancer cell lines, at a concentration of 10 mM. Consequently, KS-01 induced cell death in breast cancer cell lines. The compound displayed high specificity to the cancer cells, while not affecting cholesterol content or cell viability in normal cells. *In vivo* MDA-MB-231 mouse xenograft studies found 100%, 93.1% and 73.9% tumour reduction for the early, intermediate, and late stages of breast cancer, respectively. These results identify KS-01 as a promising molecule for the treatment of breast cancer. Currently, no studies have been performed using KS-01 as an anti-cancer compound in the context of CRC.

1.10 Introduction to this study

CRC is a highly metastatic disease which confers poor patient prognosis and limited strategies for treatment. FOLFOX is one of the most common chemotherapy regimens administered to patients with mCRC. Despite improving the OS of patients, the regimen is associated with several limitations such as increasing toxicity and acquired drug resistance. Therefore, there is a pressing need to improve on existing chemotherapies. EMT, a key

characteristic of metastasis, is a major contributor to MDR and difficulties in treatment. Therefore, the process of EMT has become an attractive therapeutic strategy against tumour progression and invasion. Current strategies used for targeting EMT are aimed at interfering with the EMT signalling process but very few studies focus on targeting the mesenchymal phenotype, which presents an alternative strategy.

Additionally, increasing evidence highlights the central role of the cholesterol biosynthesis pathway in EMT progression. The lipid composition of epithelial cells compared to mesenchymal cells are distinct and cells that undergo EMT show a major elevation in cholesterol levels (Morandi et al., 2017). This upregulation is likely to increase membrane fluidity necessary for cytoskeletal remodelling, changes in cell motility and cell polarity. Additionally, cholesterol enhances EMT related signalling pathways such as TGF-β and Wnt, which promotes cell survival and invasiveness (Jiang et al., 2019). As a result of modified cholesterol content, EMT cancer cells exhibit increased sensitivity to cholesterol reducing drugs, such as statins. Importantly, regulating cell cholesterol levels may either promote or impede the conversion to a mesenchymal phenotype (Morandi et al., 2017).

In this study, the HT-29 CRC cell line was induced to undergo EMT following the exposure to IL-6. The change in cholesterol content post-EMT induction was characterised. Thereafter, cholesterol depleting agents, MβCD and KS-01, were utilised to observe the effect of cholesterol depletion on the mesenchymal phenotype of cells. Additionally, we explored the effect of cholesterol depletion on the susceptibility of EMT induced cells to the FOLFOX chemotherapy.

2. Aim and Objectives

2.1 Aims

This study aims to investigate the effect of cholesterol depletion in EMT induced colorectal cancer and explores how cholesterol depletion influences the susceptibility of EMT induced cells to the FOLFOX chemotherapy.

2.2 Objectives

1. To establish the optimal FOLFOX concentration suitable for the treatment of HT-29 cells
2. To optimise the concentration of IL-6 needed to successfully induce EMT in HT-29 cells
3. To validate EMT induction by assessing changes in cell morphology and immunofluorescent analysis of epithelial and mesenchymal markers
4. To assess changes in cholesterol content in EMT induced cells following cholesterol depletion
5. To ascertain the effect of cholesterol depletion on the EMT phenotype
6. To determine the effect of cholesterol depletion on the invasive potential in EMT induced cells
7. To determine the effect of cholesterol depletion on FOLFOX-induced cell death in EMT induced cells
8. To determine the effect of cholesterol depletion on FOLFOX-induced multidrug resistance in EMT induced cells

3. Methodology

In this study, the human colorectal adenocarcinoma HT-29 cell line was utilised as an *in vitro* model to explore the effect of cholesterol depletion on EMT induced cells. The outline of the project is represented in Figure 3.1. In summary, following EMT induction of HT-29 cells by IL-6, changes in cholesterol content were characterised together with cholesterol depleting agents, MβCD and KS-01. Immunofluorescence was performed with epithelial marker E-cadherin and mesenchymal marker vimentin to observe the effect of cholesterol depletion on the EMT phenotype. Additionally, we explored the effect of cholesterol depletion on the invasive potential of EMT induced cells as well as on the susceptibility of FOLFOX-induced apoptosis and MDR in EMT induced cells.

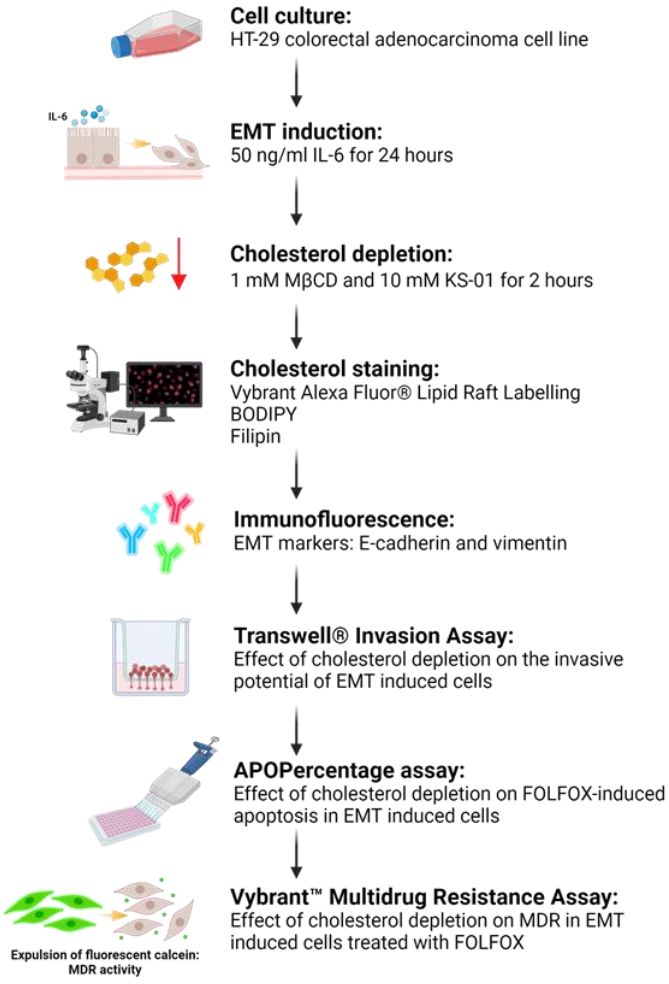


Figure 3.1: Project workflow. *Figure created with BioRender.com*

3.1 Cell Culture

The following methodology was performed with the human colorectal adenocarcinoma HT-29 cell line. The cell line was isolated from a primary tumour of a 44 year-old Caucasian female, in 1964. Cells from the HT-29 cell line are adherent, maintain an epithelial morphology and are sensitive to chemotherapeutic drugs 5-FU and oxaliplatin (Leteurtre et al., 2003). The HT-29 cells utilised in this project were obtained from Cellonex South Africa. Cells were maintained in culture from passage numbers p24 to p30. HT-29 cells were cultured in McCoy's 5a (Modified) Medium (Sigma Aldrich, UK), supplemented with 10% Foetal Bovine Serum (FBS) (Celtic Molecular Diagnostics, SA) and 1% penicillin-streptomycin (Sigma Aldrich, UK). McCoy's 5a (Modified) Medium provided essential nutrients and energy for optimal cell survival and growth. The use of penicillin-streptomycin antibiotic was to reduce the risk of bacterial and fungal contamination. Cells were incubated at 37 °C and 5% carbon dioxide (CO_2) incubator, maintaining a constant pH through a carbon dioxide-bicarbonate buffer system, to mimic *in-vivo* conditions.

3.2 IL-6 induced EMT

HT-29 cells were treated with recombinant human IL-6 cytokine (PeproTech, US) to induce EMT. IL-6 was diluted down to a working stock solution of 1 µg/ml in 0.1% Bovine Serum Albumin (BSA) (VWR Life Sciences, US) in 1× Phosphate Buffered Saline (PBS) (Sigma Aldrich, UK). EMT induction was assessed at increasing concentrations of 20, 30 and 50 ng/ml IL-6 after 24 hours (Rokavec et al., 2014; Liu et al., 2015; Wang et al., 2019). 50 ng/ml of IL-6 was selected to induce EMT after 24 hours. EMT-induced changes in cell morphology were observed under a Nikon Phase Contrast microscope.

3.3 Cell Counting

Cell counting was performed prior to plating cells, which ensured an equal number of cells plated per well. The Countess™ II Automated Cell Counter (Thermo Fisher Scientific, USA) was used to perform all cell counts for plating. Initially, the media was removed from the flask and washed twice with 2 ml of pre-warmed PBS (Sigma Aldrich, UK). Cells were detached from the flask, following the addition of 2 ml of dissociation reagent 1× trypsin/ethylenediaminetetraacetic acid (EDTA) (Sigma Aldrich, UK; Celtic Molecular Diagnostics, SA) and incubated for 5-10 minutes, at 37 °C. The cells were neutralised with an equal volume of media. Subsequently, 100 µl of cells were added to an equal volume of 0.4% trypan blue (Sigma Aldrich, UK) and mixed thoroughly. 10 µl of the cell solution was loaded

into disposable countess chamber slide and inserted into the cell counter, where viable and dead cells were counted automatically. Viable cells have intact membranes which prevents the uptake of the dye, leaving cells white in colour. The membranes of dead cells become disrupted, allowing dye uptake and staining cells blue. For the accurate detection of cell number, three readings were recorded, and an average cell number/ml was obtained.

Thereafter, cells were seeded at the desired density in 6-well, 24-well or 96-well plates. The following calculations were used to determine the volume of cells and media required for plating:

Total cell count = Cell count/ml × Volume in flask (ml)

Total Volume (Vt) = Plating volume per well (µl) × Number of wells

Volume of cells (µl) = [Volume in flask (µl) × Desired cell number per well × Number of wells] / Total cell count

Volume of media (µl) = Vt - Volume of cells

3.4 Cell Viability Assay

A 3-(4,5-dimethylthiazol-2-yl)-2-5-diphenyltetrazolium bromide (MTT) (Sigma Aldrich, UK) assay was performed to identify the effect of single-agent chemotherapies 5-FU (Sigma Aldrich, UK, F6627) and oxaliplatin (Sigma Aldrich, UK, O9512) on cell viability. Thereafter, MTT assays were utilised to ascertain the optimal concentration of the combination of the two drugs for the treatment of "FOLFOX" *in vitro*. Oxaliplatin was prepared in dH_2O, and 5-FU was reconstituted in dimethyl sulfoxide (DMSO) and diluted to working solutions in dH_2O. The percentage of DMSO did not exceed 0.2% per well and DMSO controls were constructed, to ensure that DMSO had no effect on cell viability (Appendix; Figure A.1). MTT is a yellow tetrazolium salt that is cleaved by the mitochondrial enzyme reductase to form purple formazan crystals (Sylvester, 2011). The production of purple formazan crystals is directly proportional to cell metabolic activity and therefore, provides information on cell viability.

5000 cells/well were seeded onto 96-well plates and left to adhere for 24 hours. Cells were subsequently treated with single or combination treatments of 5-FU and oxaliplatin over another 24 or 48 hours. 5 µl from a 5 mg/ml MTT stock solution (5 mg MTT in 1 ml PBS) was added into each well and the plate was left to incubate for 3 hours, to allow cells to metabolise resulting in the production of formazan crystals. The purple formazan crystals were left to dissolve over night after adding 55 µl of MTT solubilising solution (10% sodium-dodecyl-sulphate (SDS), in 10 mM hydrochloric acid (HCl)) in to each well. The absorbance of each well was measured with the Multiskan GO Microplate Reader (Thermo Fisher Scientific, SkanIt™ software), at a wavelength of 570 nm.

The percentage of cell viability was calculated using the following equation:

(x) = Average absorbance values of samples - Average absorbance values of blanks

% Cell Viability = [**(x)** of test sample / **(x)** of untreated sample] × 100

3.5 Cell Proliferation Assay

A cell proliferation assay was performed to assess the effect of 50 ng/ml IL-6 on cell growth. 20 000 cells/well were seeded onto a 24-well plate and left to adhere for 24 hours. Following IL-6 treatment, proliferative activity was ascertained by manual counting with a Neubauer haemocytometer. Cells were counted every 24 hours, over a 4-day period. 10 µl of the trypan blue cell solution was loaded onto the haemocytometer where viable and dead cells were counted under a Nikon Phase Contrast microscope. An average was obtained from cells counted in all four quadrants, made up of 16 squares each. To calculate cell number/ml, the average cell count was multiplied by a dilution factor of 2 and the Neubauer factor (10^4), which accounts for the set area and volume of each quadrant ($0.1\ mm^3 = 10^{-4}$ ml).

Cell viability and cell count was calculated as follows:

$$\% \text{ Cell viability} = [\text{Number of viable cells (unstained)}] / [\text{Total cells counted (viable and dead)}] \times 100$$

$$\text{Cell number/ml} = \text{Average cell count of four quadrants} \times 2 \times 10^4$$

3.6 Immunofluorescent Staining

Immunofluorescent staining was performed to evaluate EMT induction. Immunofluorescence utilises fluorescently labelled antibodies for the purpose of detecting an antigen of interest and therefore, specific protein expression. The indirect immunofluorescent method was employed, which involves a two-step incubation procedure. First, the incubation with a primary antibody detects and binds the antigen of interest. Second, the incubation with a secondary antibody conjugated with a fluorophore binds the primary antibody. Indirect immunofluorescence is preferred over direct immunofluorescence for its high sensitivity (Im et al., 2019).

20 000 cells/ well were seeded onto 12 mm round glass coverslips (Carl Roth, DE) in a 24-well plate. Following cell adhesion and EMT induction (50 ng/ml IL-6), the media was discarded, and cells were washed with three PBS washes. Subsequently, the cells were fixed by adding 400 µl of 4% formaldehyde (Sigma Aldrich, UK) diluted in PBS to each well for 15 minutes at room temperature. The purpose of cell fixation is to preserve cellular organelles and proteins; and to maintain a native cellular conformation through the crosslinking of proteins to the cytoskeleton. After another two PBS washes, cells were permeabilised with 0.1% Triton^{TM} X-100 (Sigma Aldrich, UK) diluted in PBS. Triton X-100 is a non-ionic surfactant used to disrupt the cell's lipid membrane, which improves antibody uptake in the cytoplasm and nucleus. Subsequently, a blocking step was included to prevent the non-specific binding of antibodies. 1% BSA in 0.1% PBS-T (PBS-Tween-20) was added to each well to saturate excess protein-binding sites and was left for an hour, at room temperature. Antigen specific primary antibody (Table 3.1) was added to each well and left overnight on a shaker at 4 ^{o}C.

The following day, the cells were washed twice with PBS-T and the secondary antibody was added to each well (Table 3.2) for 45 minutes at room temperature. 4′,6-diamidino-2-

phenylindole (DAPI) is a blue fluorescent DNA stain, used for the visualisation of nuclei. 0.0001 mg/ml DAPI (Sigma Aldrich, UK) diluted in PBS was added to each well and left for 10 minutes at room temperature. Thereafter, cells were washed three times with PBS. The coverslips were gently removed, tapped dry and placed facing down onto microscope slides coated with Fluoromount™ Aqueous Mounting Medium (Sigma Aldrich, UK). Cells were visualised under the Floid™ Cell Imaging System (Thermo Fisher Scientific, US). Immunofluorescence intensity was quantified with the ImageJ software (NIH, USA).

Table 3.1: Primary antibodies and dilutions used for immunofluorescence

Protein	Primary antibody	Dilution	Company
E-cadherin	Mouse Anti-Human E-cadherin	1:250 in 0.1% BSA, 0.1% PBS-T	BD Pharmingen, USA
Vimentin	Rabbit Anti-Human Vimentin	1:250 in 0.1% BSA, 0.1% PBS-T	Abcam, UK
Phospho-STAT3(Y705)	Rabbit Anti-Human Phospho-STAT3(Y705)	5 µg/ml in 0.1% BSA, 0.1% PBS-T	R&D Systems, USA
Ki67	Rabbit Anti-Human Ki67	1:250 in 0.1% BSA, 0.1% PBS-T	Novus Biologicals, USA

Table 3.2: Secondary antibodies and dilutions used for immunofluorescence

Target	Secondary antibody	Dilution	Company
Mouse	Goat Anti-Mouse Alexa Flour 488	1:1000 in 0.1% BSA, 0.1% PBS-T	Thermo Fisher Scientific, USA, A-11029
Rabbit	Goat Anti-Rabbit Texas Red	1:1000 in 0.1% BSA, 0.1% PBS-T	Thermo Fisher Scientific, USA, T-2767

3.7 Reverse Transcription Quantitative Polymerase chain reaction (RT-qPCR)

RT-qPCR was performed to confirm the successful induction of EMT through the relative quantification of gene expression of EMT-TFs, *SNAI1* and *TWIST1*. The difference in gene expression between control and IL-6 treated samples were indicated as $\log_2$(fold-change) ($\log_2$FC) of expression levels.

- *RNA Extraction*

RNA extraction of control and IL-6 treated samples was achieved using the Direct-zol™ RNA MiniPrep kit (Zymo Research, Inqaba Biotec™, SA). Initially, 300 µl of TRIzol® reagent (Ambion®, Life Technologies, USA) was mixed thoroughly into ~1×10^6 pelleted cells. TRIzol® reagent disrupts cell membranes and digests cell components, while retaining the integrity of RNA. Thereafter, an equal volume of 99.9% ethanol was mixed into the samples to precipitate nucleic acids out of solution. The samples were transferred to a Zymo-Spin™ IIC Column placed in a collection tube and centrifuged. At all centrifugation steps, samples were centrifuged at 16 000 x *g* for 30 seconds. In order to digest the DNA, 5 µl of DNase I and 75 µl of DNA digestion buffer was carefully added to the spin column and left for 15 minutes at room temperature. Two wash steps were included, with 400 µl of Direct-zol™ RNA PreWash and 700 µl of RNA wash buffer, respectively. At each step the flow-through was discarded. The wash steps were performed to ensure that samples were free of DNA and phenol contamination. Finally, the RNA was eluted by adding 50 µl of DNase/RNase-Free water to the spin column and centrifuged in a fresh Eppendorf tube. All samples were stored at -80°C for future use, to prevent the degradation of RNA.

The purity and integrity of RNA was assessed prior to cDNA synthesis. Nanodrop™ 1000 spectrophotometer (Thermo Fisher Scientific, USA) was used to assess purity (A260/280 and A260/230 ratios) and RNA concentration (ng/µl). The Nanodrop™ was blanked with 1 µl nuclease free water and RNA samples were read three times, to obtain an average reading. Purity assessment detects the presence of contaminants including DNA, protein, and phenols. Nucleic acids (DNA and RNA) have an absorption maximum of 260 nm. The absorbance ratio of A260/280 assesses the purity of DNA and RNA, at ratios of ~ 1.8 and ~2.0, respectively. A260/280 ratio between 2.00 to 2.2 were accepted for extracted RNA. A ratio considerably lower, indicates the presence of protein contamination which absorbs strongly at 280 nm. A260/230 ratio was accepted ~2.0, indicating “pure” RNA with the absence of phenol or salt contamination, which absorbs near 230 nm. Additionally, RNA integrity was

evaluated with agarose gel electrophoresis. 500 ng of RNA and 2 µl of 2× RNA loading dye (Thermo Scientific, USA) was loaded onto a 1% (w/v) agarose gel (0.5 g agarose powder + 50 ml 1× Tris-borate EDTA (TBE) + 5 µl Ethidium bromide, (Thermo Scientific, USA)) and resolved for 45 minutes at 80 mV. An image of the gel was captured on the ChemiDoc™ MP system (Bio-Rad, USA) and examined for smearing and for intact 28S and 18S bands.

- *cDNA Synthesis*

Extracted RNA was reverse transcribed into cDNA, using the RevertAid First Strand cDNA Synthesis kit (Thermo Fisher Scientific, USA). After thawing, reagents were kept on ice and added to a nuclease free tube in the order indicated in Table 3.3. The RNA concentration determined by the Nanodrop^{TM}, was used to calculate 2 µg of RNA. The difference in volume was adjusted by making up the mix to 12 µl with nuclease-free water. The addition of Oligo $(dT)_{18}$ primer, complementary to the poly(A) tail, allowed for the synthesis of cDNA from all mRNA present. RiboLock RNase Inhibitor protected against RNA degradation from RNases. dNTP Mix supplied nucleotides for the extension of cDNA. Reagents were gently mixed and centrifuged briefly prior to cDNA synthesis in the MultiGene PCR machine (Labnet International, UK). Samples were incubated for 60 minutes at 42 °C (the optimal temperature for RevertAid M-MuLV Reverse Transcriptase enzyme), then at 70 °C for 5 minutes to terminate the reaction. cDNA for a no template control (NTC) was also synthesised, to ensure no contamination in the reagents.

Table 3.3: Reaction set up for RevertAid First Strand cDNA synthesis

Reagent	Volume (µl)
Template RNA	2 µg
Oligo $(dT)_{18}$ primer	1
Nuclease-free water	Total volume of 12
5× Reaction Buffer	4
RiboLock RNase Inhibitor	1
10mM dNTP Mix	2
RevertAid M-MuLV RT (200U/µl)	1
Total Volume	**20**

- *Quantitative PCR (qPCR)*

Quantitative PCR (qPCR) was performed to amplify synthesised cDNA of target genes *SNAI1* and *TWIST1*. The correlation between synthesised cDNA and mRNA expression allowed for gene expression analysis, through relative quantification by comparing the gene expression of control samples against IL-6 treated samples. The SensiFAST™ SYBR® No-ROX kit (Bioline, UK) was used for the qPCR reaction. qPCR was achieved with SYBR-based detection, where the dye SYBR green I intercalated with the minor groove of dsDNA, which emits a strong fluorescent signal once bound. After thawing, reagents were kept on ice and added to opaque 8-well PCR strips, (BIOPlastics, Netherlands; Celtic Diagnostics, SA) in the order indicated in Table 3.4. Primers were synthesised by Integrated DNA Technologies (IDT) (Illinois, USA), the sequences and annealing temperatures are reported in Table 3.5. The threshold cycle (Ct) value is precisely proportional to the input amounts of cDNA. For this reason, cDNA was quantified with the Nanodrop^{TM} prior to qPCR, where exactly 4000 µg cDNA was calculated. Reagents were mixed and centrifuged briefly; a 3-step cycling was set up on the Bio-Rad CFX-96 system (Bio-Rad, USA) (Table 3.6). A melt curve was also set up to confirm amplification specificity of target cDNA. The temperature was at 65 ^{o}C for 5 seconds and increased to 95 ^{o}C, at 5 ^{o}C increments.

Table 3.4: Reaction set up for SensiFAST™ SYBR® No-ROX qPCR reaction

Reagent	Volume (µl)	Final Concentrations
2× SensiFAST™ SYBR® No-ROX mix	5	1×
10 µM Forward Primer	0.4	400 nM
10 µM Reverse Primer	0.4	400 nM
cDNA Template	4000 µg	-
dH_2O	2.2	-
Total volume	**10**	-

Table 3.5: Sequences and annealing temperature of *SNAI1*, *TWIST1* and *GAPDH* primers

Primer	Sequence (5′-3′)	Annealing Temperature (°C)	GC Content (%)
SNAI1 (Forward)	TCGGAAGCCTAACTACAGCGA	59.2	52.38
SNAI1 (Reverse)	AGATGAGCATTGGCAGCGAG		55.00
TWIST1 (Forward)	GTCCGCAGTCTTACGAGGAG		60.00
TWIST1 (Reverse)	GCTTGAGGGTCTGAATCTTGCT		50.00
GAPDH (Forward)	CGTGTCGGTTGTGGATCTGA	57.1	55.00
GAPDH (Reverse)	TGACGAAGTGGTCGTTGAGG		55.00

Table 3.6: 3-step qPCR cycling conditions

Cycles	Temperature (°C)	Time	Step
1	95	2 min	Polymerase activation
40	95	5 sec	Denaturation
	57.1 or 59.2	10 sec	Annealing
	72	20 sec	Extension

Glyceraldehyde-3-phosphate dehydrogenase (*GAPDH*) was used as a reference gene. A reference gene is important to normalise variation between samples that can occur at events such as RNA isolation, reverse transcription efficiency, PCR reaction set up and PCR reaction amplification efficiency (Sikand et al., 2012). Reference genes are typically involved in the regulation of cellular functions and are ubiquitously expressed between cells. GAPDH is assumed to be invariably expressed and is therefore used to normalise gene expression. Additionally, a NTC sample was included, where no signal or amplification confirmed no contamination of reagents or the formation of primer dimers.

The Ct values generated using the CFX Maestro software (Bio-Rad, USA) were used to interpret the qPCR results. An increase of SYBR fluorescence intensity is proportional to the amount of the PCR product formed. The initial detection of fluorescence above the set

threshold is reported as a Ct value; where a higher the starting copy number of the cDNA target, resulted in a lower Ct value. It is assumed that the amount of PCR doubles with every cycle (PCR efficiency (E) = 2). Therefore, the Livak method was used to calculate fold change in expression (Livak and Schmittgen, 2001). Raw Ct values were exported to an Excel© spreadsheet, and the normalised fold change between control and IL-6 treated samples was calculated as follows:

$$\Delta\Delta Ct = (Ct_{(target,\ untreated)} - Ct_{(GAPDH,\ untreated)}) - (Ct_{(target,\ treated)} - Ct_{(GAPDH,\ treated)})$$

$$\text{Normalised fold change} = E^{-\Delta\Delta Ct}; \text{ where } E = 2$$

3.8 Cholesterol Staining

Three cholesterol staining techniques were utilised to observe the effect of EMT induction in lipid rafts, lipid droplets and free cholesterol. Moreover, cells were treated with 1 mM MβCD (Sigma Aldrich, UK) or 10 mM KS-01 (a novel, patented cholesterol depleting agent), reconstituted in dH_2O, and changes in the lipid profile were recorded in pre- and post-EMT induced cells.

3.8.1 Vybrant Alexa Fluor® Lipid Raft Labelling

Cholesterol accumulates in specified regions of the cell membrane, together with sphingolipids, forming micro-domains termed lipid-rafts. Vybrant Alexa Fluor® (Thermo Fisher Scientific, USA) staining fluorescently labels lipid rafts present in live cells. Alexa Fluor® staining utilises lipid raft marker cholera toxin-B (CT-B). CT-B recognises and binds to the pentasaccharide chain of plasma ganglioside GM1, that concentrates in lipid rafts. Alexa Fluor 594 fluorescently labelled specific antibody crosslinks with CT-B, to allow the visualisation of lipid rafts by fluorescence microscopy (Gianni and Campadelli-Fiume, 2012).

20 000 cells/ well were seeded onto a 24-well plate. Following EMT induction and 2 hours of cholesterol depletion with 1 mM MβCD or 10 mM KS-01, the media was discarded, and the cells were washed with three PBS washes. Subsequently, the cells were fixed by adding 400 µl of 4% formaldehyde (Sigma Aldrich, UK) to each well for 10 minutes at room temperature. Following two additional PBS washes, 1 µl of Alexa Fluor® [Subunit A: CT-B]

made up in 1 ml of PBS, was added to each well and incubated for 30 minutes at 37 ºC. Subsequently, 1 µl of Alexa Fluor® [Subunit B: Anti-CT-B antibody] was added to each well and incubated for another 30 minutes at 37 ºC. The cells were washed twice with PBS and 0.0001 mg/ml DAPI nuclear stain was added to the wells and incubated at room temperature for 10 minutes. Finally, the cells were washed three times with PBS. The coverslips were gently removed, tapped dry and placed facing down onto microscope slides coated with Fluoromount™ Aqueous Mounting Medium (Sigma Aldrich, UK). Cells were visualised under the Floid™ Cell Imaging System (Thermo Fisher Scientific, US). Immunofluorescence intensity was quantified with the ImageJ software (NIH, USA).

3.8.2 Filipin

Filipin is a fluorescent polyene macrolide with antifungal and antibacterial properties produced by *Streptomyces filipinensis*. The macrolide interacts with membrane sterols with high affinity, disrupting its membrane structure (Payero et al., 2015). Filipin is widely used for its detection and quantification of cellular cholesterol. Its highly fluorescent property allows for visualisation of unesterified cholesterol and is detected at a UV excitation of 360 nm and emission of 480 nm (Maxfield and Wüstner, 2012).

20 000 cells/ well were seeded onto a 24-well plate. Following EMT induction and 2 hours of cholesterol depletion with 1 mM MβCD or 10 mM KS-01, the media was discarded, and the cells were washed with three PBS washes. Subsequently, the cells were fixed by adding 400 µl of 4% formaldehyde to each well for 10 minutes at room temperature. Following two additional PBS washes, 2 µl of Filipin (0.01 mg/ml) (Sigma Aldrich, UK) made up in 1 ml of PBS, was added to each well and incubated for 2 hours at room temperature, in the dark. The cells were washed twice with PBS and NucRed™ Dead (Thermo Fisher Scientific, USA) nuclear stain was added to the wells and incubated at room temperature 10 minutes. Finally, the cells were washed three times with PBS. The coverslips were gently removed, tapped dry and placed facing down onto microscope slides coated with Fluoromount™ Aqueous Mounting Medium. Cells were visualised under the Floid™ Cell Imaging System. Immunofluorescence intensity was quantified with the ImageJ software.

3.8.3 BODIPY 493/503

BODIPY (4,4-difluoro-1,3,5,7,8-pentamethyl-4-bora-3a,4a-diaza-s-indacene) is a green lipophilic fluorophore with a nonpolar structure that allows the binding and staining of neutral lipid droplets. Lipid droplets are ubiquitous structures important for lipid storage, with

a core of neutral lipids and cholesteryl esters, surrounded by a phospholipid monolayer. Lipid droplets are important for various cellular functions including membrane homeostasis and lipid-based signalling. The dye binds to neutral lipids, emitting a green fluorescence at a wavelength 520 nm, when excited by blue light (460–490 nm) (Qiu and Simon, 2016).

20 000 cells/ well were seeded onto a 24-well plate. Following EMT induction and 2 hours of cholesterol depletion with 1 mM MβCD or 10 mM KS-01, the media was discarded, and the cells were washed with three PBS washes. Subsequently, the cells were fixed by adding 400 µl of 4% formaldehyde to each well for 10 minutes at room temperature. Following two additional PBS washes, 4 µl of BODIPY (Thermo Fisher Scientific, USA) made up in 1 ml of PBS, was added to each well and incubated for 30 minutes at 37 ^{o}C. The cells were washed twice with PBS and 0.0001 mg/ml DAPI nuclear stain was added to the wells and incubated at room temperature 10 minutes. Finally, the cells were washed three times with PBS. The coverslips were gently removed, tapped dry and placed facing down onto microscope slides coated with Fluoromount™ Aqueous Mounting Medium. Cells were visualised under the Floid™ Cell Imaging System. Immunofluorescence intensity was quantified with the ImageJ software.

3.9 Transwell® Invasion Assay

An important characteristic of EMT is the enhanced invasive and migratory abilities of cells that allowing for travel to distant sites. The Transwell® Invasion assay measures the ability of cells to attach and invade the extracellular matrix (ECM) and migrate towards a chemo-attractant (Justus et al., 2014). The directional migration of single cells occurs through a porous membrane insert, that is coated with ECM. The number of cells that invade through the membrane is stained and counted under a microscope. This assay was performed to assess the effects of FOLFOX and cholesterol depletion on the migratory and invasive potential of EMT induced cells.

Each plate was set up by adding 500 µl of complete medium (McCoy's 5a (Modified) Medium with 10% FBS) to the lower chamber in a 24-well plate. FBS contains essential growth factors, hormones, and lipids necessary for cell growth therefore, the supplemented 10% FBS served as the chemo-attractant gradient. Following the appropriate treatments, cells were resuspended in serum-free media to a total of 100 000 viable cells/ml. Prior to resuspension, the Haemocytometer was utilised for cell counts and to calculate %100 cell viability. Subsequently, 160 µl of cells in serum-free media were mixed with 40 µl of

Geltrex™ (Thermo Fisher Scientific, UK). Geltrex™ is a soluble form of basement membrane, containing ECM components such as collagen IV, laminin, heparin sulphate proteoglycans and entactin. The total cell mixture of 200 µl was carefully coated onto 0.8 µM-pore transwell chamber (Thermo Fisher Scientific, UK) and incubated for 24 hours at 37 °C. The following day, non-invasive cells were gently wiped off from the upper chamber with a cotton swab and cells that had invaded to the lower chamber were fixed with 4% formaldehyde for 10 minutes, at room temperature. Thereafter, the cells on the lower chamber of the inserts were stained with 0.0001 mg/ml DAPI for 10 minutes, at room temperature. In between each step, the inserts were washed twice with chilled PBS. The membrane was carefully cut from the insert, using a sterile blade, and mounted onto microscope slides. Cells were counted under the Floid™ Cell Imaging System, in different fields of view of the microscope and the averaged sum of invaded cells were calculated. Data was presented as percentage of invasive cells relative to the control.

3.10 Apoptosis Assay

An apoptosis assay was performed to compare the effect of cholesterol depletion and FOLFOX treatments following EMT induction on apoptosis. The Cell-APOPercentage™ Apoptosis Assay (Biocolor, UK) is a colorimetric assay, used to detect incidences of early apoptosis in anchorage dependent cells. Flippases and floppases functions to maintain lipid asymmetry in the cell membrane. During the early stages of apoptosis, flippases become inactivated by lipid scramblases leading to the loss of lipid asymmetry resulting in a membrane flip. The exposure of phosphatidylserine phospholipid to the extracellular space is an apoptotic marker (Mariño and Kroemer, 2013). The phosphatidylserine transmembrane movement selectively imports the APOPercentage dye into apoptotic cells, in a uni-directional manner. The dye concentrates within the cell, as the cell shrinks in volume, allowing for apoptosis to be assessed via spectrophotometry.

5000 cells/well were seeded onto a 96-well plate and left to adhere for 24 hours. Following EMT induction, cells were treated with cholesterol depleting agents (1 mM MβCD or 10 mM KS-01) alone or together with FOLFOX (20 µM 5-FU and 8 µM Oxaliplatin), for 2 hours. Cells treated for longer than 2 hours resulted in loss of cell adhesion leading to cell detachment, resulting in washing away of cells and lead to inaccurate readings. After 2 hours, the media was discarded, and each well was gently washed with 100 µl of PBS. 65 µl of the dye mix (0.5 µl of APOPercentage™ dye and 64.5 µl PBS) was added to each well and

incubated for 10 minutes at 37 ºC. Thereafter, the cells were washed twice with 100 µl of PBS and 50 µl of PBS was then added in to each well, to prevent the cells from drying out. The absorbance of each well was measured with the Multiskan GO Microplate Reader (Thermo Fisher Scientific, SkanIt™ software), at a wavelength of 550 nm.

The percentage of cell viability was calculated using the following equation:

(x) = Average absorbance values of samples - Average absorbance values of blanks

% Cell Viability = [**(x)** of test sample / **(x)** of untreated sample] × 100

3.11 Vybrant™ Multidrug Resistance Assay

EMT is known to contribute towards drug resistance which allows for cancer recurrence and metastasis, following treatments with chemotherapy. The Vybrant™ Multidrug Resistance Assay was performed to observe the effects of cholesterol depleting agents on MDR. The purpose of this assay was to record cell fluorescence intensity, caused by fluorogenic dye calcein. Calcein acetoxymethyl ester (calcein AM) is a nonfluorescent, lipophilic dye that easily penetrates the cell membrane of normal cells. In the cytoplasm, the ester bonds of calcein AM are cleaved by endogenous esterases, transforming calcein AM into highly fluorescent calcein. Due to its hydrophilic nature, calcein becomes retained in the cytoplasm. Under conditions of drug resistance, the transmembrane efflux transporter, P-gp, functions to export non-fluorescent calcein AM from the cell interior (Hammond et al., 2007). The degree of P-gp activity, pertaining to increasing MDR, is measured by a decrease in intracellular calcein fluorescence.

5000 cells/well were seeded onto a black 96-well fluorescent plate (Thermo Fisher Scientific, USA) and left to adhere for 24 hours. Following EMT induction, cells were treated with cholesterol depleting agents (1 mM MβCD or 10 mM KS-01) alone or together with FOLFOX (20 µM 5-FU and 8 µM Oxaliplatin), for 2 hours. Cells treated for longer than 2 hours resulted in loss of cell adhesion leading to cell detachment, resulting in washing away of cells and lead to inaccurate readings. After 2 hours, the media was discarded, and each well was gently washed with 200 µl of PBS. Verapamil is a calcium channel blocker known to inhibit P-gp. 1 µM of verapamil was included as a positive control based on its ability to

reduce drug efflux pump activity. Subsequently, 50 µl of 0.25 µM calcein-AM was added to each well and incubated at 37 °C for 30 minutes in the dark. Finally, cells were washed twice with 200 µl of PBS. Fluorescence intensity was measured with the Victor Nivo multi-mode microplate reader (Perkin Elmer, USA) at an excitation maximum of 494 nm and an emission maximum of 517 nm. Fluorescence intensity, pertaining to amount of calcein retention, indicated MDR activity and was calculated as percentage of fluorescence intensity relative to the control.

3.12 Statistical Analysis

All assays were performed in technical duplicates or triplicates, and an average of the data was obtained (technical repeats). For data reproducibility, experiments were repeated three times (biological repeats). Statistical analysis was performed on the repeated experiments (n=3). All statistical analysis was performed on the raw data. Statistical analysis and graphs were generated through GraphPad Prism8®. Values were considered significant at $p > 0.05$, at a confidence interval (CI) of 95%.

For each assay performed in a 96-well plate, a Z-factor (Zhang et al., 1999) was calculated, where a Z-factor represents the robustness of the technical repeats and indicates the trustworthiness of the assay. Only data with a Z-factor > 0.7 were reported, which suggests excellent robustness. Z-factors were calculated on Microsoft Office Excel©.

A Student's T test was performed when comparing the means between two groups; specifically, when measuring the differences between control and IL-6 treated samples. A one-way analysis of variance (ANOVA) was performed when analysing the difference between the means of more than two groups, with one independent variable. A one-way ANOVA was performed when comparing variation between samples treated with combinations of FOLFOX and cholesterol depleting agents.

Both Student's T test and one-way ANOVA are parametric tests. Therefore prior to statistical analysis of each data set, a Shapiro-Wilk test of normality was performed to confirm a normal distribution of data. For pairwise analysis, either Least Significant Difference (LSD) or a Bonferroni test was performed and will be specified for each result. A Bonferroni test is used to correct for Type I error, which becomes inflated when performing multiple comparisons.

4. Results

4.1 Optimisation of FOLFOX chemotherapy suitable for HT-29 cells

FOLFOX is one of the most common combination chemotherapies used to treat metastatic CRC. Before being able to observe the effects of FOLFOX on EMT induced cells, it was necessary to optimise the concentrations of 5-FU and oxaliplatin suitable for inducing cytotoxicity in HT-29 cells. Initially, MTT assays were performed to obtain a dose response curve of 5-FU and oxaliplatin at 24 and 48 hours (Figure 4.1). Both drugs were ineffective at inducing cytotoxicity at 24 hours at concentration ranges of 1 µM, 5 µM, 10 µM, 20 µM, 50 µM, 100 µM and 200 µM for 5-FU; and 0.5 µM, 1 µM, 5 µM, 10 µM, 20 µM, 50 µM and 100 µM for oxaliplatin. After 48 hours of exposure to 5-FU and oxaliplatin, both 5-FU and oxaliplatin showed ~50% inhibition of cell viability at concentrations up to 50 µM.

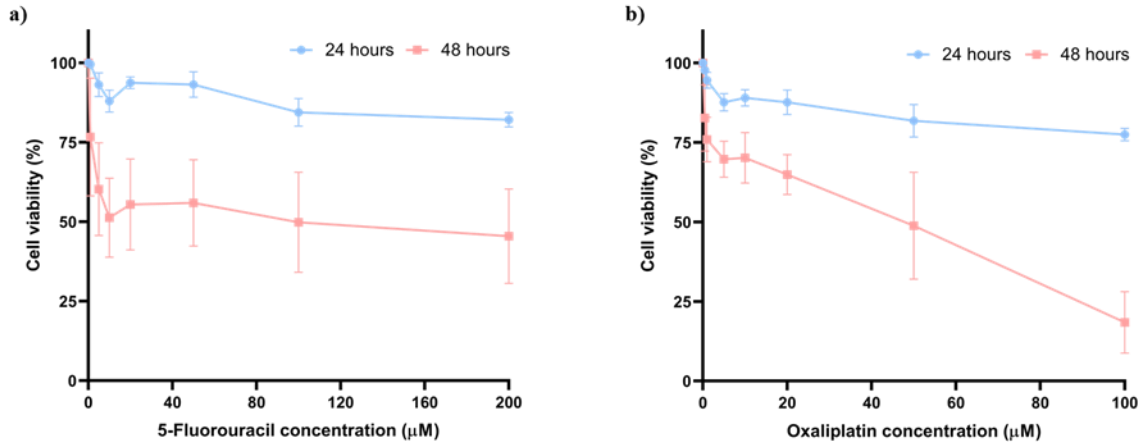


Figure 4.1: Dose-response curves of 5-fluorouracil and oxaliplatin at 24 and 48 hours. a) *The effect of 5-FU on HT-29 cell viability at 1 µM, 5 µM, 10 µM, 20 µM, 50 µM, 100 µM and 200 µM* ***b)*** *The effect of oxaliplatin on HT-29 cell viability at 0.5 µM 1 µM, 5 µM, 10 µM, 20 µM, 50 µM and 100 µM. n=3*

Thereafter, a 5-FU concentration range of 5 µM, 10 µM, 20 µM, 30 µM and 50 µM; and oxaliplatin concentration range of 1 µM, 2 µM, 4 µM and 8 µM was selected for combination treatments. Cells were exposed to combinations of these drug concentrations for 24 hours and an MTT assay was performed to observe the cytotoxic effect (Figure 4.2).

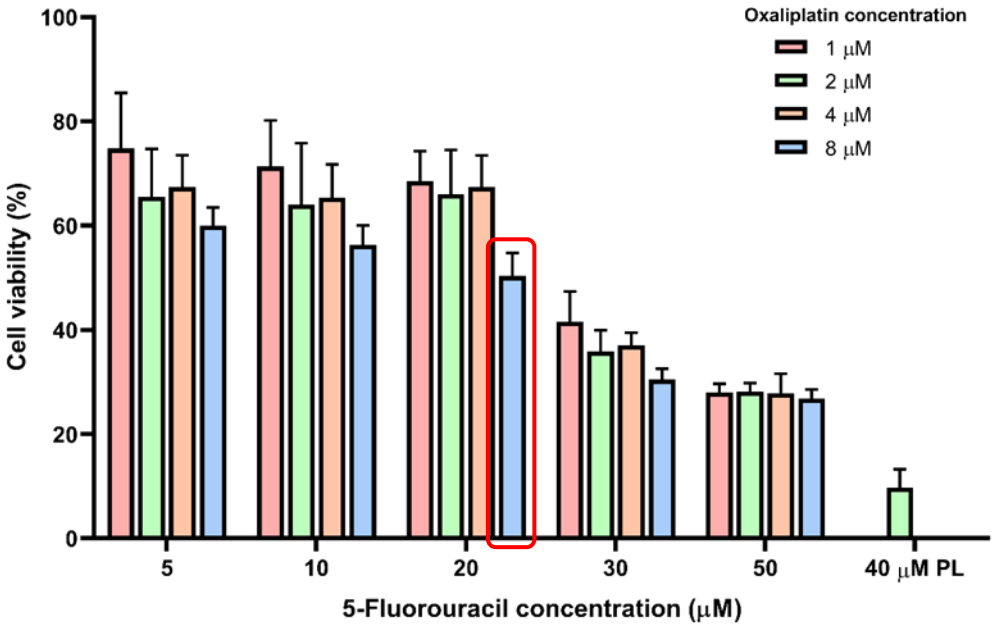


Figure 4.2: HT-29 cell viability following combination treatments with 5-fluorouracil and oxaliplatin. *Cells were exposed to combinations of 5-FU and oxaliplatin at concentrations of 5 μM, 10 μM, 20 μM, 30 μM and 50 μM; and 1 μM, 2 μM, 4 μM and 8 μM, respectively. Treatment with 20 μM 5-FU and 8 μM oxaliplatin showed 50.3% cell viability after 24 hours. 40 μM plumbagin (PL) acted as the positive control. A one-way ANOVA ($P < 0.05$) was performed for statistical analysis. n=3*

It was noted that combinations 5-FU and oxaliplatin exhibited higher cytotoxicity after 24 hours compared to single treatments. The purpose of optimising 5-FU and oxaliplatin for the treatment of HT-29 cells was to analyse the downstream effects of FOLFOX following EMT induction. Therefore, when selecting a concentration of 5-FU and oxaliplatin it was necessary to maintain ~50% cell viability. It was observed that a combination of 20 μM 5-FU and 8 μM oxaliplatin displayed 50.3% cell viability after 24 hours. 5-FU concentrations above 20 μM (i.e., 30 μM and 50 μM) exhibited cell inhibition >50%. Folinic acid (F7878, Sigma Aldrich, UK) did not improve 5-FU cytotoxicity and was therefore excluded from combination treatments (Appendix; Figure A.2).

Ultimately, 24 hours exposure to 20 μM 5-FU and 8 μM oxaliplatin was selected as the FOLFOX treatment in cells. For simplicity, throughout the results section, 20 μM 5-FU and 8 μM oxaliplatin will be referred to as "FOLFOX".

4.2 Increasing concentrations of IL-6 represses E-cadherin protein expression

Cancer cells undergoing EMT are involved in the formation of a favourable microenvironment for cancer progression and metastasis, which contributes to difficulties in treatment and poorer prognosis (Iwatsuki et al., 2010). In order to investigate the characteristics of EMT in colorectal cancer cells, the proinflammatory cytokine IL-6 was utilised as an inducer of EMT.

Initially, it was necessary to establish an optimal concentration of IL-6 needed to induce an EMT phenotype in cells. E-cadherin was selected as a marker to observe changes in the HT-29 epithelial phenotype. Immunofluorescent staining of E-cadherin was performed after cells were exposed to increasing concentrations of IL-6 at 20 ng/ml, 30 ng/ml, and 50 ng/ml for 24 hours. Preliminary data demonstrated the reduction of E-cadherin levels, at increasing IL-6 concentrations (Figure 4.3). Consistent with decreased E-cadherin levels, cells exhibited decreased cell-cell contacts with a more dispersed cell arrangement.

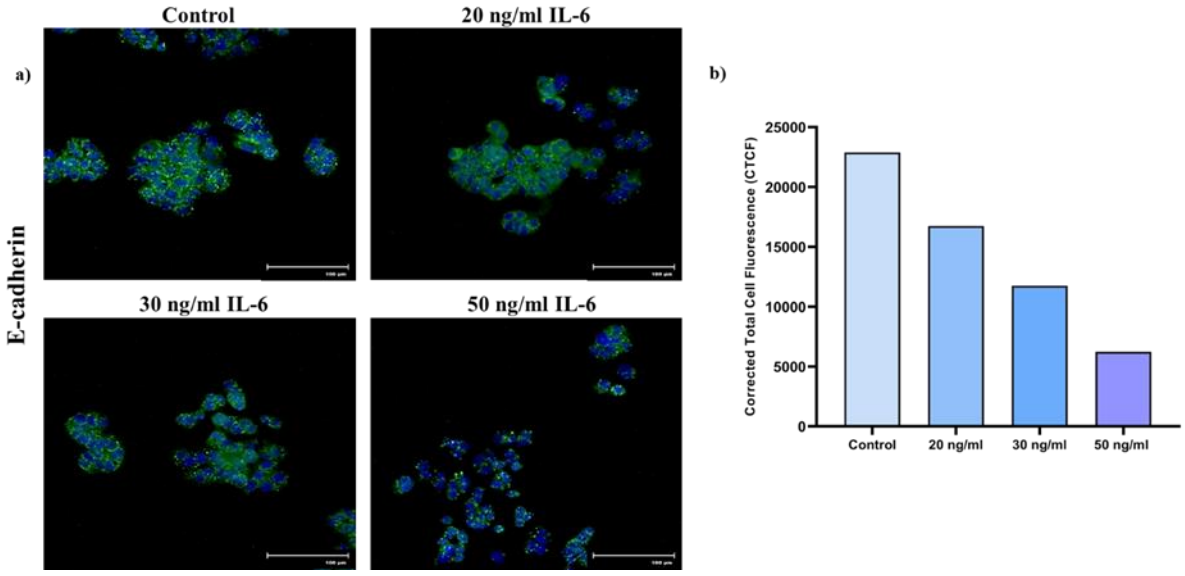


Figure 4.3: E-cadherin expression following exposure of HT-29 cells to increasing concentrations of IL-6. a) *The visual representation of E-cadherin EMT molecular marker expression at concentrations of 20, 30 and 50 ng/ml IL-6 for 24 hours. E-cadherin expression is illustrated by Alexa Fluor 488 staining (green) and nuclei were stained with DAPI nuclear stain (blue).* ***b)*** *Preliminary analysis of E-cadherin expression by ImageJ, represented by corrected total cell fluorescence. The scale bar on the micrographs represents 100 µm. n=1 for initial optimisation of IL-6 concentration.*

After exposure for 24 hours with 20 ng/ml, 30 ng/ml and 50 ng/ml of IL-6, preliminary analysis indicated a respective 26.8%, 48.7% and 72.8% reduction in E-cadherin expression

relative to the control. Seeing that 50 ng/ml IL-6 exhibited the greatest reduction of E-cadherin expression, this concentration was selected for further validation of EMT induction.

4.3 IL-6 exposure promotes an EMT phenotype in colorectal cancer cells

It was necessary to further validate that IL-6 was successfully inducing an EMT phenotype in HT-29 cells. EMT-induced changes in cell morphology were observed under the Floid™ Cell Imaging System microscope. HT-29 cells usually have a rounded cobblestone morphology and grow in clusters. Following exposure to 50 ng/ml IL-6 for 24 hours, it was noted that cell-cell contacts were reduced, and cells adopted a spindle-shaped morphology, resembling a mesenchymal phenotype (Figure 4.4).

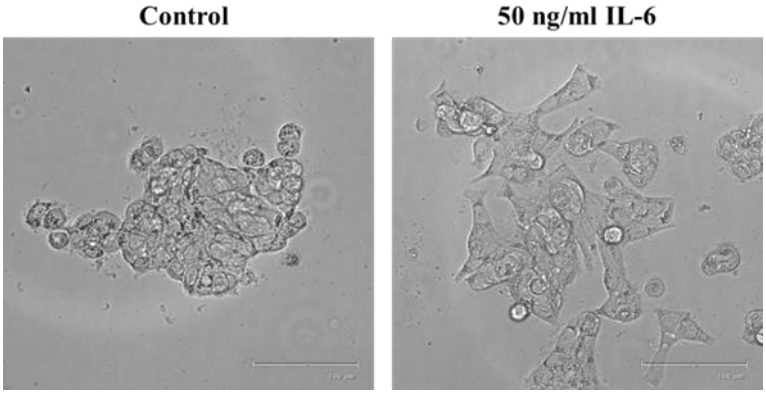


Figure 4.4: Changes in HT-29 cell morphology following exposure to 50 ng/ml IL-6. *HT-29 control cells (left) show an epithelial, cobblestone phenotype. Following exposure to 50 ng/ml IL-6, cells show reduced cell-cell contacts and the appearance of a more spindle shape (right). Cells were viewed under the Floid™ Cell Imaging System. The scale bar on the micrographs represents 100 µm.*

The extent to which IL-6 can induce an EMT phenotype, was analysed with immunofluorescent staining of both E-cadherin and vimentin. E-cadherin is a transmembrane glycoprotein that mediates cell-cell adhesion between epithelial cells. Vimentin is a type III intermediate filament, uniquely expressed in mesenchymal cells, and is important for maintaining a mesenchymal cell structure. Figure 4.5 depicts the changes in E-cadherin and vimentin protein expression, following treatment with 50 ng/ml IL-6. Analysis presented a 60.0% decrease in E-cadherin (n=3) as well as a significant increase in vimentin by 50.7%. These changes in protein expression of EMT molecular markers indicates the successful induction of EMT in HT-29 cells.

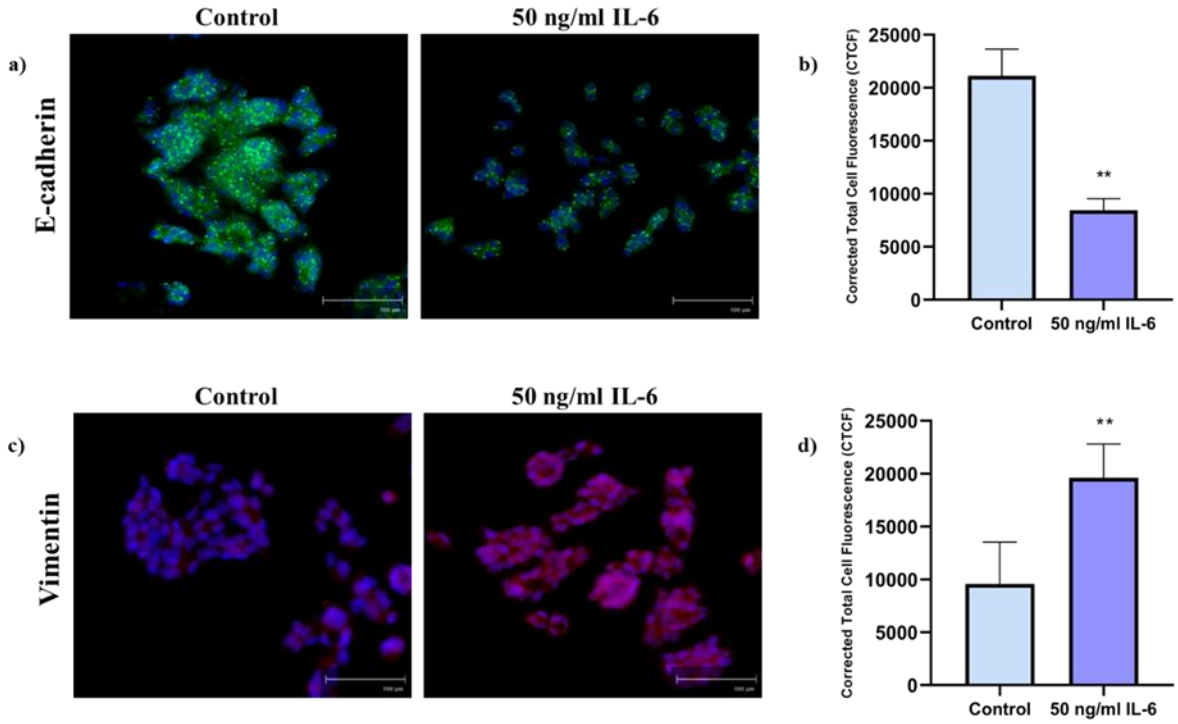


Figure 4.5: Changes in E-cadherin and Vimentin expression levels following 50 ng/ml IL-6 exposure. a) *Visual representation of changes in E-cadherin expression levels pre and post IL-6 treatment. E-cadherin was stained by Alexa Fluor 488 (green) and nuclei were stained with DAPI nuclear stain (blue).* ***b)*** *ImageJ analysis confirms a significant decrease in E-cadherin fluorescence following IL-6 treatment.* ***c)*** *Vimentin was stained by Texas Red (red) and nuclei were stained with DAPI nuclear stain (blue).* ***d)*** *ImageJ analysis confirms a significant increase in vimentin fluorescence following IL-6 treatment. The scale bar on the micrographs represents 100 µm. Data represents the mean ± standard deviation. A two-tailed, paired T-test was performed for statistical analysis where * P < 0.05, ** P < 0.01, *** P < 0.001 and ns = not significant at 95% CI. n=3.*

EMT induction was further validated by gene expression analysis of EMT-TFs *SNAI1* and *TWIST1*. SNAI1 and TWIST1 are key mediators of EMT that function to downregulate E-cadherin and upregulate vimentin as well as other mesenchymal markers such as N-cadherin and fibronectin. Additionally, these transcription factors modulate gene expression of key proteins that function to enhance cell migration and invasiveness, promote apoptotic resistance and multidrug resistance (Vu and Datta, 2017).

RT-qPCR analysis substantiated that the changes in gene expression of *SNAI1* and *TWIST1* were consistent with EMT induction. The $\log_2$FC of *SNAI1* and *TWIST1* mRNA expression levels, relative to the control, are illustrated in Figure 4.6. Following IL-6 exposure, gene expression of *SNAI1* and *TWIST1* changed by a $\log_2$FC of 0.96 and 1.20, respectively.

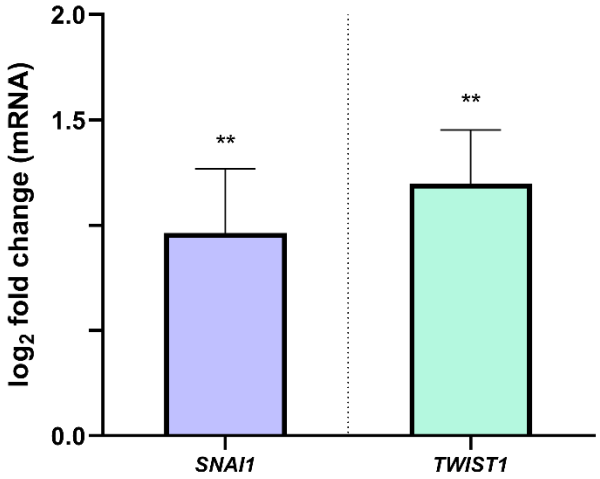


Figure 4.6: SNAI1 and TWIST1 expression levels are upregulated in HT-29 cells exposed to IL-6. *qPCR confirmed that EMT-TFs, SNAI1 and TWIST1, expression levels are increased following treatment with IL-6. Data is presented as relative gene expression by comparing control samples against IL-6 treated samples. Data represents the mean ± standard deviation. A two-tailed, paired T-test was performed for statistical analysis where * P < 0.05, ** P < 0.01, *** P < 0.001 and ns = not significant at 95% CI. n=3.*

Several studies report that IL-6 utilises the JAK/STAT3 pathway to induce EMT. STAT3 is phosphorylated by JAK2 following IL-6 ligand binding to IL-6R leading to the homodimerization and translocation of STAT3 into the nucleus. The phosphorylation of STAT3 mediates several pathways that are involved in EMT induction including the upregulation of *SNAI1* and *TWIST1* transcription factors (Yadav et al., 2011; Kim et al., 2016).

STAT3 is activated through phosphorylation of the Tyr705 residue. Therefore, to establish if STAT3 phosphorylation is upregulated following exposure to IL-6, immunofluorescence was performed targeting phospho-STAT3(Y705). The treatment with IL-6 significantly increased STAT3 phosphorylation by 50%, in comparison to control cells (Figure 4.7). These findings support the view that IL-6 utilises STAT3 to induce EMT.

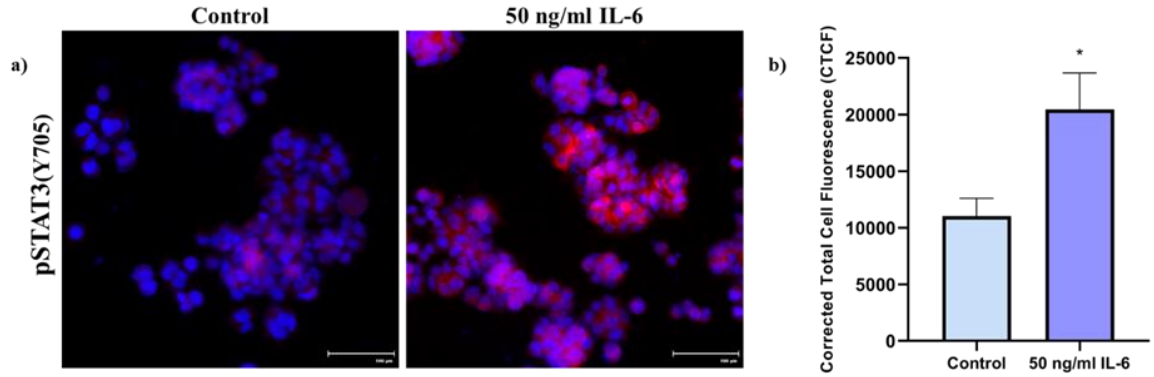


Figure 4.7: IL-6 treatment increases STAT3 phosphorylation at Tyrosine 705. a) *Visual representation of the increase in STAT3 phosphorylation at Tyrosine 705 following IL-6 treatment. pSTAT3(Y705) was stained by Texas Red (red) and nuclei were stained with DAPI nuclear stain (blue).* ***b)*** *ImageJ analysis confirms a significant increase in STAT3 phosphorylation following IL-6 treatment. The scale bar on the micrographs represents 100 µm. Data represents the mean ± standard deviation. A two-tailed, paired T-test was performed for statistical analysis where * $P < 0.05$, ** $P < 0.01$, *** $P < 0.001$ and ns = not significant at 95% CI. n=3.*

The activity of the STAT3 is important for relaying signals from the cell membrane to the nucleus. The transcription factor is involved in regulating numerous processes that promote tumorigenesis and EMT including cell survival, migration and proliferation (Siveen et al., 2014). It was necessary to identify the state of proliferation in the EMT cells particularly when establishing effective anti-cancer therapeutics.

It is for this reason that a cell proliferation assay was employed. The assay assessed the effect of IL-6 on cell proliferation over 4-days. 20 000 cells/well were treated with 50 ng/ml of IL-6 at Day 0; after every 24 hours the cells were counted and the differences in cell number between treated and control samples were recorded. It was observed that IL-6 had a stimulatory effect on the growth of HT-29 cells over the 4-day period (Figure 4.8a). At the time of EMT induction (Day 1), the number of treated cells doubled in comparison to the control cells. On Day 2, cells treated with IL-6 showed 1.4 times greater cell growth relative to the control cells. Overall, treated cells maintained a greater cell count than untreated cells.

To validate these findings, immunofluorescence was performed to examine the effect of IL-6 on Ki67 protein levels. Ki67 is an important marker expressed in proliferating cancerous cells. The protein is only detected during the active cell cycle phases and is not expressed in the quiescent phase (Li et al., 2015). Following IL-6 treatment, the antigen was detected with immunofluorescent staining and quantified by ImageJ (Figure 4.8b and c). It was noted that Ki67 levels increased by 42.4% in cells exposed to IL-6 for 24 hours; further signifying that IL-6 acts to stimulate proliferation.

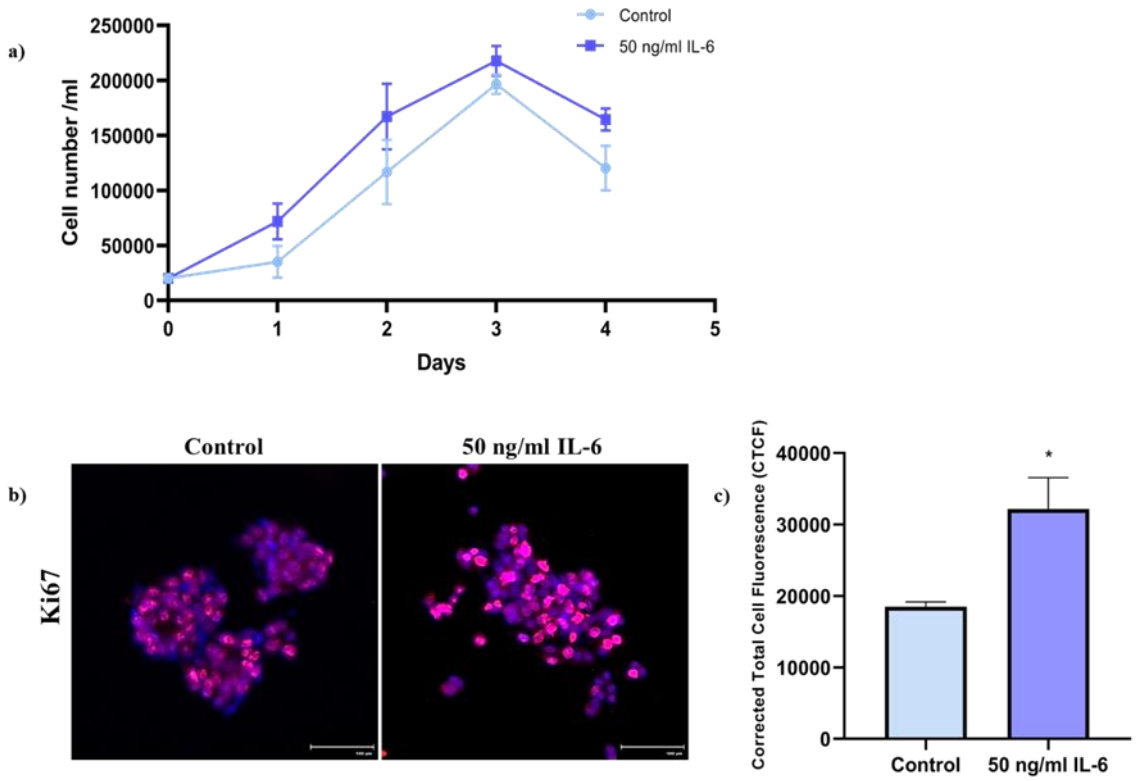


Figure 4.8: IL-6 increases HT-29 cell proliferation. a) *A growth curve that was generated through a cell proliferation assay recorded increased cell counts in treated samples over 4-days.* ***b)*** *Immunofluorescence of proliferative marker Ki67 shows increased staining with 50 ng/ml IL-6 after 24 hours. Ki67 was stained by Texas Red (red) and nuclei were stained with DAPI nuclear stain (blue).* ***c)*** *ImageJ analysis confirms a significant increase in Ki67 following IL-6 treatment. The scale bar on the micrographs represents 100 µm. Data represents the mean ± standard deviation. A two-tailed, paired T-test was performed for statistical analysis where * P < 0.05, ** P < 0.01, *** P < 0.001 and ns = not significant at 95% CI. n=3.*

4.4 Cholesterol depleting agents successfully reduce cellular cholesterol following EMT induction

Numerous malignant tumours exhibit cholesterol accumulation and an overwhelming amount of evidence shows that cholesterol plays an important role in cancer development (Ding et al., 2019). Therefore, cholesterol staining was performed to evaluate the effect of EMT induction on cellular cholesterol levels. Additionally, changes in cholesterol content and membrane fluidity have resulted in the suppression of metastatic potential and is capable of impeding the EMT process (Zhao et al., 2016; Tisza et al., 2016). Cholesterol depleting agents are gaining interest as potential anticancer compounds for their ability to induce cancer cell death in several cancers, disrupting lipid rafts and subsequent signalling pathways (Gu et al., 2019). Two cholesterol depleting agents were utilised, namely MβCD and KS-01. Cells were treated

for 2 hours with 1 mM MβCD and 10 mM KS-01 and cholesterol content was quantified in the form of lipid rafts, LDs, and free cholesterol. Concentrations of MβCD and KS-01 were previously established in our laboratory.

The first cholesterol staining assay performed was the Vybrant Alexa Fluor® Lipid Raft Labelling assay. Cancer cells require excess cholesterol for membrane synthesis to sustain high levels of proliferation as well as to mediate oncogenic signalling for metastatic activity. Cellular cholesterol is shown to accumulate in lipid-rafts, an important site for oncogenic signalling (Cruz et al., 2013). Cells were treated with 50 ng/ml of IL-6 for 24 hours to induce EMT. Following EMT induction, cells were treated with 1 mM MβCD and 10 mM KS-01 for 2 hours, to deplete cholesterol. Following treatment with IL-6 alone (pre-EMT untreated vs post-EMT untreated), it was found that, although not significant, lipid raft levels were increased by 34.7%. Interestingly, treatments with 1 mM MβCD and 10 mM KS-01 had a similar effect on cholesterol levels in pre- and post-EMT samples, despite the 34.7% increase in lipid levels post-EMT. This corresponded to a 50.4% and 49.2% decrease in lipid rafts pre-EMT and a 71.0% and 67.2% decrease in lipid rafts when treated with 1 mM MβCD and 10 mM KS-01, respectively. Notably, both MβCD and KS-01 displayed a similar effect on lipid raft levels (Figure 4.9).

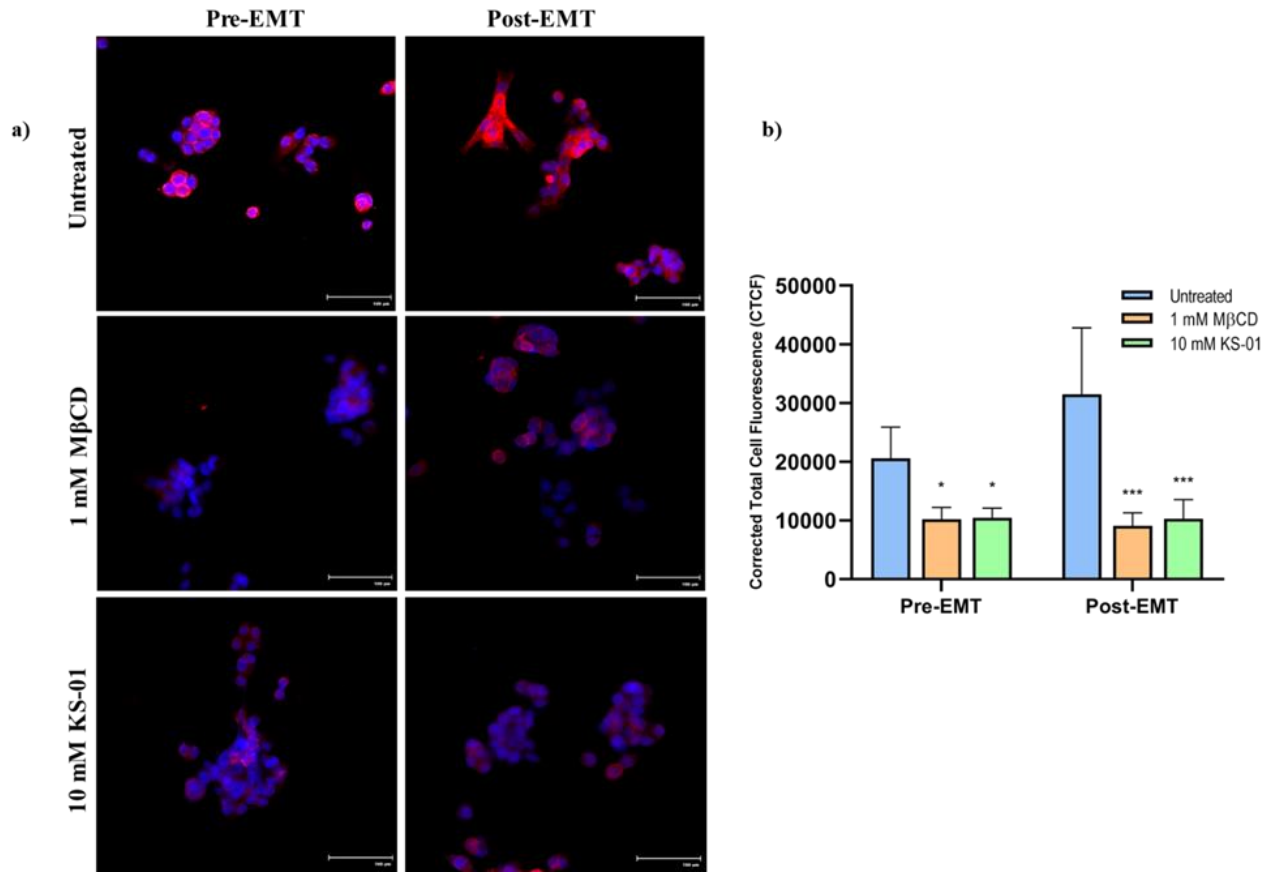


Figure 4.9: Vybrant Alexa Fluor® Lipid Raft Labelling of cells pre- and post-EMT induction. a) *Cholesterol staining shows that lipid raft levels increase following EMT induction. Subsequently, treatment with 1 mM MβCD or 10 mM KS-01 successfully decrease lipid raft levels in pre- and post-EMT cells. Lipid rafts were stained by Alexa Fluor 555 (red) and nuclei were stained with DAPI (blue)* ***b)*** *ImageJ analysis confirms a significant decrease in lipid raft levels following MβCD and KS-01 treatment in pre- and post-EMT cells. The scale bar on the micrographs represents 100 µm. Data represents the mean ± standard deviation. A one-way ANOVA ($P < 0.01$) was performed for statistical analysis. Bonferroni's multiple comparisons test was performed for pairwise analysis where * $P < 0.05$, ** $P < 0.01$, *** $P < 0.001$ and ns = not significant at 95% CI. Pairwise analysis was performed comparing MβCD and KS-01 against untreated samples in pre-EMT cells and in post-EMT cells. n=3.*

In addition to disrupting lipid raft integrity, MβCD and KS-01 function to extract membrane cholesterol (Mahammad and Parmryd, 2015). The Filipin assay was utilised to assess changes in free cholesterol levels at the cell membrane and intracellular cholesterol. Following exposure to IL-6, it was found that cholesterol levels increased by 33.8%. Treatments with 1 mM MβCD and 10 mM KS-01 decreased cellular cholesterol in pre-EMT cells by 44.1% and 52.1% and decreased cholesterol levels by 65.3% and 67.8% in post-EMT cells, respectively (Figure 4.10). This result is consistent with the effects of MβCD and KS-01 on lipid rafts.

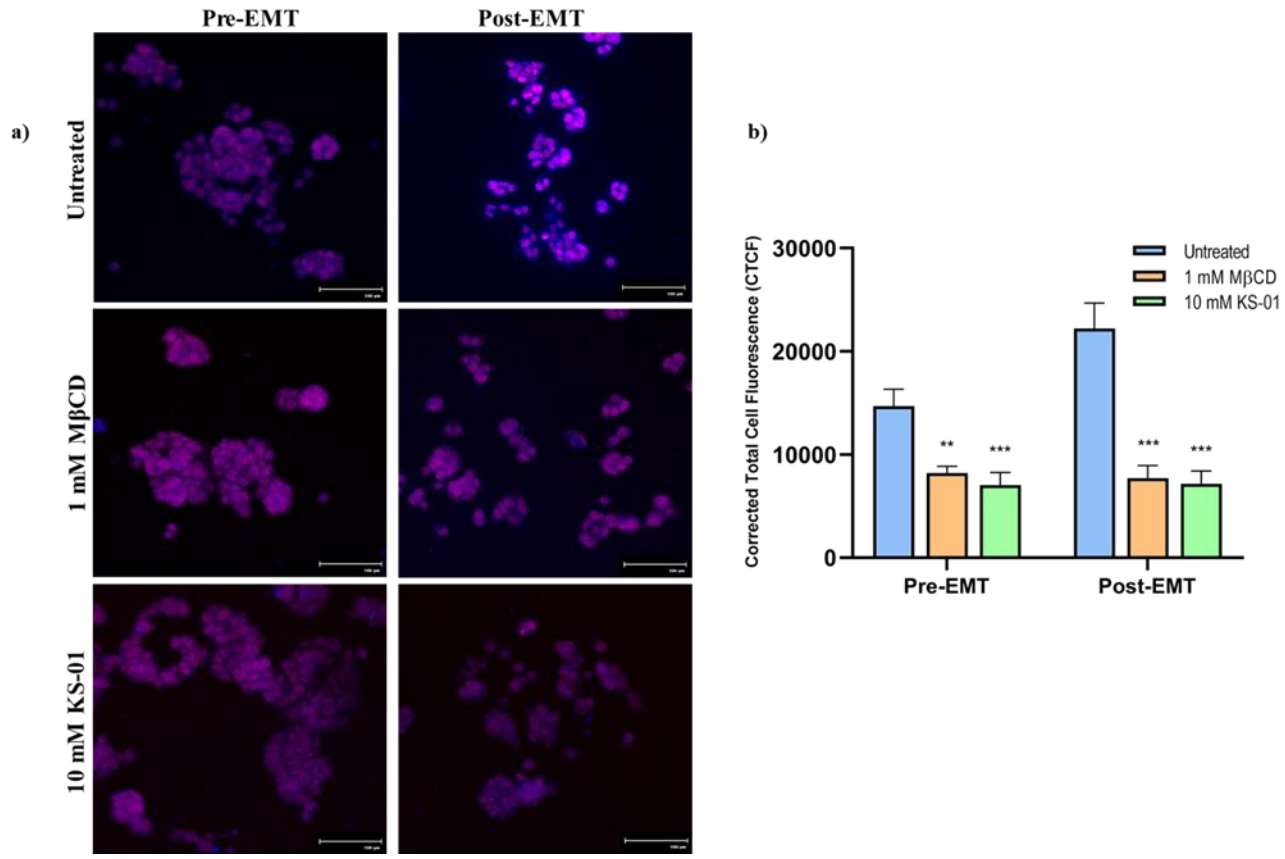


Figure 4.10: Filipin staining of free cholesterol in cells pre- and post-EMT induction. a) *Staining shows that cholesterol levels increase following EMT induction. Subsequently, treatment with 1 mM MβCD or 10 mM KS-01 successfully decrease cholesterol levels in pre- and post-EMT cells. Cholesterol was stained by filipin (blue), and nuclei were stained with NucRed™ Dead (red)* ***b)*** *ImageJ analysis confirms a significant decrease in cholesterol levels following MβCD and KS-01 treatment in pre- and post-EMT cells. The scale bar on the micrographs represents 100 µm. Data represents the mean ± standard deviation. A one-way ANOVA ($P < 0.001$) was performed for statistical analysis. Bonferroni's multiple comparisons test was performed for pairwise analysis where * $P < 0.05$, ** $P < 0.01$, *** $P < 0.001$ and ns = not significant at 95% CI. Pairwise analysis was performed comparing MβCD and KS-01 against untreated samples in pre-EMT cells and in post-EMT cells. n=3.*

Lipid droplets serves as an important storage organelle for cholesteryl esters and are important for various cellular functions including membrane homeostasis and lipid-based signalling. Cells were stained with green BODIPY fluorophore for the analysis of lipid droplets. Following EMT induction, there was a 28.8% increase in LD levels. It was observed that 1 mM MβCD and 10 mM KS-01 respectively decreased lipid droplet levels in pre-EMT cells by 60.8% and 64.2% and decreased cholesterol levels by 72.0% and 71.3% in post-EMT cells (Figure 4.11). These findings suggest lipid droplets are affected by cholesterol depletion to maintain cholesterol homeostasis.

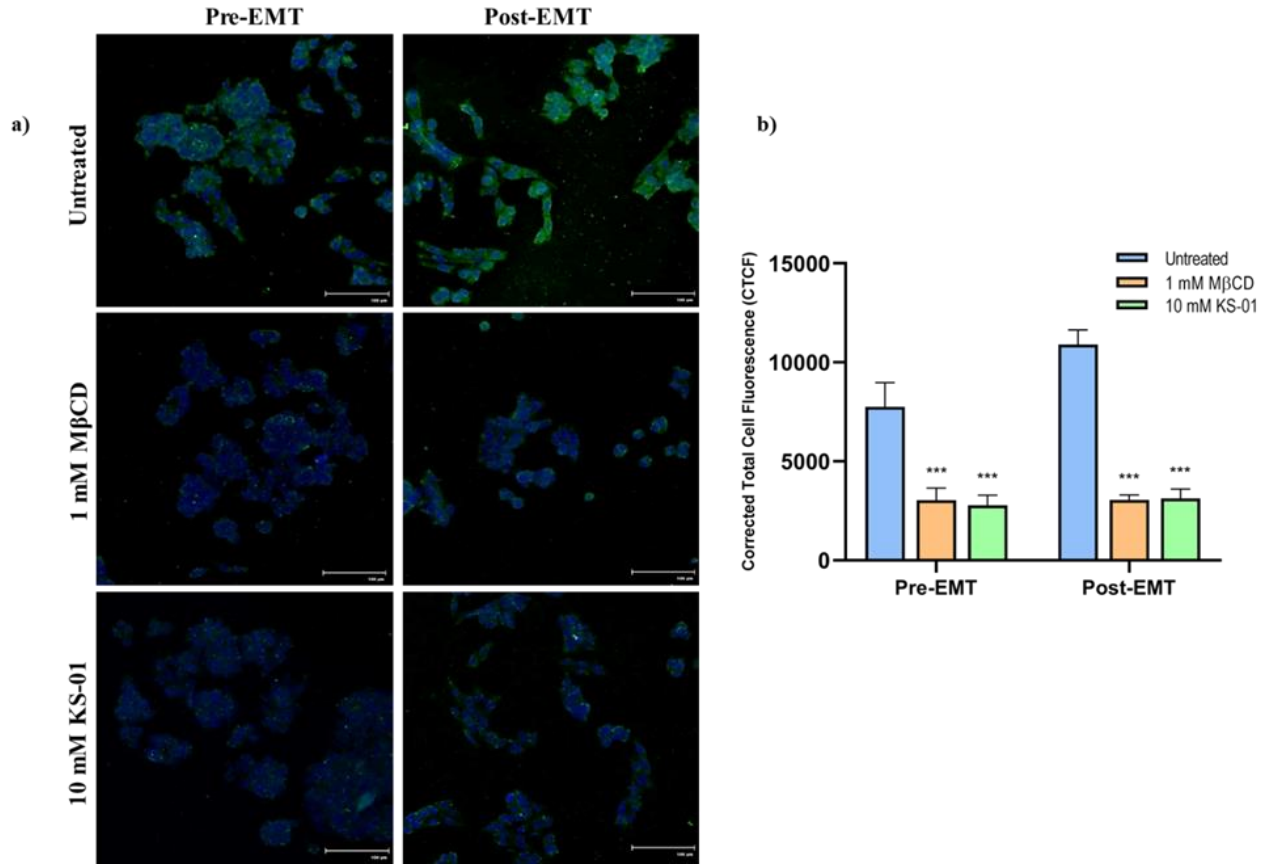


Figure 4.11: BODIPY staining of lipid droplets in cells pre- and post-EMT induction. a) *Cholesterol staining shows that lipid droplet levels increase following EMT induction. Subsequently, treatment with 1 mM MβCD or 10 mM KS-01 successfully decrease lipid droplet levels in pre- and post-EMT cells. Lipid droplets were stained by BODIPY (green), and nuclei were stained with DAPI (blue)* ***b)*** *ImageJ analysis confirms a significant decrease in lipid droplet levels following MβCD and KS-01 treatment in pre- and post-EMT cells. The scale bar on the micrographs represents 100 µm. Data represents the mean ± standard deviation. A one-way ANOVA ($P < 0.001$) was performed for statistical analysis. Bonferroni's multiple comparisons test was performed for pairwise analysis where * $P < 0.05$, ** $P < 0.01$, *** $P < 0.001$ and ns = not significant at 95% CI. Pairwise analysis was performed comparing MβCD and KS-01 against untreated samples in pre-EMT cells and in post-EMT cells. n=3.*

Ultimately, an overall increase in lipid content was observed in post-EMT HT-29. Cholesterol depleting agents, MβCD and KS-01, successfully depleted cholesterol from the cell membrane and lipid rafts resulting in reduced intracellular cholesterol and lipid droplets. It is noted that MβCD and KS-01 depleted a greater percentage of cholesterol in post-EMT cells compared to pre-EMT cells. This is most likely a result of the observed increase in cholesterol levels, following EMT induction.

4.5 Cholesterol depletion promotes an epithelial phenotype in EMT induced cells

Following confirmation of increased cholesterol in EMT induced cells, we wanted to observe how cholesterol depletion would influence the expression of EMT molecular markers. Therefore, immunofluorescence was performed with E-cadherin and vimentin in EMT induced cells, following 2 hours of cholesterol depletion with 1 mM MβCD and 10 mM KS-01.

E-cadherin protein expression increased by 46.9% in the presence of 1 mM MβCD and significantly increased by 55.3% in the presence of 10 mM KS-01 (compared to untreated Post-EMT) (Figure 4.12). Additionally, vimentin expression significantly decreased by 41.0% and 52.8% when exposed to 1 mM MβCD and 10 mM KS-01, respectively (Figure 4.13). This outcome validates that cholesterol is important for EMT induction and is involved in the maintenance of the mesenchymal phenotype. This result also provided initial evidence that cholesterol depletion may be able to reverse the EMT phenotype.

Immunofluorescence was also performed together with FOLFOX, to ensure that the observed phenotype reversal was maintained when treated together with the chemotherapy. Interestingly, EMT induced cells treated with FOLFOX alone showed 39.5% increase in E-cadherin and 11.7% decrease in vimentin. Furthermore, it was observed that when EMT induced cells were treated with FOLFOX together with cholesterol depleting agents, the reversal of the EMT phenotype was maintained. It was found that cells exposed to MβCD/FOLFOX had a 60.0% increase in E-cadherin and 40.9% reduction in vimentin. EMT induced KS-01/FOLFOX exposed cells showed 61.9% rise in E-cadherin and 47.3% decrease in vimentin protein expression. Ultimately, these results suggest that cholesterol depletion may be involved in reversing the EMT phenotype, even in the presence of a chemotherapy.

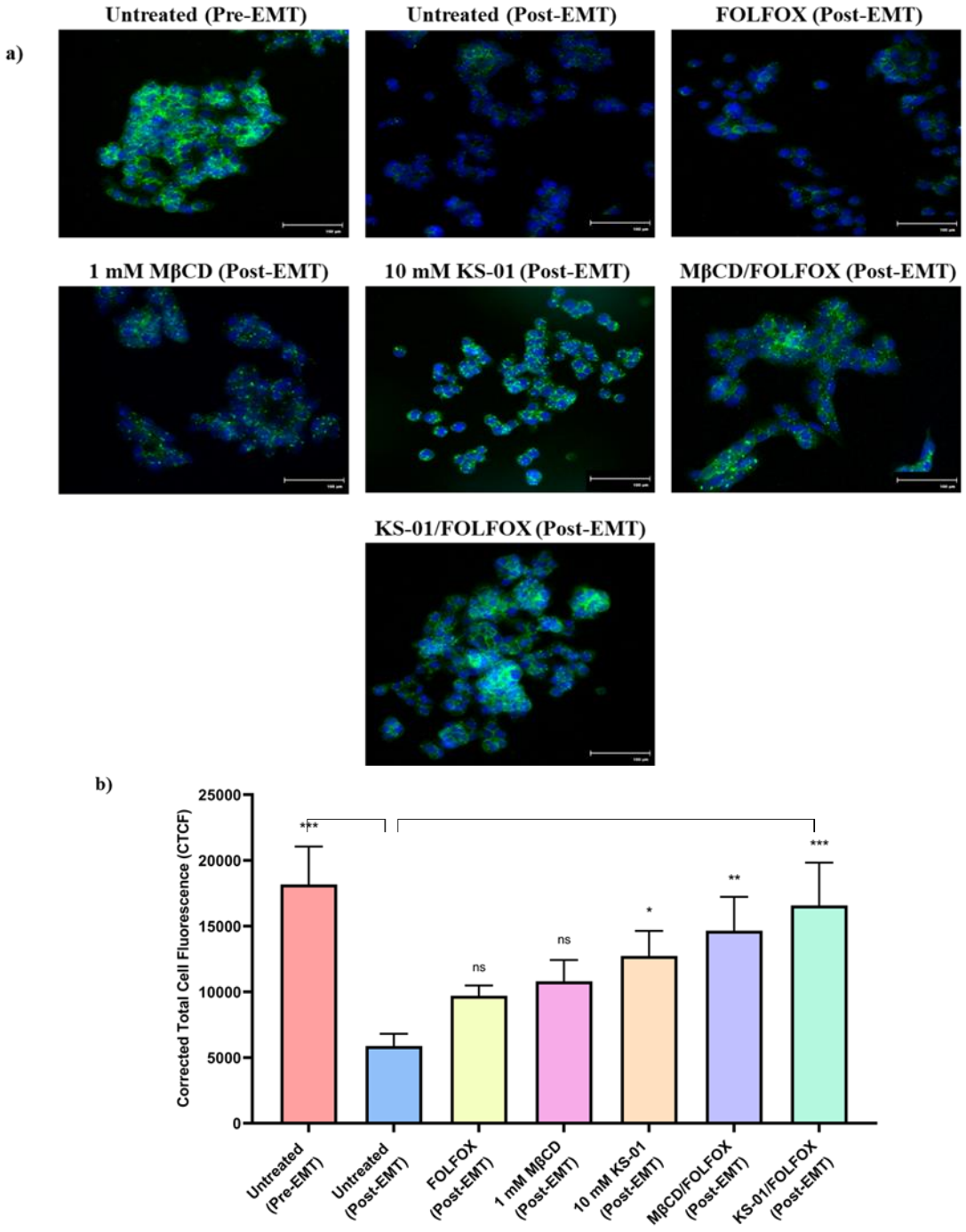


Figure 4.12: Treatment with cholesterol depleting agents increases E-cadherin epithelial marker in EMT induced cells. a) *Visual representation of changes in E-cadherin expression following treatment with cholesterol depleting agents MβCD and KS-01 in the presence of FOLFOX in EMT induced cells. E-cadherin was stained by Alexa Fluor 488 (green) and nuclei were stained with DAPI (blue).* ***b)*** *ImageJ analysis shows cholesterol depletion to increase E-cadherin levels in EMT induced cells, compared to untreated EMT induced cells. The scale bar on the micrographs represents 100 µm. Data represents the mean ± standard deviation. A one-way ANOVA ($P < 0.001$) was performed for statistical analysis. Bonferroni's multiple comparisons test was performed for pairwise analysis where * $P < 0.05$, ** $P < 0.01$, *** $P < 0.001$ and ns = not significant at 95% CI. n=3.*

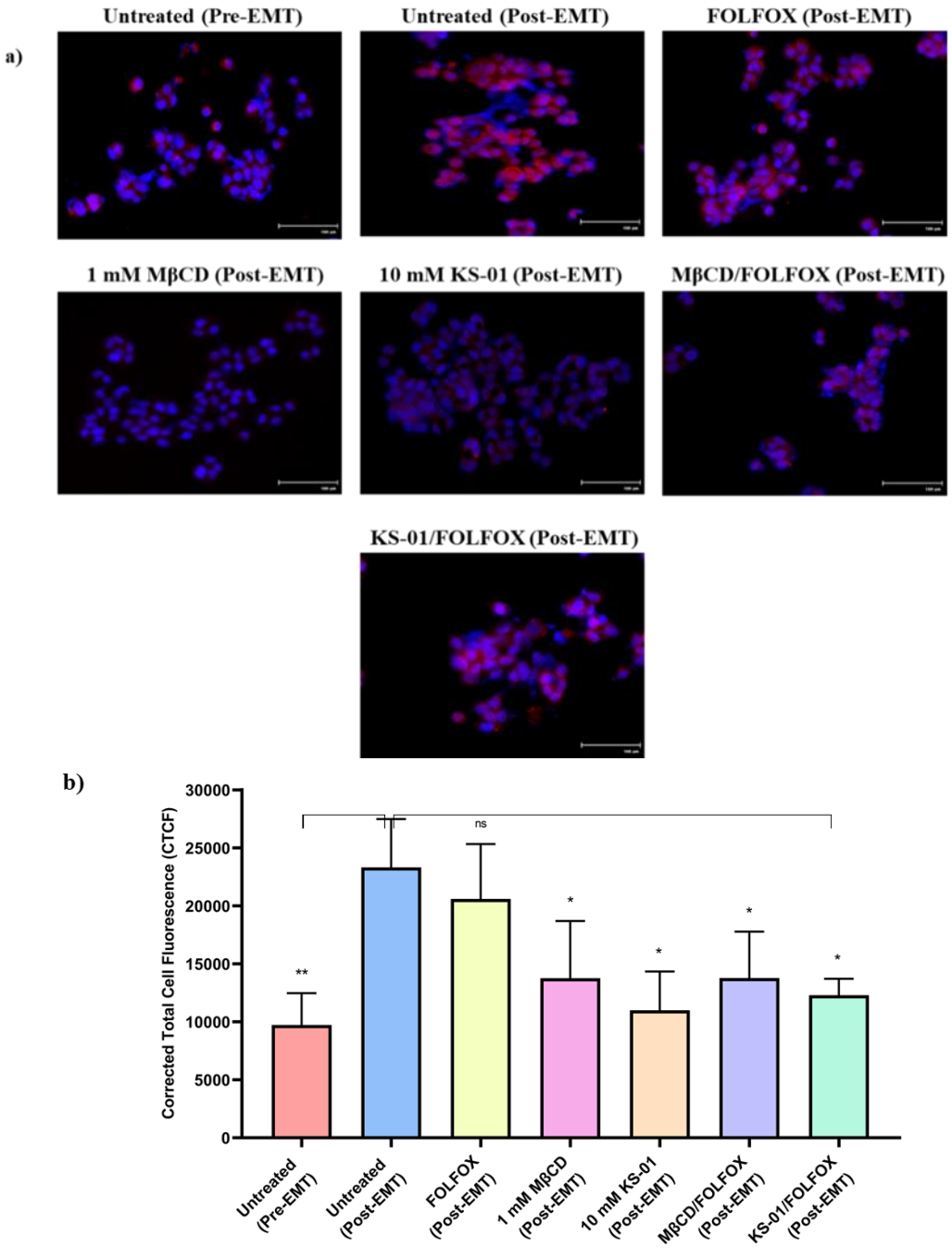


Figure 4.13: Treatment with cholesterol depleting agents decreases vimentin mesenchymal marker in EMT induced cells. ***a)*** *Visual representation of changes in vimentin expression following treatment with cholesterol depleting agents MβCD and KS-01 in the presence of FOLFOX in EMT induced cells. Vimentin was stained by Texas Red (red) and nuclei were stained with DAPI (blue).* ***b)*** *ImageJ analysis shows cholesterol depletion to decrease vimentin levels in EMT induced cells, compared to untreated EMT induced cells. The scale bar on the micrographs represents 100 µm. Data represents the mean ± standard deviation. A one-way ANOVA ($P < 0.05$) was performed for statistical analysis. Bonferroni's multiple comparisons test was performed for pairwise analysis where * $P < 0.05$, ** $P < 0.01$, *** $P < 0.001$ and ns = not significant at 95% CI. n=3.*

4.6 Cholesterol depletion and exposure to FOLFOX reduces the invasive potential of EMT induced cells

Following the observation of EMT phenotype reversal, changes in the invasive potential of EMT induced cells were investigated. The Transwell® Invasion assay measures the ability of cells to attach and invade the ECM and migrate towards a chemo-attractant (Justus et al., 2014). The assay was performed on EMT induced cells with cholesterol depleting agents and FOLFOX chemotherapy. The number of cells that had invaded through the membrane was stained and counted under the Floid™ Cell Imaging System.

Figure 4.14 highlights the relative invasion detected in treated cells, where untreated EMT induced cells are reported as 100% invaded cells. It was found that EMT induced cells exposed to MβCD had 43.0% reduced invasiveness and cells exposed to KS-01 showed a 47.8% reduction in invasive potential. The exposure of EMT induced cells to FOLFOX had a significant effect on invasive potential by reducing invasion by 72.2%. Treatments of FOLFOX together with cholesterol depleting agents indicated greater reduction of invasive potential to 78.2% and 84.5% treated with MβCD/FOLFOX and KS-01/FOLFOX, respectively.

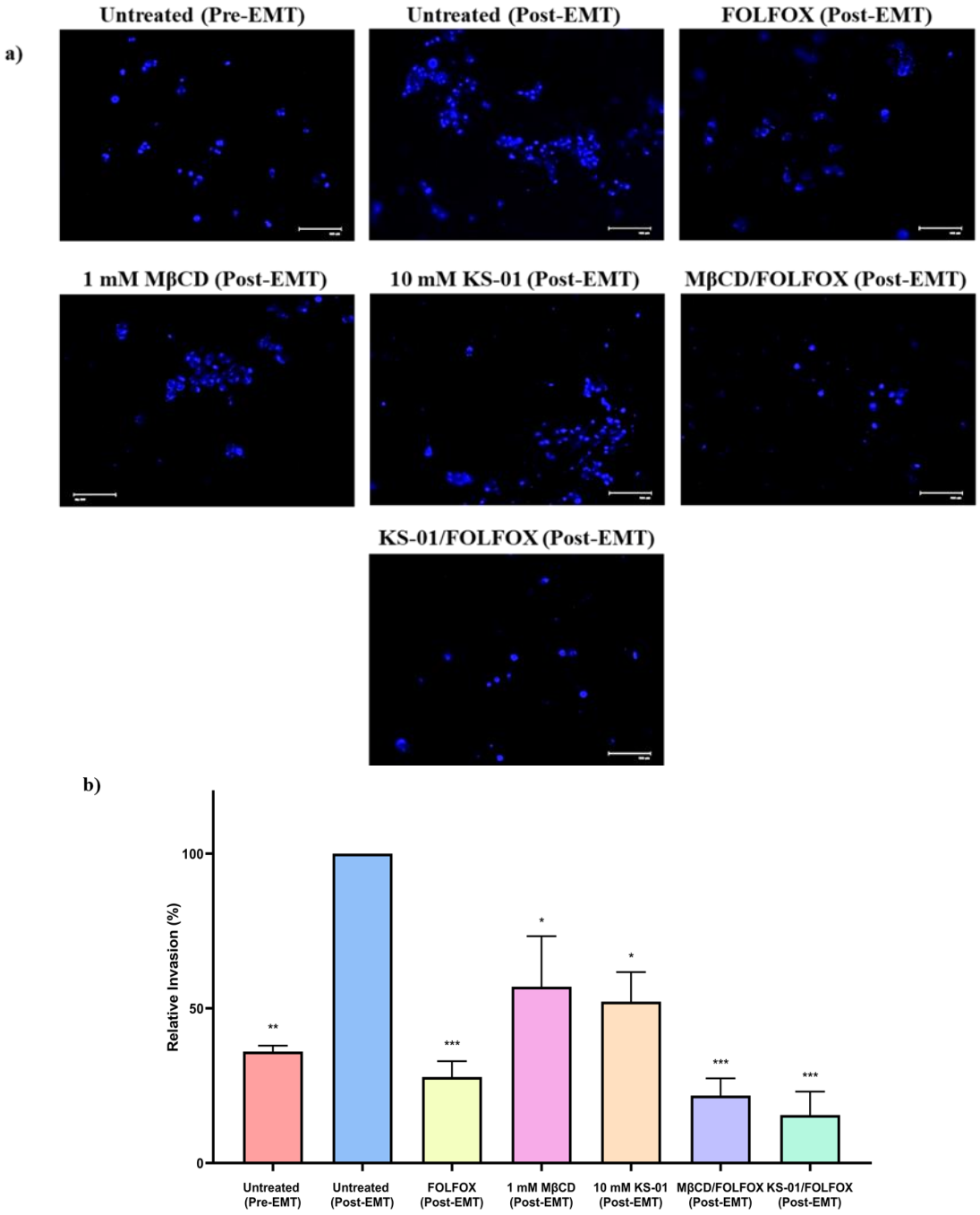


Figure 4.14: Treatment with cholesterol depleting agents decreases invasive potential in EMT induced cells. ***a)*** *Visual representation demonstrating change in number of cells that invaded following treatment with cholesterol depleting agents MβCD and KS-01 in the presence of FOLFOX in EMT induced cells. Nuclei were stained with DAPI (blue).* ***b)*** *Graphical representation depicting number of cells invaded, represented as relative invasion. Data is presented as relative invasion set against EMT induced untreated cells. EMT induction leads to a significant increase in invasive potential. Treatment with cholesterol depleting agents significantly decrease percent of invaded cells. The scale bar on the micrographs represents 100 µm. Data represents the mean ± standard deviation. A one-way ANOVA ($P < 0.001$) was performed for statistical analysis. Bonferroni's multiple comparisons test was performed for pairwise analysis where * $P < 0.05$, ** $P < 0.01$, *** $P < 0.001$ and ns = not significant at 95% CI. n=3.*

4.7 The effect of cholesterol depletion on apoptosis of EMT induced cells exposed to FOLFOX

An important characteristic of EMT is resistance to apoptotic stimuli. An APOPercentage™ apoptosis assay was performed to investigate if EMT induction confers resistance to FOLFOX treatment as well as to investigate if cholesterol depletion can promote apoptosis in these cells. The APOPercentage™ assay was performed to detect the early stages of apoptosis, therefore, cells were treated for 2 hours with combinations of cholesterol depleting agents and FOLFOX.

Figure 4.16a provides a visual representation of the APOPercentage™ dye uptake in apoptotic cells. Untreated (Pre-EMT) acts as a visual control for no dye uptake. It is observed that cells treated with FOLFOX (before induced to undergo EMT) increased uptake of the pink dye. However, following EMT induction, cells treated with FOLFOX exhibited reduced uptake of the dye, indicating that EMT facilitates apoptosis resistance. Following treatments with cholesterol depleting agents (alone and together with FOLFOX), an increase in dye uptake is observed.

Spectrophotometry analysis revealed that FOLFOX-induced apoptosis decreased from 61.2% to 25.7% following EMT induction (Figure 4.16b), verifying that EMT induction plays a role in resistance to apoptosis. It was noted that EMT induced cells exposed to 1mM MβCD and 10 mM KS-01 were more susceptible to cell death than FOLFOX treated cells. Post-EMT cells treated with 1 mM MβCD and 10 mM KS-01 detected 59.7% and 77.2% of early-stage apoptosis, respectively. Additionally, the treatment with MβCD and KS-01, in post-EMT cells, increased FOLFOX-induced apoptosis from 25.7% to 46.7% and 68.3% respectively. 40 μM plumbagin was included as a positive control.

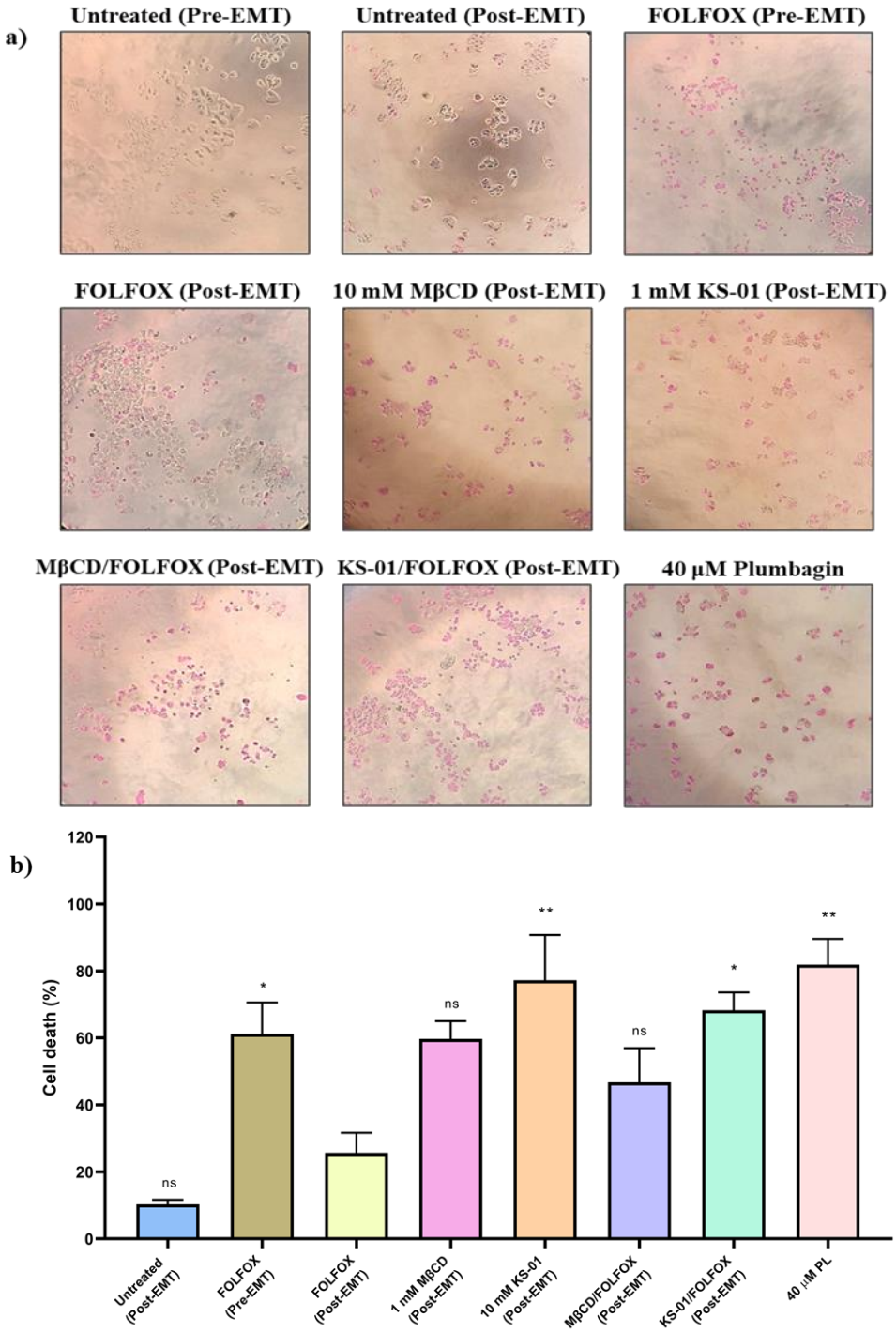


Figure 4.15: Effect of cholesterol depleting agents on susceptibility to apoptosis in EMT induced cells. ***a)*** *Visual representation of APOPercentage™ dye uptake following treatment with FOLFOX and cholesterol depleting agents: MβCD and KS-01. Cells were captured under the Nikon Phase Contrast microscope* ***b)*** *Graphical representation depicting percent cell death of cells. Cells treated with FOLFOX chemotherapy showed resistance to apoptosis following EMT induction. Treatment with 10 mM KS-01 lead to a significant increase in apoptosis. 40 µM Plumbagin acts as the positive control. Data represents the mean ± standard deviation. A one-way ANOVA ($P < 0.01$) was performed for statistical analysis. Bonferroni's multiple comparisons test was performed for pairwise analysis where * $P < 0.05$, ** $P < 0.01$, *** $P < 0.001$ and ns = not significant at 95% CI. n=3.*

4.8 The effect of cholesterol depletion on multidrug resistance of EMT induced cells exposed to FOLFOX

Drug resistance is often reported after prolonged use of chemotherapies and remains one of the greatest obstacles in the treatment of metastatic CRC. A Vybrant™ Multidrug Resistance assay was performed to observe how cholesterol depletion would influence MDR in cells exposed to a chemotherapy. Fluorescence intensity pertains to the amount of calcein dye retained intracellularly. Low fluorescence intensity reflects high MDR activity. 1 μM verapamil acts as the positive control by inhibiting the activity of P-gp transmembrane efflux transporter.

Figure 4.17 reports the relative fluorescence intensity detected in cells, where untreated pre-EMT cells are recorded as 100% relative fluorescence intensity (pertaining to no MDR activity). Fluorescence intensity decreased to 63.2% following EMT induction, which indicates that EMT induced cells exhibits some MDR activity. Following exposure to the FOLFOX chemotherapy, relative intracellular fluorescence intensity dropped to 32.8%, which denotes that FOLFOX contributes to significant MDR activity in EMT induced cells. Following cholesterol depletion, MβCD treatment increased fluorescence intensity at 69.7%. Additionally, when treated together with FOLFOX, MβCD significantly increased fluorescence intensity to 80.6%. KS-01 treatment alone in EMT induced cells showed 60.1% relative fluorescence and 71.8% relative fluorescence when treated together with FOLFOX. These results indicate that cholesterol depletion abrogates MDR activity that is elicited in cells exposed to a chemotherapy. Ultimately, the treatment with cholesterol depleting agents is a promising means to overcome chemotherapy induced MDR.

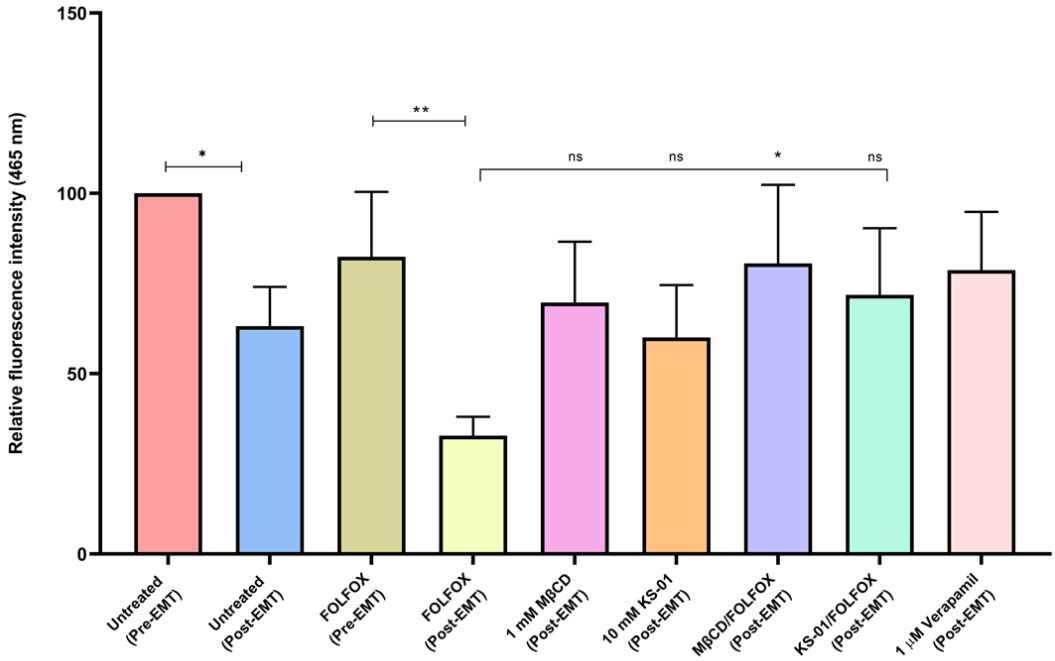


Figure 4.16: Treatment with cholesterol depleting agents decreases drug resistance in EMT induced cells*. Graphical representation depicting relative fluorescence intensity. EMT induced cells showed decreased retention of fluorescent calcein. Cholesterol depleting agents increases intracellular calcein retention. 1 μM Verapamil acts as the positive control. Data represents the mean ± standard deviation. A one-way ANOVA (P < 0.01) was performed for statistical analysis. Uncorrected LSD test was performed for pairwise analysis where * P < 0.05, ** P < 0.01, *** P < 0.001 and ns = not significant at 95% CI. n=3.*

5. Discussion

It is recognised that several cancer types, such as prostate, breast and CRC have higher membrane and cellular cholesterol levels compared to normal cells. An upregulation of cholesterol levels has shown to facilitate increased proliferation and oncogenic signalling. These cancer cells are more susceptible to cell-death induced by cholesterol lowering (Matusewicz et al., 2015). It is for this reason that cholesterol is viewed as an attractive target for anti-cancer therapies. Utilising cholesterol depleting agents to improve on existing chemotherapies is a novel concept. This study explored the effect of cholesterol depletion on the ability of FOLFOX to induce apoptosis, to decrease invasion and MDR, during the metastatic EMT stage. It was observed that the use of cholesterol depleting agents enhanced the effectiveness of the FOLFOX chemotherapy, by enhancing FOLFOX-induced apoptosis and decreasing FOLFOX-induced multidrug resistance.

5.1 IL-6 mediated EMT induction in colorectal cancer

Tumours can be regarded as wounds that do not heal and therefore inflammatory pathways are aberrantly activated. Tumour-associated inflammation is a known hallmark of cancer that advances cancers towards metastasis (Hanahan and Weinberg, 2011). A metastatic cascade usually favours the execution of the EMT program, which enhances cell migratory and invasive potential and confers stem-like properties which contributes to cancer aggressiveness (Mittal, 2018). The EMT program can also promote the production of proinflammatory molecules (Suarez-Carmona et al., 2017). Consequently, inflammation and EMT can sustain each other in the interest of metastasis.

IL-6 is one of the most abundant cytokines in the TME and is well-known for promoting an inflammatory response. Elevated IL-6 levels are associated with poor patient outcome in a number of cancers (Dominguez et al., 2017). The link between IL-6 expression and EMT pathways has been established through several independent studies (Rokavec et al., 2014; Liu et al., 2015; Wang et al., 2019). JAK/STAT3 is regarded as the key signalling pathway exploited by IL-6 to promote EMT, by transcriptionally regulating several TFs and miRNAs. In accordance with these studies, the immunofluorescent staining of HT-29 cells confirmed a significant increase of phosphorylated STAT3(Y705) following exposure to IL-6. Importantly, the STAT3 homodimer can directly promote EMT by enhancing the transcriptional activity of EMT-TFs TWIST, SNAIL and ZEB1 (Xiong et al., 2012; Zhang et al., 2015; Saitoh et al., 2016).

The activation of EMT-TFs results in significant genetic reprogramming. These EMT-TFs function interactively to modify the gene expression of cytoskeletal and adhesive complex proteins and to alter the cells interactions with the ECM. SNAI1 and SLUG function to repress transcriptional activity of epithelial genes by binding at the E-box promotor region (Herranz et al., 2008; Lamouille et al., 2014). Target genes of SNAIL include genes encoding E-cadherin, claudins, occludin and cytokeratin. Repression of these genes dissolves apical tight junctions and promotes cytoskeletal reorganisation (Lamouille et al., 2014). Similar to SNAIL, TWIST TF downregulates E-cadherin expression and upregulates mesenchymal N-cadherin, the 'cadherin-switch' modifies cell adhesive contacts (Yang et al., 2012). ZEB1 and ZEB2 binds to E-box regulatory sequences that can either activate or repress gene expression. ZEB TFs recruit transcriptional co-repressors or interact with coactivators to mediate epithelial suppression and mesenchymal upregulation (Postigo et al., 2003). Additionally, EMT-TFs can regulate the expression of other EMT-TFs. SNAI1 has shown to positively regulate the expression of SLUG, TWIST1 and ZEB1 (Taube et al., 2010; Hugo et al., 2011). IL-6 exposure in HT-29 cells upregulated *SNAI1* and *TWIST1* gene expression levels by a $\log_2$FC of ~1 (Figure 4.6). As a result of EMT-TF cooperative activity, the expression of one EMT-TF would result in the activation of other core groups of EMT-TFs (Shibue and Weinberg, 2017).

E-cadherin was selected as a marker for EMT induction during the optimisation stages of recombinant IL-6 concentration. E-cadherin is a cell adhesion transmembrane glycoprotein that mediates cell-cell interactions and is uniquely expressed in epithelial tissue (Bruner and Derksen, 2018). In landmark studies, it was demonstrated that the inhibition of E-cadherin activity is sufficient to stimulate the dissociation and invasion of cancerous cells (Behrens et al., 1985; Vleminckx et al., 1991). The loss of E-cadherin expression is an indicator of cancer progression and provided the initial evidence that EMT had been induced at 50 ng/ml IL-6.

Vimentin serves as a downstream effector of SNAIL, TWIST1 and ZEB-mediated EMT (Usman et al., 2021). Vimentin is a type III intermediate filament that forms a major cytoskeletal component in mesenchymal cells. Vimentin becomes upregulated in the context of carcinogenesis and replaces cytokeratin (epithelial intermediate filament) at more advanced stages of cancer (Usman et al., 2021). Its overexpression is used as a marker for cells undergoing EMT and consequently to predict poorer patient outcome (Wu et al., 2018; Kim et al., 2020). Following IL-6 exposure to HT-29 cells, vimentin expression levels increased by 50.7% (Figure 4.5). The upregulation of vimentin facilitates cytoskeletal

reorganization that occurs during EMT in order to enhance changes in cell adhesion, migration and promote invasion (Liu et al., 2015).

Importantly, EMT cells exhibit plasticity in the transition between epithelial and mesenchymal states. Partial EMT (pEMT) is the process where cells transition through a spectrum of intermediate states exhibiting a hybrid of epithelial and mesenchymal markers (Nieto et al., 2016). This would explain the ~50% upregulation of vimentin in the HT-29 cells, and why the cells retained 40% E-cadherin expression (Figure 4.5). This hybrid expression of EMT markers is considered to be a common event, while the transition to a complete mesenchymal phenotype has shown to be infrequent in normal and tumorigenic human tissue (Derynck and Weinberg, 2019). pEMT is considered most relevant in cancer progression because these cells sustain high migratory properties while maintaining cell-cell adhesions, which allows cells to travel efficiently in clusters. Additionally, the retention of epithelial characteristics allows for cells to colonise more effectively at secondary sites through MET and so pEMT has found to be more aggressive than complete EMT (Jolly et al., 2015; Nieto et al., 2016).

The reversible activation of EMT is important to allow invasion and dissemination to secondary niches. EMT-inducing factors are shown to attenuate cell proliferation which favours de-differentiation and invasion. SNAIL expression has shown to initiate cell cycle arrest by repressing the expression of *CCND1* (gene encoding Cyclin D1) (Vega et al., 2004). However, during the process of MET, EMT-TFs are downregulated and proliferation is initiated for cells to re-differentiate and for the formation of micro-metastases (Tsai et al., 2012; Weidenfeld and Barkan, 2018). These findings support the notion that EMT drives epithelial cells into a quiescent state in order to acquire mesenchymal features. Interestingly, we found that IL-6 increased HT-29 cell proliferation, which was validated by increased expression of proliferative marker Ki67. IL-6 can act as both a growth factor or a growth inhibitory factor in several cancers, including in the context of EMT induction (Kanazawa et al., 2007; Sullivan et al., 2009; Chen et al., 2018). Weidenfeld and Barkan, 2018, proposed a model that may clarify the contradictions seen between different studies (Figure 5.1). This model further supports the view that EMT progresses along a spectrum of intermediate states and highlights the high levels of plasticity within the EMT program. Most likely, the HT-29 cells exposed to IL-6 are at an “equilibrium” state between the two complete epithelial and mesenchymal phenotypes.

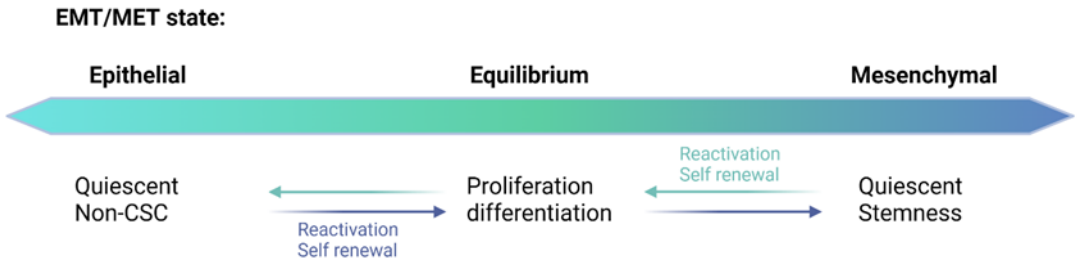


Figure 5.1: The EMT/MET spectrum. *The model proposed by Weidenfeld and Barkan suggests that cells travel between an EMT/MET state. Cancer cells that fluctuate between epithelial and mesenchymal phenotypes observe corresponding changes in proliferation and differentiation/stemness. CSC: Cancer stem cell Figure created with BioRender.com. Figure adapted from (Weidenfeld and Barkan, 2018).*

5.2 Cholesterol: an important driver of EMT induction

Inflammatory diseases and chronic inflammation can stimulate changes in lipid metabolism, including reduction of serum HDL levels and a rise in triglycerides and LDL cholesterol levels (Tsoupras et al., 2018). The increase in lipid content helps sustain the immune response, supported by evidence reporting that several immune receptors and immune-related transcription factors are sterol dependent (Bilotta et al., 2020). However, as a consequence, persistent inflammation can result in increased risk of atherosclerosis (Tsoupras et al., 2018). Specifically, IL-6 mediated inflammation is associated with cholesterol-related disorders including atherosclerosis and coronary artery disease (Omoigui, 2007).

Inflammatory stress through IL-6 signalling is understood to increase cholesterol accumulation by enhancing expression of SREBP2, LDLR and HMGCR in several cell types, leading to cellular uptake of plasma LDL and promoting *de novo* biosynthesis (Gierens et al., 2000; Zhao et al., 2011; Chen et al., 2014; DiNicolantonio and McCarty, 2018). Currently, there is limited literature delineating the link between IL-6 mediated cholesterol accumulation and cancer progression. It is well known that increased cholesterol content is associated with increased cancer aggressiveness (Ding et al., 2019). The pathways involved in deregulated cholesterol metabolism in EMT have been discussed previously (Section 1.8). It can be hypothesised that cholesterol accumulation stimulated by IL-6 expression is involved in driving tumorigenesis and consequently fuels EMT. This hypothesis is supported by our findings, where following IL-6 mediated EMT induction there was a notable increase in cholesterol content in lipid rafts, free cholesterol, and lipid droplets, by 34.7%, 33.8% and

28.8% respectively. Several EMT-related signalling pathways are dependent on lipid raft composition such as TGF-β and Wnt signalling. Additionally, the IL-6R has shown to associate with lipid rafts and that a significant proportion of phosphorylated STAT3 accumulates in the lipid raft (Kim et al., 2004). Consequently, the IL-6 mediated accumulation of cholesterol in lipid rafts domains is likely to enhance a proinflammatory feedback loop, EMT and ultimately, cancer aggressiveness.

It is estimated that ~90% of free cellular cholesterol exists in the plasma membrane of numerous cell types (Kim et al., 1991; Lange, 1991). The observation of increased free cholesterol in EMT induced HT-29 cells is likely to enhance membrane fluidity necessary for mesenchymal morphological alterations and to facilitate the observed increase in cell proliferation (Morandi et al., 2017). Free cholesterol may also serve as a precursor for cholesterol derivatives such as bile acids. Increased production of cholesterol-derived bile acids acid is recognised as a major driver of CRC (Rossin et al., 2017). Secondary bile acids including lithocholic acid and deoxycholic acid are understood to stimulate CRC by causing damage to epithelial cells, elevating reactive oxygen species (ROS), apoptosis inhibition, and to promote stemness of cells (Nguyen et al., 2018). Any excess cellular cholesterol is toxic to cells and is therefore stored in lipid droplets. Readily available cholesterol in the form of CEs, reduces the energetic demand that would be required through *de novo* biosynthesis. IL-6 signalling facilitates abnormal accumulation of lipid droplets, which subsequently act as reservoirs of cholesterol, to enable membrane biogenesis and modify lipid raft structure which ultimately enhances cancer aggressiveness. (Sahini and Borlak, 2014; Ayyagari et al., 2020).

As discussed previously, cellular cholesterol is tightly regulated through *de novo* biosynthesis, efflux, and influx pathways. Control of cholesterol metabolism in the intestine is balanced by the intestinal absorption of dietary cholesterol and intracellular synthesis (Cohen, 2008). However, an *in vitro* model has limited access to circulating cholesterol, where supplemented media with 10% FBS only provides 2–3% of cholesterol that is available to cells in the body (Else, 2020). Therefore, the observed increase in cellular cholesterol of HT-29 cells is likely attributed to an upregulation of the cholesterol biosynthesis pathway. This hypothesis would need to be validated following RT-qPCR analysis of genes encoding SREBP2, LDLR and HMGCR, following treatment with IL-6 in HT-29 cells. Consequently, we hypothesised that depleting excess cholesterol from EMT induced cells may reduce cancer aggressiveness *in vitro* through disrupting cholesterol

mediated oncogenic signalling. β-CDs effectively disrupt lipid rafts and subsequent signalling pathways, while showing no disturbances to normal cholesterol in the human body (Gu et al., 2019).

Results showed that MβCD and KS-01 depleted cholesterol from lipid rafts (by 71.0% and 67.2%, respectively), lipid droplets (by 72.0% and 71.3%, respectively) and free cholesterol (by 65.3% and 67.8%, respectively), following EMT induction. β-CD derivatives have high affinity towards cholesterol and are very effective in extracting excess cholesterol from cell membranes (Jansook et al., 2018). β-CDs show high affinity to lipid rafts because they are cholesterol dense, containing 30-50% of plasma membrane cholesterol. Therefore, MβCD is often used as an anticancer agent by decreasing membrane cholesterol through the disruption of lipid rafts (Zidovetzki and Levitan, 2007). Moreover, studies do show that β-CDs can extract cholesterol from non-raft domains as well as lipid rafts, where cholesterol at the plasma membrane can regulate intracellular cholesterol levels. It is suggested that exposing cells to CDs promotes CD-induced cholesterol efflux to the membrane in order to maintain cholesterol homeostasis and membrane integrity (Zidovetzki and Levitan, 2007). Lange et al., 1999, found that treating fibroblast cells to 2% HPβCD led to a ~25% decrease in total membrane cholesterol, and simultaneously depleting 76% of intracellular cholesterol at the endoplasmic reticulum (Lange et al., 1999). Additionally, cholesterol depletion has shown to degrade lipid droplets through autophagy (Ouimet and Marcel, 2012). These findings would explain the observed decrease of lipid droplet content following cholesterol depletion, which would function to maintain cholesterol homeostasis.

The observation that treatment with MβCD and KS-01 depleted ~10-20% more cholesterol from EMT induced cells compared to pre-EMT cells, suggests that cells in the EMT stage should be more susceptible to cholesterol depleting agents than epithelial cells. The downstream effects of this observed cholesterol depletion are discussed in greater detail below.

5.3 Cholesterol depletion as a novel strategy for EMT phenotype reversal

It has been established that cholesterol plays an important role in EMT induction. However, the effect of cholesterol in maintaining an EMT phenotype has not been fully elucidated. Therefore, MβCD and KS-01 were utilised to examine how cholesterol depletion affects the EMT phenotype in HT-29 cells. Interestingly, it was found that following exposure to MβCD and KS-01, E-cadherin expression increased by 46.9% and 55.3%, respectively and vimentin

levels decreased by 41.0% and 52.8%, respectively (Figure 4.12 and 4.13). Regulating cell cholesterol levels has shown to either promote or impede the conversion to a mesenchymal phenotype (Morandi et al., 2017). Several studies report that the interference of lipid rafts inhibits the activity of key EMT-related signalling pathways which promotes the expression of epithelial markers and downregulates mesenchymal marker expression (Zuo and Chen, 2009; Guerra et al., 2016; Wu et al., 2020).

The disruption of lipid rafts shows to attenuate IL-6 signalling. A study conducted by Sehgal et al., 2002, showed that treatment of human hepatoma cells with MβCD prevented the activation of STAT3, through disruption of lipid rafts (Sehgal et al., 2002). Moreover, IL-6 and TGF-β signalling are closely linked and have shown to act synergistically in promoting EMT (Zhang et al., 2005). Modulation of MAPK-dependent EMT induction via TGF-β is dependent on the integrity of lipid raft domains. Cholesterol depletion consequently disrupted TGF-β activation of MAPK resulting in the upregulation of E-cadherin and suppression of actin stress fibres (Zuo and Chen, 2009; Wu et al., 2020). Wnt/β-catenin is another EMT-related signalling pathway that becomes disrupted by membrane cholesterol depletion (Guerra et al., 2016). These findings highlight the importance of lipid raft integrity in maintaining an EMT phenotype.

An important property of mesenchymal cells is increased membrane fluidity which modulates changes in cell adhesion, migration and differentiation (Kashirina et al., 2020). Cholesterol depletion with β-CDs increases membrane stiffness which results in deceased cell migration, stem cell characteristics and has shown to inhibit EMT induction *in vitro* (Byfield et al., 2004; Zhao et al., 2016). Therefore, the alteration of membrane fluidity is another likely mechanism that causes the observed changes in the EMT phenotype in the HT-29 cells. Additionally, changes to membrane fluidity can enhance the activity of anti-metastatic drugs, by decreasing the activity of efflux pump ABCA1 where its expression is highly dependent on membrane fluidity (Zhao et al., 2016).

Increased motility and invasiveness are characteristics of mesenchymal cells, facilitated by E-cadherin inhibition and vimentin upregulation. The observed restoration of E-cadherin and downregulation of vimentin, following treatment with MβCD and KS-01 in EMT induced cells, is consistent with the Transwell® Invasion results, which showed reduced invasive potential of HT-29 cells by 43.0% and 47.8%, respectively. Vimentin allows for cytoskeletal rearrangement of mesenchymal cells, protecting cells from mechanical stress during

migration (Usman et al., 2021). E-cadherin expression prevents invasion by preventing dissociation of epithelial cells from the tumour (Bruner and Derksen, 2018). Consequently, the mediation of E-cadherin and vimentin expression through cholesterol depletion influences cell invasion, promoting a less aggressive cancer phenotype. Studies show that increased membrane cholesterol is related to increased membrane fluidity, which enhances that invasive properties of cells, while reduced membrane fluidity deceases cell migration (Guerra et al., 2016; Zhao et al., 2016). Additionally, disruption of lipid rafts with MβCD decreases the secretion of MMPs which suppresses the invasiveness of cancer cells, through the cells' limited ability to degrade ECM components (Greenlee et al., 2021) Therefore, alterations to lipid content affects invasive potential and cancer aggressiveness in HT-29 cells.

In addition to invasiveness, EMT upregulates pro-survival signalling for the survival of cells in circulation and to maintain a favourable microenvironment at secondary niches. IL-6/JAK/STAT3 is one of the major pro-survival signalling networks in EMT (Thomson et al., 2011). IL-6/STAT3 signalling stimulates the expression of several pro-survival proteins including Bcl-2, Bcl-xL and survivin. Pro-survival PI3K signalling pathway is also stimulated by IL-6 (Masjedi et al., 2018). Importantly, treatments with MβCD and KS-01 showed to induce 59.7% and 77.2% of early-stage apoptosis in EMT induced cells, respectively (Figure 4.15). Cholesterol depletion is recognised to induce cellular apoptosis in a range of invasive cell lines. Studies show that cancer cells with elevated cholesterol at lipid rafts are increasingly sensitive to apoptosis through cholesterol depletion (Li et al., 2006) β-CDs are able to induce cell death by elevating caspase-3/7 activity and inhibiting Bcl-xL, c-myc, Wnt receptor LRP6 and β-catenin (Li et al., 2006; Onodera et al., 2013; Badana et al., 2018). Additionally, PI3K activates Akt by recruiting Akt and PDK1 to lipid rafts. MβCD has shown to inhibit Akt phosphorylation and upregulate protein degradation in breast and prostate cancer cell lines, by depleting lipid raft cholesterol (Li et al., 2006). Based on these findings, it can be concluded that cholesterol depleting agents may be an effective strategy in reversing the aggressive EMT phenotype, impeding invasiveness and enhancing apoptosis in CRC cells.

The use of CDs presents an alternative approach to reduce cellular cholesterol levels in cancerous cells. Statin treatment is a common strategy used to target cellular cholesterol, through cholesterol synthesis inhibition. Statins exhibit anti-cancer properties in mesenchymal-like cells and have reported to suppress EMT by restoring E-cadherin and decreasing vimentin expression (Warita et al., 2021; Nishikawa et al., 2019). Cholesterol

synthesis inhibition has shown to be successful in a laboratory setting, however, the effects of statins extend past the lipid profile, causing metabolic disruptions in the production of steroid hormones, vitamin D and bile acids, in normal cells (Golomb and Evans, 2008). Consequently, the severe side effects of statins have raised questions about its usefulness in a clinical setting. Additionally, a study performed by Chen et al., 2014, showed that inflammatory stress confers statin resistance through enhancing HMGCR expression, thus weakening statins suppressive effects (Chen et al., 2014). Results obtained from this study highlights CDs as an alternative strategy to remove excess cholesterol in cancers.

5.4 Cholesterol depletion enhances the effectiveness of the FOLFOX chemotherapy

The FOLFOX chemotherapy is associated with a number of limitations mainly severe systemic toxicity and acquired drug resistance after prolonged use. This project explored the novel concept of utilising cholesterol depletion to improve on existing chemotherapies. The effect of cholesterol depletion on enhancing FOLFOX-induced cytotoxicity and reducing multidrug resistance was explored. A concentration of 20 μM 5-FU and 8 μM oxaliplatin was selected as the *in vitro* FOLFOX treatment at 24 hours. An MTT assay of combined treatments showed 50.3% cell viability. This was to ensure that treatments with FOLFOX alone and in combination with cholesterol depleting agents maintained a cell population large enough to analyse the downstream effects. Stem cells have intrinsic chemoresistance which suggests that, in a clinical setting, continuous chemotherapeutic exposure may select for cells with increased stemness. Treatment with MβCD and KS-01 following EMT induction allowed to examine if cholesterol depletion may sensitise the population of FOLFOX-surviving cells to chemotherapeutic cytotoxicity.

It was important to establish that the phenotype reversal that was exhibited by cholesterol depletion was maintained when cells were treated together with the chemotherapy. Interestingly, not only was the phenotype reversal maintained, but FOLFOX chemotherapy alone showed to non-significantly increase E-cadherin levels by 39.5% and decrease vimentin by 11.7% (Figures 4.12 and 4.13). Cells exposed to FOLFOX following cholesterol depletion showed an enhanced upregulation in E-cadherin and downregulation in vimentin, compared to cholesterol depletion alone. Additionally, FOLFOX reduced the invasiveness of EMT induced cells by 72.2% and reduced the invasive potential of cells exposed to MβCD and KS-01 by 78.2% and 84.5%, respectively. Wang et al., 2018, showed that oxaliplatin significantly upregulated E-cadherin and downregulated SNAIL, TWIST and N-cadherin in gastric cancer

which resulted in reduced invasiveness (Wang et al., 2018). Another study showed that following exposure to oxaliplatin, N-cadherin levels were suppressed in CRC cells which correlated with decreased migratory activity (Skarkova et al., 2018). Moreover, 5-FU has shown to act synergistically with chemotherapeutic compounds to suppress the EMT phenotype in gastric cancer and reduce the invasiveness of gastric cancer cells (Kurata et al., 2018). The findings from these studies support our observations, however, the mechanisms that FOLFOX utilises to influence the EMT phenotype is not known.

Resistance to apoptosis is closely linked to drug resistance and poses a major problem for anticancer chemotherapies. HT-29 treatment with MβCD and KS-01, in post-EMT cells, increased FOLFOX-induced apoptosis from 25.7% to 46.7% and 68.3% respectively (Figure 4.15). These results indicate that cholesterol depletion sensitises CRC cells to chemotherapeutic cytotoxicity. Cholesterol is largely implicated in acquired drug resistance in cancers, by modifying cholesterol-related MDR signalling pathways and/or regulating the activity of multidrug transporters (Abdulla et al., 2021). Cancer cells increase cellular cholesterol levels either through increased biosynthesis or uptake through LDLR, where the inhibition of these mechanisms can sensitise cells to chemotherapeutic agents (Guillaumond et al., 2015; Kong et al., 2018). Importantly, high cholesterol in lipid rafts can reduce sensitivity to anticancer agents. Cholesterol targeting agents such as simvastatin and MβCD can re-sensitise cells to chemotherapies by disrupting the activity of drug resistance related pathways such as integrin β3/focal adhesion kinase (FAK)/ERK and PI3K/Akt signalling (Chen et al., 2018; Jin et al., 2019).

MβCD/FOLFOX and KS-01/FOLFOX treatments did not induce the same cytotoxicity as MβCD and KS-01 alone in EMT induced cells. A likely explanation for this result is that cells employ several MDR mechanisms to confer chemotherapy resistance, including the over-expression of efflux pumps such as ABC transporters (other than P-gp efflux, as discussed below), reduced drug uptake, activation of detoxifying systems, DNA repair activation and evasion of apoptosis (Cho and Kim, 2020). Interestingly, Escalante et al., 2021, reported the overexpression of genes involved in 5-FU metabolism, detoxification and DNA repair as a result of EMT-TF SLUG, ZEB1 and TWIST1 binding at their response elements, which impairs cells response to FOLFOX treatment (Escalante et al., 2021). Additionally, cancer cells employ several mechanisms to reduce the effectiveness of platinum-based anticancer compounds including oxaliplatin such as the active efflux of platinum-based compounds, detoxification systems preventing the formation of DNA-adducts

and enhanced DNA repair programs (Zhou et al., 2020). The ability of cholesterol depleting agents to enhance FOLFOX-induced apoptosis allows us to hypothesis that, in a clinical setting, the combination of these two treatments may result in increased effectiveness of FOLFOX at a lower dose, which may reduce off-target effects and systemic toxicity.

Importantly, cholesterol depletion reduced MDR activity, mediated by the P-gp efflux pump. Results from the Vybrant™ Multidrug Resistance assay is reported with an inverse relationship between relative fluorescence intensity and MDR activity (Figure 4.16). Initially, relative fluorescence intensity decreased to 63.19%, following EMT induction, indicating that EMT promoted an upregulation of P-gp expression. This result is consistent with studies that IL-6 signalling promotes chemoresistance by inducing *ABCB1* (encoding P-gp) gene expression (Conze et al., 2001). Subsequently, post-EMT cells treated with FOLFOX showed reduced fluorescence intensity of 32.8%, indicating high MDR activity. One mechanism that FOLFOX utilises to promote resistance is through initiating alternative splicing of CD44, which upregulates *ABCB1* expression and subsequently P-gp activity (Ghatak et al., 2021). MβCD and KS-01 increased relative fluorescence intensity in cells FOLFOX treated cells by 80.6% and 71.8%, respectively. Cholesterol depletion can reduce MDR activity in cancer cells by decreasing ABC transporter activity, destabilising lipid rafts and subsequent pro-survival signalling and can also increase membrane fluidity which enhances chemotherapeutic drug influx (Yan et al., 2020). Additionally, it was found that cholesterol acts as a regulator for P-gp activity. P-gp efflux activity is largely dependent on its lipid environment, where cholesterol can modulate transporter conformation by binding at P-gp substrate sites and therefore, regulates P-gp catalytic activity and efflux (Abdulla et al., 2021). Cholesterol depletion would therefore disrupt the activity of P-gp, which would enhance the cellular accumulation of chemotherapies, leading to improved cytotoxicity. These findings provide novel and exciting insights into the possibility that cholesterol depletion may improve the effectiveness of FOLFOX chemotherapy.

6. Conclusions

It is well-understood that cholesterol directly regulates signalling pathways involved in EMT progression thereby driving cancer aggressiveness and conferring chemotherapy resistance. However, no publication to date has attempted to utilise cholesterol as a target as a means of improving current chemotherapies. To address this gap in the literature, this study explored the dynamics of cholesterol in IL-6 mediated EMT induction and investigated the effect of cholesterol depletion on the susceptibility of EMT induced cells to FOLFOX.

Following the successful induction of EMT by proinflammatory cytokine IL-6 in HT-29 cells, total cellular cholesterol levels increased in lipid rafts, lipid droplets and free cholesterol. To the best of our knowledge, this is the first study recording the link between IL-6 mediated cholesterol accumulation and EMT induction. The observed increase in cellular cholesterol is likely utilised by EMT induced cells to facilitate oncogenic signalling and enhanced membrane fluidity for proliferation and migration.

Interestingly, targeting cholesterol in EMT induced cells with compounds MβCD and KS-01 showed to reverse EMT phenotypic changes by significantly increasing epithelial marker E-cadherin and decreasing mesenchymal marker vimentin. Most likely, cholesterol depletion of EMT induced cells disrupted EMT-related signalling at lipid rafts and suppressed the metastatic mesenchymal phenotype by reducing membrane fluidity. Consequently, cholesterol depletion reduced invasiveness and increased apoptosis in EMT induced cells.

When MβCD and KS-01 were treated together with the FOLFOX chemotherapy, cholesterol depletion increased FOLFOX-induced apoptosis and decreased the effects of FOLFOX-induced multidrug resistance. Cholesterol depletion is likely to modulate drug resistance by reducing the activity of efflux transporters such as P-gp at lipid rafts, inhibiting pro-survival signalling at lipid rafts and increasing membrane permeability for chemotherapy uptake. These results highlight the multifaceted role of cholesterol in enhancing EMT and regulating drug resistance (Figure 6.1).

Ultimately, this study demonstrated that cholesterol plays a vital role in contributing to the aggressiveness of CRC and is implicated in the complex molecular pathways of EMT induction. This study provided novel evidence revealing that the use of cholesterol depleting agents may pose as an alternative strategy to improve on current chemotherapies for the treatment of metastatic CRC.

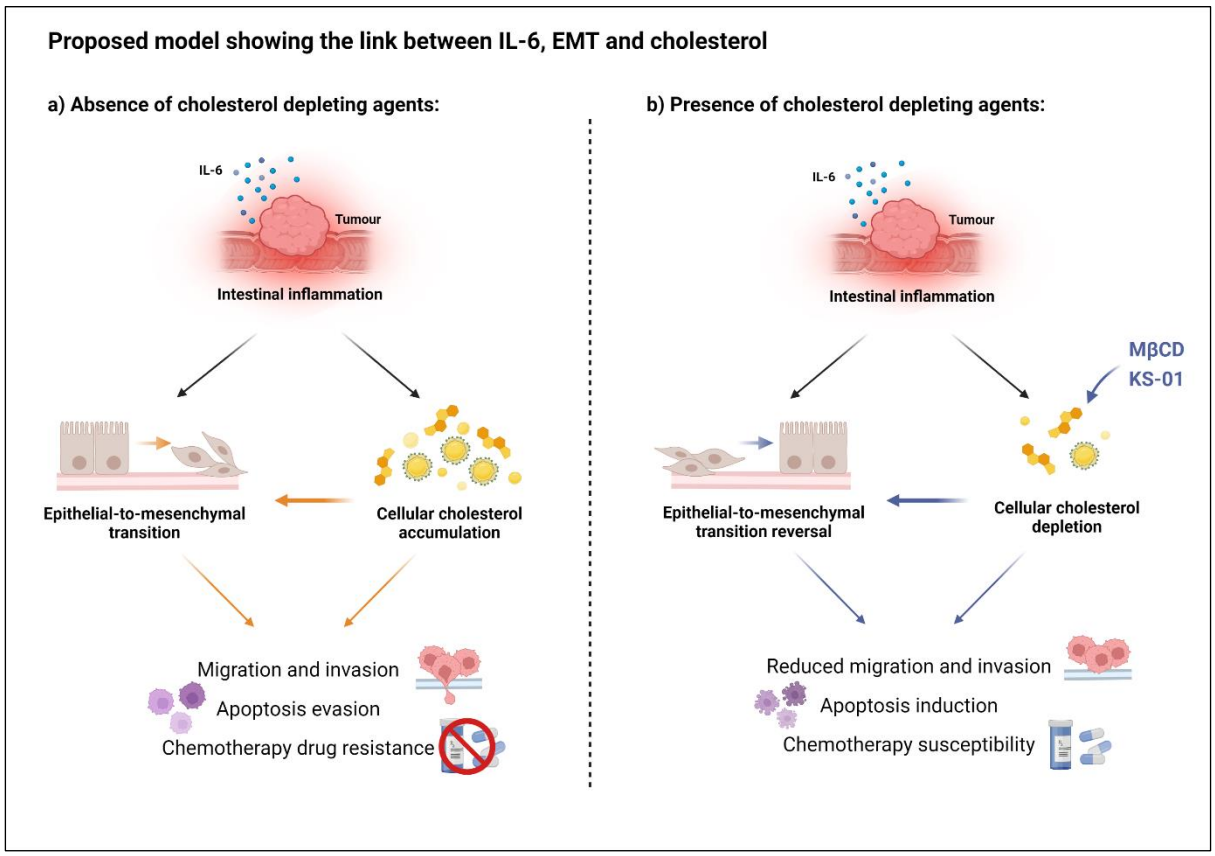


Figure 6.1: Proposed model exploring the link between IL-6, EMT and cholesterol in cancer. *Tumour-associated intestinal inflammation drives cancer aggressiveness through promoting cellular cholesterol accumulation and EMT progression.* ***a)*** *Increased cellular cholesterol helps drive EMT by mediating EMT related signalling pathways. Both EMT and cholesterol accumulation promotes invasiveness, apoptosis evasion and enhances cancer drug resistance.* ***b)*** *The use of cholesterol depleting agents (MBCD and KS-01) poses a novel strategy to deplete cellular cholesterol, which is needed to sustain EMT. Therefore, cholesterol depletion results in the reversal of the EMT phenotype. Consequently, cells show a less aggressive phenotype, displaying reduced invasiveness, increased susceptibility to apoptosis and importantly, increased sensitivity to chemotherapeutics.*

7. Future work

The biological mechanisms of cholesterol involved in maintaining an EMT phenotype is unknown. Future work may include performing RT-qPCR and western blot analysis with cholesterol related genes involved in biosynthesis, influx and efflux which may be implicated in maintaining the EMT phenotype. Thereafter, analysis may be performed to see how the expression of these genes and proteins would be affected following cholesterol depletion. This may provide insight into which cholesterol related genes are fundamental for the reversal of the EMT phenotype. Additionally, it would be worthwhile to identify the expression of cholesterol related genes that are involved in reducing MDR acquired by FOLFOX.

The Wnt/β-catenin signalling pathway is considered to be the driving event of CRC carcinogenesis and is implicated in tumour growth, metastasis and importantly EMT. It is important to explore the link between other EMT-related signalling pathways, specifically Wnt signalling and cellular cholesterol accumulation following EMT induction. Therefore, knockdown and overexpression studies may be performed with effectors in the Wnt pathway to elucidate the role of Wnt signalling in EMT induction and cholesterol accumulation. The effects of knockdown and overexpression may be observed using several assays including RT-qPCR analysis, western blots, cholesterol staining, cell viability assays such as APOPercentage assay and Transwell® Invasion assay.

Finally, due to the highly heterogenous nature of tumours and the complexity of the EMT program, it would be worthwhile to validate these results in a more realistic model. Results will need to be validated i*n vivo* with a mouse xenograft model. However, taking into consideration the costs associated with obtaining a murine cell model for EMT, a more viable option would be to generate *in vitro* 3D organoids, derived from CRC tissue samples, which can be induced to undergo EMT. 3D organoid cultures will provide a more accurate physiological response of EMT induced cells to cholesterol depletion, than 2D cell culture.

8. Limitations to the study

In vitro models are critical in research to provide insights into cell behaviour and mechanisms of drug toxicity. However, the behaviour of *in vitro* 2D cell culture is not a true reflection of the physiological conditions and metabolic responses of *in vivo* human tissue. Tumour progression including EMT induction and metastasis are not homogenous events. There is complex interplay between tumour cells, different cell types and the microenvironment. The homogenous nature of 2D cell culture limits our ability to explore the true complexity of heterogenous EMT induction. The TME promotes the production of diverse cytokines, at different stages of cancers. While IL-6 has proven to be a critical molecule in driving EMT, the isolated exposure to IL-6 alone limits a true analysis of inflammation-induced EMT and, in turn, how the cells would respond to the plethora of signalling molecules in the TME.

Furthermore, *in vitro* 2D cell culture limits our ability to accurately perform anticancer drug analysis. *In vitro* cell models may respond differently to chemotherapeutics compared to a whole-body system. Cell models do not provide appropriate information on drug bioavailability and off target adverse effects. Moreover, it is difficult to ascertain *in vivo* doses from *in vitro* concentrations. Finally, it is difficult to establish the effects of long-term exposure from an *in vitro* model. It is for these reasons that animal models are utilised before any drugs undergo preclinical trials.

Ultimately, this study explored a novel concept of utilising cholesterol depletion to improve on chemotherapies. The work presented in this study utilised an *in vitro* 2D cell model which provides significant and exciting data that can be used in the future, to design 3D *in vitro* and *in vivo* experiments and possibly clinical trials.

References

Abdulla, N., Vincent, C.T. and Kaur, M. 2021. Mechanistic Insights Delineating the Role of Cholesterol in Epithelial Mesenchymal Transition and Drug Resistance in Cancer. *Frontiers in Cell and Developmental Biology*. **9**, p.728325.

Arnold, D.R. and Kwiterovich, P.O. 2003. Cholesterol: Absorption, Function, and Metabolism. *Encyclopedia of Food Sciences and Nutrition (Second Edition)*. pp.1226–1237.

Ayyagari, V.N., Wang, X., Diaz-Sylvester, P.L., Groesch, K. and Brard, L. 2020. Assessment of acyl-CoA cholesterol acyltransferase (ACAT-1) role in ovarian cancer progression-An in vitro study. *PloS One*. **15**(1), p.e0228024.

Babcook, M.A., Joshi, A., Montellano, J.A., Shankar, E. and Gupta, S. 2016. Statin Use in Prostate Cancer: An Update. *Nutrition and Metabolic Insights*. **9**(14), pp.43–50.

Badana, A.K., Chintala, M., Gavara, M.M., Naik, S., Kumari, S., Kappala, V.R., Iska, B.R. and Malla, R.R. 2018. Lipid rafts disruption induces apoptosis by attenuating expression of LRP6 and survivin in triple negative breast cancer. *Biomedicine & Pharmacotherapy*. **97**, pp.359–368.

Bebington, B., Singh, E., Fabian, J., Jan Kruger, C., Prodehl, L., Surridge, D., Penny, C., McNamara, L. and Ruff, P. 2018. Design and methodology of a study on colorectal cancer in Johannesburg, South Africa. *JGH Open*. **2**(4), pp.139–143.

Beckwitt, C.H., Brufsky, A., Oltvai, Z.N. and Wells, A. 2018. Statin drugs to reduce breast cancer recurrence and mortality. *Breast Cancer Research*. **20**(1), p.144.

Behrens, J., Birchmeier, W., Goodman, S.L. and Imhof, B.A. 1985. Dissociation of Madin-Darby canine kidney epithelial cells by the monoclonal antibody anti-arc-1: mechanistic aspects and identification of the antigen as a component related to uvomorulin. *The Journal of Cell Biology*. **101**(4), pp.1307–1315.

Berg, J.M., Tymoczko, J.L. and Stryer, L. 2002. The Complex Regulation of Cholesterol Biosynthesis Takes Place at Several Levels. *Biochemistry. 5th edition*.

Beseničar, M.P., Bavdek, A., Kladnik, A., Maček, P. and Anderluh, G. 2008. Kinetics of cholesterol extraction from lipid membranes by methyl-β-cyclodextrin—A surface plasmon resonance approach. *Biochimica et Biophysica Acta (BBA) - Biomembranes*. **1778**(1), pp.175–184.

Bilotta, M.T., Petillo, S., Santoni, A. and Cippitelli, M. 2020. Liver X Receptors: Regulators of Cholesterol Metabolism, Inflammation, Autoimmunity, and Cancer. *Frontiers in Immunology*. **11**.

Bonovas, S., Filioussi, K., Flordellis, C.S. and Sitaras, N.M. 2007. Statins and the risk of colorectal cancer: a meta-analysis of 18 studies involving more than 1.5 million patients. *Centre for Reviews and Dissemination (UK)*.

Boudreau, D.M., Yu, O. and Johnson, J. 2010. Statin Use and Cancer Risk: A Comprehensive Review. *Expert opinion on drug safety*. **9**(4), pp.603–621.

Brand, M., Gaylard, P. and Ramos, J. 2018. Colorectal cancer in South Africa: An assessment of disease presentation, treatment pathways and 5-year survival. *South African Medical Journal*. **108**(2), pp.118–122.

Briffa, R., Langdon, S.P., Grech, G. and J.Harrison, D. 2017. Acquired and Intrinsic Resistance to Colorectal Cancer Treatment. *Colorectal Cancer - Diagnosis, Screening and Management*.

Brown, A.J. 2007. Cholesterol, Statins and Cancer. *Clinical and Experimental Pharmacology and Physiology*. **34**(3), pp.135–141.

Bruner, H.C. and Derksen, P.W.B. 2018. Loss of E-Cadherin-Dependent Cell–Cell Adhesion and the Development and Progression of Cancer. *Cold Spring Harbor Perspectives in Biology*. **10**(3), p.a029330.

Byfield, F.J., Aranda-Espinoza, H., Romanenko, V.G., Rothblat, G.H. and Levitan, I. 2004. Cholesterol depletion increases membrane stiffness of aortic endothelial cells. *Biophysical Journal*. **87**(5), pp.3336–3343.

Campbell, M.J., Esserman, L.J., Zhou, Y., Shoemaker, M., Lobo, M., Borman, E., Baehner, F., Kumar, A.S., Adduci, K., Marx, C., Petricoin, E.F., Liotta, L.A., Winters, M.,

Benz, S. and Benz, C.C. 2006. Breast Cancer Growth Prevention by Statins. *Cancer Research*. **66**(17), pp.8707–8714.

Cao, H., Xu, E., Liu, H., Wan, L. and Lai, M. 2015. Epithelial-mesenchymal transition in colorectal cancer metastasis: A system review. *Pathology, Research and Practice*. **211**(8), pp.557–569.

Chen, Q., Pan, Z., Zhao, M., Wang, Q., Qiao, C., Miao, L. and Ding, X. 2018. High cholesterol in lipid rafts reduces the sensitivity to EGFR-TKI therapy in non-small cell lung cancer. *Journal of Cellular Physiology*. **233**(9), pp.6722–6732.

Chen, S., Deng, G., Li, K., Zheng, H., Wang, G., Yu, B. and Zhang, K. 2018. Interleukin-6 Promotes Proliferation but Inhibits Tenogenic Differentiation via the Janus Kinase/Signal Transducers and Activators of Transcription 3 (JAK/STAT3) Pathway in Tendon-Derived Stem Cells. *Medical Science Monitor : International Medical Journal of Experimental and Clinical Research*. **24**, pp.1567–1573.

Chen, Y., Ku, H., Zhao, L., Wheeler, D.C., Li, L.-C., Li, Q., Varghese, Z., Moorhead, J.F., Powis, S.H., Huang, A. and Ruan, X.Z. 2014. Inflammatory stress induces statin resistance by disrupting 3-hydroxy-3-methylglutaryl-CoA reductase feedback regulation. *Arteriosclerosis, Thrombosis, and Vascular Biology*. **34**(2), pp.365–376.

Cho, Y. and Kim, Y.K. 2020. Cancer Stem Cells as a Potential Target to Overcome Multidrug Resistance. *Frontiers in Oncology*. **10**.

Cohen, D.E. 2008. Balancing Cholesterol Synthesis and Absorption in the Gastrointestinal Tract. *Journal of clinical lipidology*. **2**(2), pp.S1–S3.

Comella, P., Casaretti, R., Sandomenico, C., Avallone, A. and Franco, L. 2009. Role of oxaliplatin in the treatment of colorectal cancer. *Therapeutics and Clinical Risk Management*. **5**, pp.229–238.

Conze, D., Weiss, L., Regen, P.S., Bhushan, A., Weaver, D., Johnson, P. and Rincón, M. 2001. Autocrine Production of Interleukin 6 Causes Multidrug Resistance in Breast Cancer Cells. *Cancer Research*. **61**(24), pp.8851–8858.

Cruz, P., Mo, H., McConathy, W., Sabnis, N. and Lacko, A. 2013. The role of cholesterol metabolism and cholesterol transport in carcinogenesis: a review of scientific findings, relevant to future cancer therapeutics. *Frontiers in Pharmacology*. **4**.

Dekker, E., Tanis, P.J., Vleugels, J.L.A., Kasi, P.M. and Wallace, M.B. 2019. Colorectal cancer. *The Lancet*. **394**(10207), pp.1467–1480.

Derynck, R. and Weinberg, R.A. 2019. EMT and Cancer: More Than Meets the Eye. *Developmental Cell*. **49**(3), pp.313–316.

Ding, X., Zhang, W., Li, S. and Yang, H. 2019. The role of cholesterol metabolism in cancer. *American Journal of Cancer Research*. **9**(2), pp.219–227.

DiNicolantonio, J.J. and McCarty, M.F. 2018. Is interleukin-6 the link between low LDL cholesterol and increased non-cardiovascular mortality in the elderly? *Open Heart*. **5**(1), p.e000789.

Dominguez, C., David, J.M. and Palena, C. 2017. Epithelial-mesenchymal transition and inflammation at the site of the primary tumor. *Seminars in cancer biology*. **47**, pp.177–184.

Douillard, J.Y., Cunningham, D., Roth, A.D., Navarro, M., James, R.D., Karasek, P., Jandik, P., Iveson, T., Carmichael, J., Alakl, M., Gruia, G., Awad, L. and Rougier, P. 2000. Irinotecan combined with fluorouracil compared with fluorouracil alone as first-line treatment for metastatic colorectal cancer: a multicentre randomised trial. *Lancet (London, England)*. **355**(9209), pp.1041–1047.

Else, P.L. 2020. The highly unnatural fatty acid profile of cells in culture. *Progress in Lipid Research*. **77**, p.101017.

Escalante, P.I., Quiñones, L.A. and Contreras, H.R. 2021. Epithelial-Mesenchymal Transition and MicroRNAs in Colorectal Cancer Chemoresistance to FOLFOX. *Pharmaceutics*. **13**(1), p.75.

Fleming, M., Ravula, S., Tatishchev, S.F. and Wang, H.L. 2012. Colorectal carcinoma: Pathologic aspects. *Journal of Gastrointestinal Oncology*. **3**(3), pp.153–173.

Folprecht, G., Pericay, C., Saunders, M.P., Thomas, A., Lopez, R.L., Roh, J.K., Chistyakov, V., Höhler, T., Kim, J.-S., Hofheinz, R.-D., Ackland, S.P., Swinson, D., Kopp, M.,

Udovitsa, D., Hall, M., Iveson, T., Vogel, A. and Zalcberg, J.R. 2016. Oxaliplatin and 5-FU/folinic acid (modified FOLFOX6) with or without aflibercept in first-line treatment of patients with metastatic colorectal cancer: the AFFIRM study. *Annals of Oncology*. **27**(7), pp.1273–1279.

Friis, S., Riis, A.H., Erichsen, R., Baron, J.A. and Sørensen, H.T. 2015. Low-Dose Aspirin or Nonsteroidal Anti-inflammatory Drug Use and Colorectal Cancer Risk: A Population-Based, Case-Control Study. *Annals of Internal Medicine*. **163**(5), pp.347–355.

Gao, Y., Nan, X., Shi, X., Mu, X., Liu, B., Zhu, H., Yao, B., Liu, X., Yang, T., Hu, Y. and Liu, S. 2019. SREBP1 promotes the invasion of colorectal cancer accompanied upregulation of MMP7 expression and NF-κB pathway activation. *BMC Cancer*. **19**(1), p.685.

Garbers, C. and Rose-John, S. 2018. Dissecting Interleukin-6 Classic- and Trans-Signaling in Inflammation and Cancer. *Methods in Molecular Biology (Clifton, N.J.)*. **1725**, pp.127–140.

Geng, F., Cheng, X., Wu, X., Yoo, J.Y., Cheng, C., Guo, J.Y., Mo, X., Ru, P., Hurwitz, B., Kim, S.-H., Otero, J., Puduvalli, V., Lefai, E., Ma, J., Nakano, I., Horbinski, C., Kaur, B., Chakravarti, A. and Guo, D. 2016. Inhibition of SOAT1 Suppresses Glioblastoma Growth via Blocking SREBP-1-Mediated Lipogenesis. *Clinical Cancer Research: An Official Journal of the American Association for Cancer Research*. **22**(21), pp.5337–5348.

Ghafouri-Fard, S., Abak, A., Tondro Anamag, F., Shoorei, H., Fattahi, F., Javadinia, S.A., Basiri, A. and Taheri, M. 2021. 5-Fluorouracil: A Narrative Review on the Role of Regulatory Mechanisms in Driving Resistance to This Chemotherapeutic Agent. *Frontiers in Oncology*. **11**.

Ghatak, S., Hascall, V.C., Markwald, R.R. and Misra, S. 2021. FOLFOX Therapy Induces Feedback Upregulation of CD44v6 through YB-1 to Maintain Stemness in Colon Initiating Cells. *International Journal of Molecular Sciences*. **22**(2), p.753.

Giacchetti, S., Perpoint, B., Zidani, R., Le Bail, N., Faggiuolo, R., Focan, C., Chollet, P., Llory, J.F., Letourneau, Y., Coudert, B., Bertheaut-Cvitkovic, F., Larregain-Fournier, D., Le Rol, A., Walter, S., Adam, R., Misset, J.L. and Lévi, F. 2000. Phase III

multicenter randomized trial of oxaliplatin added to chronomodulated fluorouracil-leucovorin as first-line treatment of metastatic colorectal cancer. *Journal of Clinical Oncology: Official Journal of the American Society of Clinical Oncology*. **18**(1), pp.136–147.

Gianni, T. and Campadelli-Fiume, G. 2012. αVβ3-Integrin Relocalizes nectin1 and Routes Herpes Simplex Virus to Lipid Rafts. *Journal of Virology*. **86**(5), pp.2850–2855.

Gierens, H., Nauck, M., Roth, M., Schinker, R., Schürmann, C., Scharnagl, H., Neuhaus, G., Wieland, H. and März, W. 2000. Interleukin-6 Stimulates LDL Receptor Gene Expression via Activation of Sterol-Responsive and Sp1 Binding Elements. *Arteriosclerosis, Thrombosis, and Vascular Biology*. **20**(7), pp.1777–1783.

Giovannucci, E. and Michaud, D. 2007. The Role of Obesity and Related Metabolic Disturbances in Cancers of the Colon, Prostate, and Pancreas. *Gastroenterology*. **132**(6), pp.2208–2225.

Golomb, B.A. and Evans, M.A. 2008. Statin Adverse Effects: A Review of the Literature and Evidence for a Mitochondrial Mechanism. *American journal of cardiovascular drugs : drugs, devices, and other interventions*. **8**(6), pp.373–418.

Gonzalez, D.M. and Medici, D. 2014. Signaling mechanisms of the epithelial-mesenchymal transition. *Science signaling*. **7**(344), p.re8.

de Gramont, A., Figer, A., Seymour, M., Homerin, M., Hmissi, A., Cassidy, J., Boni, C., Cortes-Funes, H., Cervantes, A., Freyer, G., Papamichael, D., Le Bail, N., Louvet, C., Hendler, D., de Braud, F., Wilson, C., Morvan, F. and Bonetti, A. 2000. Leucovorin and fluorouracil with or without oxaliplatin as first-line treatment in advanced colorectal cancer. *Journal of Clinical Oncology: Official Journal of the American Society of Clinical Oncology*. **18**(16), pp.2938–2947.

Greenlee, J.D., Subramanian, T., Liu, K. and King, M.R. 2021. Rafting Down the Metastatic Cascade: The Role of Lipid Rafts in Cancer Metastasis, Cell Death, and Clinical Outcomes. *Cancer Research*. **81**(1), pp.5–17.

Gresham, G., Sidhu, J., Malhi, N. and Cheung, W.Y. 2014. Predicting toxicities from adjuvant treatment in a population-based cohort of early colon cancer (CC) patients

(pts): A strategy to improve use of curative chemotherapy. *Journal of Clinical Oncology*. **32**(3), pp.412–412.

Gu, L., Saha, S.T., Thomas, J. and Kaur, M. 2019. Targeting cellular cholesterol for anticancer therapy. *The FEBS Journal*. **286**(21), pp.4192–4208.

Guerra, F.S., Sampaio, L. da S., Konig, S., Bonamino, M., Rossi, M.I.D., Costa, M.L., Fernandes, P. and Mermelstein, C. 2016. Membrane cholesterol depletion reduces breast tumor cell migration by a mechanism that involves non-canonical Wnt signaling and IL-10 secretion. *Translational Medicine Communications*. **1**(1), p.3.

Guillaumond, F., Bidaut, G., Ouaissi, M., Servais, S., Gouirand, V., Olivares, O., Lac, S., Borge, L., Roques, J., Gayet, O., Pinault, M., Guimaraes, C., Nigri, J., Loncle, C., Lavaut, M.-N., Garcia, S., Tailleux, A., Staels, B., Calvo, E., Tomasini, R., Iovanna, J.L. and Vasseur, S. 2015. Cholesterol uptake disruption, in association with chemotherapy, is a promising combined metabolic therapy for pancreatic adenocarcinoma. *Proceedings of the National Academy of Sciences*. **112**(8), pp.2473–2478.

Guo, D., Reinitz, F., Youssef, M., Hong, C., Nathanson, D., Akhavan, D., Kuga, D., Amzajerdi, A.N., Soto, H., Zhu, S., Babic, I., Tanaka, K., Dang, J., Iwanami, A., Gini, B., DeJesus, J., Lisiero, D.D., Huang, T.T., Prins, R.M., Wen, P.Y., Robins, H.I., Prados, M.D., DeAngelis, L.M., Mellinghoff, I.K., Mehta, M.P., James, C.D., Chakravarti, A., Cloughesy, T.F., Tontonoz, P. and Mischel, P.S. 2011. An LXR Agonist Promotes Glioblastoma Cell Death through Inhibition of an EGFR/AKT/SREBP-1/LDLR–Dependent Pathway. *Cancer Discovery*. **1**(5), pp.442–456.

Gustavsson, B., Carlsson, G., Machover, D., Petrelli, N., Roth, A., Schmoll, H.-J., Tveit, K.-M. and Gibson, F. 2015. A Review of the Evolution of Systemic Chemotherapy in the Management of Colorectal Cancer. *Clinical Colorectal Cancer*. **14**(1), pp.1–10.

Hammond, C.L., Marchan, R., Krance, S.M. and Ballatori, N. 2007. Glutathione Export during Apoptosis Requires Functional Multidrug Resistance-associated Proteins *. *Journal of Biological Chemistry*. **282**(19), pp.14337–14347.

Hanahan, D. and Weinberg, R.A. 2011. Hallmarks of Cancer: The Next Generation. *Cell*. **144**(5), pp.646–674.

Hanahan, D. and Weinberg, R.A. 2000. The Hallmarks of Cancer. *Cell*. **100**(1), pp.57–70.

Hendrayani, S.-F., Al-Harbi, B., Al-Ansari, M.M., Silva, G. and Aboussekhra, A. 2016. The inflammatory/cancer-related IL-6/STAT3/NF-κB positive feedback loop includes AUF1 and maintains the active state of breast myofibroblasts. *Oncotarget*. **7**(27), pp.41974–41985.

Hendrayani, S.-F., Al-Khalaf, H.H. and Aboussekhra, A. 2014. The Cytokine IL-6 Reactivates Breast Stromal Fibroblasts through Transcription Factor STAT3-dependent Up-regulation of the RNA-binding Protein AUF1 *. *Journal of Biological Chemistry*. **289**(45), pp.30962–30976.

Herbst, C., Miot, J.K., Moch, S.L. and Ruff, P. 2020. Colorectal Cancer (CRC) treatment and associated costs in the public sector compared to the private sector in Johannesburg, South Africa. *BMC Health Services Research*. **20**(1), p.290.

Herranz, N., Pasini, D., Díaz, V.M., Francí, C., Gutierrez, A., Dave, N., Escrivà, M., Hernandez-Muñoz, I., Di Croce, L., Helin, K., García de Herreros, A. and Peiró, S. 2008. Polycomb Complex 2 Is Required for E-cadherin Repression by the Snail1 Transcription Factor. *Molecular and Cellular Biology*. **28**(15), pp.4772–4781.

Holmer, R., Wätzig, G.H., Tiwari, S., Rose-John, S. and Kalthoff, H. 2015. Interleukin-6 trans-signaling increases the expression of carcinoembryonic antigen-related cell adhesion molecules 5 and 6 in colorectal cancer cells. *BMC Cancer*. **15**, p.975.

Huang, B., Song, B. and Xu, C. 2020. Cholesterol metabolism in cancer: mechanisms and therapeutic opportunities. *Nature Metabolism*. **2**(2), pp.132–141.

Hugo, H.J., Kokkinos, M.I., Blick, T., Ackland, M.L., Thompson, E.W. and Newgreen, D.F. 2011. Defining the E-cadherin repressor interactome in epithelial-mesenchymal transition: the PMC42 model as a case study. *Cells, Tissues, Organs*. **193**(1–2), pp.23–40.

Iliopoulos, D., Hirsch, H.A. and Struhl, K. 2009. An epigenetic switch involving NF-κB, Lin28, let-7 microRNA, and IL6 links inflammation to cell transformation. *Cell*. **139**(4), pp.693–706.

Im, K., Mareninov, S., Diaz, M.F.P. and Yong, W.H. 2019. An introduction to Performing Immunofluorescence Staining. *Methods in molecular biology (Clifton, N.J.)*. **1897**, pp.299–311.

Iwatsuki, M., Mimori, K., Yokobori, T., Ishi, H., Beppu, T., Nakamori, S., Baba, H. and Mori, M. 2010. Epithelial-mesenchymal transition in cancer development and its clinical significance. *Cancer Science*. **101**(2), pp.293–299.

Jansook, P., Ogawa, N. and Loftsson, T. 2018. Cyclodextrins: structure, physicochemical properties and pharmaceutical applications. *International Journal of Pharmaceutics*. **535**(1–2), pp.272–284.

Jiang, S., Wang, Xuetong, Song, D., Liu, X., Gu, Y., Xu, Z., Wang, Xiaodong, Zhang, X., Ye, Q., Tong, Z., Yan, B., Yu, J., Chen, Y., Sun, M., Wang, Y. and Gao, S. 2019. Cholesterol Induces Epithelial-to-Mesenchymal Transition of Prostate Cancer Cells by Suppressing Degradation of EGFR through APMAP. *Cancer Research*. **79**(12), pp.3063–3075.

Jin, H., He, Y., Zhao, P., Hu, Y., Tao, J., Chen, J. and Huang, Y. 2019. Targeting lipid metabolism to overcome EMT-associated drug resistance via integrin β3/FAK pathway and tumor-associated macrophage repolarization using legumain-activatable delivery. *Theranostics*. **9**(1), p.265.

Johnson, D.E., O'Keefe, R.A. and Grandis, J.R. 2018. Targeting the IL-6/JAK/STAT3 signalling axis in cancer. *Nature Reviews Clinical Oncology*. **15**(4), pp.234–248.

Johnston, P.G. and Kaye, S. 2001. Capecitabine: a novel agent for the treatment of solid tumors. *Anti-Cancer Drugs*. **12**(8), pp.639–646.

Jolly, M.K., Boareto, M., Huang, B., Jia, D., Lu, M., Ben-Jacob, E., Onuchic, J.N. and Levine, H. 2015. Implications of the Hybrid Epithelial/Mesenchymal Phenotype in Metastasis. *Frontiers in Oncology*. **5**, p.155.

Jung, J.E., Lee, H.G., Cho, I.H., Chung, D.H., Yoon, S.-H., Yang, Y.M., Lee, J.W., Choi, S., Park, J.-W., Ye, S.-K. and Chung, M.-H. 2005. STAT3 is a potential modulator of HIF-1-mediated VEGF expression in human renal carcinoma cells. *FASEB journal: official publication of the Federation of American Societies for Experimental Biology*. **19**(10), pp.1296–1298.

Justus, C.R., Leffler, N., Ruiz-Echevarria, M. and Yang, L.V. 2014. In vitro Cell Migration and Invasion Assays. *Journal of Visualized Experiments : JoVE*. (88), p.51046.

Kanazawa, T., Nishino, H., Hasegawa, M., Ohta, Y., Iino, Y., Ichimura, K. and Noda, Y. 2007. Interleukin-6 directly influences proliferation and invasion potential of head and neck cancer cells. *European Archives of Oto-Rhino-Laryngology*. **264**(7), pp.815–821.

Kashirina, A.S., López-Duarte, I., Kubánková, M., Gulin, A.A., Dudenkova, V.V., Rodimova, S.A., Torgomyan, H.G., Zagaynova, E.V., Meleshina, A.V. and Kuimova, M.K. 2020. Monitoring membrane viscosity in differentiating stem cells using BODIPY-based molecular rotors and FLIM. *Scientific Reports*. **10**(1), p.14063.

Kim, J., Adam, R.M., Solomon, K.R. and Freeman, M.R. 2004. Involvement of Cholesterol-Rich Lipid Rafts in Interleukin-6-Induced Neuroendocrine Differentiation of LNCaP Prostate Cancer Cells. *Endocrinology*. **145**(2), pp.613–619.

Kim, J.A., Maxwell, K., Hajjar, D.P. and Berliner, J.A. 1991. Beta-VLDL increases endothelial cell plasma membrane cholesterol. *Journal of Lipid Research*. **32**(7), pp.1125–1131.

Kim, M.S., Jeong, J., Seo, J., Kim, H.-S., Kim, S.-J. and Jin, W. 2016. Dysregulated JAK2 expression by TrkC promotes metastasis potential, and EMT program of metastatic breast cancer. *Scientific Reports*. **6**.

Kim, T.W., Lee, Y.S., Yun, N.H., Shin, C.H., Hong, H.K., Kim, H.H. and Cho, Y.B. 2020. MicroRNA-17-5p regulates EMT by targeting vimentin in colorectal cancer. *British Journal of Cancer*. **123**(7), pp.1123–1130.

Kong, Y., Cheng, L., Mao, F., Zhang, Z., Zhang, Y., Farah, E., Bosler, J., Bai, Y., Ahmad, N., Kuang, S., Li, L. and Liu, X. 2018. Inhibition of cholesterol biosynthesis

overcomes enzalutamide resistance in castration-resistant prostate cancer (CRPC). *The Journal of Biological Chemistry*. **293**(37), pp.14328–14341.

Kubatka, P., Kruzliak, P., Rotrekl, V., Jelinkova, S. and Mladosievicova, B. 2014. Statins in oncological research: from experimental studies to clinical practice. *Critical Reviews in Oncology/Hematology*. **92**(3), pp.296–311.

Kuoppala, J., Lamminpää, A. and Pukkala, E. 2008. Statins and cancer: A systematic review and meta-analysis. *European Journal of Cancer*. **44**(15), pp.2122–2132.

Kurata, T., Fushida, S., Kinoshita, J., Oyama, K., Yamaguchi, T., Okazaki, M., Miyashita, T., Tajima, H., Ninomiya, I. and Ohta, T. 2018. Low-dose eribulin mesylate exerts antitumor effects in gastric cancer by inhibiting fibrosis via the suppression of epithelial–mesenchymal transition and acts synergistically with 5-fluorouracil. *Cancer Management and Research*. **10**, pp.2729–2742.

Lamouille, S., Xu, J. and Derynck, R. 2014. Molecular mechanisms of epithelial–mesenchymal transition. *Nature reviews. Molecular cell biology*. **15**(3), pp.178–196.

Lange, Y. 1991. Disposition of intracellular cholesterol in human fibroblasts. *Journal of Lipid Research*. **32**(2), pp.329–339.

Lange, Y., Ye, J., Rigney, M. and Steck, T.L. 1999. Regulation of endoplasmic reticulum cholesterol by plasma membrane cholesterol. *Journal of Lipid Research*. **40**(12), pp.2264–2270.

Leteurtre E., Gouyer, V., Rousseau, K., Moreau, O., Barbat, A., Swallow, D., Huet, G., Lesuffleur, T. 2004. Differential mucin expression in colon carcinoma HT-29 clones with variable resistance to 5-fluorouracil and methotrexate. *Biol Cell*. **96**(2), pp.145-51.

Li, L.T., Jiang, G., Chen, Q., and Zheng, J.N. 2015. Ki67 is a promising molecular target in the diagnosis of cancer (Review). *Molecular Medicine Reports*. **11**(3), pp.1566–1572.

Li, Y.C., Park, M.J., Ye, S.-K., Kim, C.-W. and Kim, Y.-N. 2006. Elevated Levels of Cholesterol-Rich Lipid Rafts in Cancer Cells Are Correlated with Apoptosis Sensitivity Induced by Cholesterol-Depleting Agents. *The American Journal of Pathology*. **168**(4), pp.1107–1118.

Lin, Y., He, Z., Ye, J., Liu, Z., She, X., Gao, X. and Liang, R. 2020. Progress in Understanding the IL-6/STAT3 Pathway in Colorectal Cancer. *OncoTargets and therapy*. **13**, pp.13023–13032.

Liu, C.-Y., Lin, H.-H., Tang, M.-J. and Wang, Y.-K. 2015. Vimentin contributes to epithelial-mesenchymal transition cancer cell mechanics by mediating cytoskeletal organization and focal adhesion maturation. *Oncotarget*. **6**(18), pp.15966–15983.

Liu, H., Ren, G., Wang, T., Chen, Y., Gong, C., Bai, Y., Wang, B., Qi, H., Shen, J., Zhu, L., Qian, C., Lai, M. and Shao, J. 2015. Aberrantly expressed Fra-1 by IL-6/STAT3 transactivation promotes colorectal cancer aggressiveness through epithelial–mesenchymal transition. *Carcinogenesis*. **36**(4), pp.459–468.

Livak, K.J. and Schmittgen, T.D. 2001. Analysis of relative gene expression data using real-time quantitative PCR and the 2(-Delta Delta C(T)) Method. *Methods (San Diego, Calif.)*. **25**(4), pp.402–408.

Long, A.G., Lundsmith, E.T. and Hamilton, K.E. 2017. Inflammation and Colorectal Cancer. *Current colorectal cancer reports*. **13**(4), pp.341–351.

López, C.A., Vries, A.H. de and Marrink, S.J. 2011. Molecular Mechanism of Cyclodextrin Mediated Cholesterol Extraction. *PLOS Computational Biology*. **7**(3), p.e1002020.

Luo, J., Yang, H. and Song, B.-L. 2020. Mechanisms and regulation of cholesterol homeostasis. *Nature Reviews Molecular Cell Biology*. **21**(4), pp.225–245.

Mahammad, S. and Parmryd, I. 2015. Cholesterol Depletion Using Methyl-β-cyclodextrin *In*: D. M. Owen, ed. *Methods in Membrane Lipids*.

Manne, U., Shanmugam, C., Katkoori, V.R., Bumpers, H.L. and Grizzle, W.E. 2010. Development and progression of colorectal neoplasia. *Cancer biomarkers : section A of Disease markers*. **9**(1–6), pp.235–265.

Mariño, G. and Kroemer, G. 2013. Mechanisms of apoptotic phosphatidylserine exposure. *Cell Research*. **23**(11), pp.1247–1248.

Masjedi, A., Hashemi, V., Hojjat-Farsangi, M., Ghalamfarsa, G., Azizi, G., Yousefi, M. and Jadidi-Niaragh, F. 2018. The significant role of interleukin-6 and its signaling

pathway in the immunopathogenesis and treatment of breast cancer. *Biomedicine & Pharmacotherapy*. **108**, pp.1415–1424.

Matusewicz, L., Meissner, J., Toporkiewicz, M. and Sikorski, A.F. 2015. The effect of statins on cancer cells--review. *Tumour Biology: The Journal of the International Society for Oncodevelopmental Biology and Medicine*. **36**(7), pp.4889–4904.

Maxfield, F.R. and Wüstner, D. 2012. Analysis of cholesterol trafficking with fluorescent probes. *Methods in Cell Biology*. **108**, pp.367–393.

Mittal, V. 2018. Epithelial Mesenchymal Transition in Tumor Metastasis. *Annual Review of Pathology*. **13**, pp.395–412.

Morandi, A., Taddei, M.L., Chiarugi, P. and Giannoni, E. 2017. Targeting the Metabolic Reprogramming That Controls Epithelial-to-Mesenchymal Transition in Aggressive Tumors. *Frontiers in Oncology*. **7**, p.40.

Nakamura, K., Nakamura, T., Iino, T., Hagi, T., Kita, K., Asanuma, K. and Sudo, A. 2020. Expression of Interleukin-6 and the Interleukin-6 Receptor Predicts the Clinical Outcomes of Patients with Soft Tissue Sarcomas. *Cancers*. **12**(3), p.585.

Negrei, C., Hudita, A., Ginghina, O., Galateanu, B., Voicu, S.N., Stan, M., Costache, M., Fenga, C., Drakoulis, N. and Tsatsakis, A.M. 2016. Colon Cancer Cells Gene Expression Signature As Response to 5- Fluorouracil, Oxaliplatin, and Folinic Acid Treatment. *Frontiers in Pharmacology*. **7**, p.172.

Nguyen, T.T., Ung, T.T., Kim, N.H. and Jung, Y.D. 2018. Role of bile acids in colon carcinogenesis. *World Journal of Clinical Cases*. **6**(13), pp.577–588.

Nie, D., Fu, Jiewen, Chen, H., Cheng, J. and Fu, Junjiang 2019. Roles of MicroRNA-34a in Epithelial to Mesenchymal Transition, Competing Endogenous RNA Sponging and Its Therapeutic Potential. *International Journal of Molecular Sciences*. **20**(4), p.861.

Nieto, M.A., Huang, R.Y., Jackson, R.A. and Thiery, J.P. 2016. EMT: 2016. *Cell*. **166**(1), pp.21–45.

Nishikawa, S., Menju, T., Takahashi, K., Miyata, R., Chen-Yoshikawa, T., Sonobe, M., Yoshizawa, A., Sabe, H., Sato, T., Date, H. Statins may have double-edged effects in

patients with lung adenocarcinoma after lung resection. 2019. *Cancer Manag Res*. **11**, pp.3419-3432.

Omoigui, S. 2007. The Interleukin-6 inflammation pathway from cholesterol to aging – Role of statins, bisphosphonates and plant polyphenols in aging and age-related diseases. *Immunity & Ageing*. **4**(1), p.1.

Onodera, R., Motoyama, K., Okamatsu, A., Higashi, T., Kariya, R., Okada, S. and Arima, H. 2013. Involvement of cholesterol depletion from lipid rafts in apoptosis induced by methyl-β-cyclodextrin. *International Journal of Pharmaceutics*. **452**(1), pp.116–123.

Ouimet, M. and Marcel, Y.L. 2012. Regulation of Lipid Droplet Cholesterol Efflux From Macrophage Foam Cells. *Arteriosclerosis, Thrombosis, and Vascular Biology*. **32**(3), pp.575–581.

Payero, T.D., Vicente, C.M., Rumbero, Á., Barreales, E.G., Santos-Aberturas, J., de Pedro, A. and Aparicio, J.F. 2015. Functional analysis of filipin tailoring genes from Streptomyces filipinensis reveals alternative routes in filipin III biosynthesis and yields bioactive derivatives. *Microbial Cell Factories*. **14**(1), p.114.

Pino, M.S. and Chung, D.C. 2010. The chromosomal instability pathway in colon cancer. *Gastroenterology*. **138**(6), pp.2059–2072.

Pires, B.R.B., Mencalha, A.L., Ferreira, G.M., de Souza, W.F., Morgado-Díaz, J.A., Maia, A.M., Corrêa, S. and Abdelhay, E.S.F.W. 2017. NF-kappaB Is Involved in the Regulation of EMT Genes in Breast Cancer Cells. *PLoS ONE*. **12**(1), p.e0169622.

Postigo, A.A., Depp, J.L., Taylor, J.J. and Kroll, K.L. 2003. Regulation of Smad signaling through a differential recruitment of coactivators and corepressors by ZEB proteins. *The EMBO Journal*. **22**(10), pp.2453–2462.

Qiu, B. and Simon, M.C. 2016. BODIPY 493/503 Staining of Neutral Lipid Droplets for Microscopy and Quantification by Flow Cytometry. *Bio-protocol*. **6**(17), p.e1912.

Rawla, P., Sunkara, T. and Barsouk, A. 2019. Epidemiology of colorectal cancer: incidence, mortality, survival, and risk factors. *Gastroenterology Review/Przegląd Gastroenterologiczny*. **14**(2), pp.89–103.

Reiner, Z. 2014. Resistance and intolerance to statins. *Nutrition, metabolism, and cardiovascular diseases: NMCD*. **24**(10), pp.1057–1066.

Resnik, N., Repnik, U., Kreft, M.E., Sepčić, K., Maček, P., Turk, B. and Veranič, P. 2015. Highly Selective Anti-Cancer Activity of Cholesterol-Interacting Agents Methyl-β-Cyclodextrin and Ostreolysin A/Pleurotolysin B Protein Complex on Urothelial Cancer Cells. *PLOS ONE*. **10**(9), p.e0137878.

Roche, J. 2018. The Epithelial-to-Mesenchymal Transition in Cancer. *Cancers*. **10**(2), p.52.

Röhrl, C. and Stangl, H. 2018. Cholesterol metabolism—physiological regulation and pathophysiological deregulation by the endoplasmic reticulum. *Wiener Medizinische Wochenschrift*. **168**(11), pp.280–285.

Rokavec, M., Öner, M.G., Li, H., Jackstadt, R., Jiang, L., Lodygin, D., Kaller, M., Horst, D., Ziegler, P.K., Schwitalla, S., Slotta-Huspenina, J., Bader, F.G., Greten, F.R. and Hermeking, H. 2014. IL-6R/STAT3/miR-34a feedback loop promotes EMT-mediated colorectal cancer invasion and metastasis. *The Journal of Clinical Investigation*. **124**(4), pp.1853–1867.

Rossin, D., Calfapietra, S., Sottero, B., Poli, G. and Biasi, F. 2017. HNE and cholesterol oxidation products in colorectal inflammation and carcinogenesis. *Free Radical Biology and Medicine*. **111**, pp.186–195.

Sahini, N. and Borlak, J. 2014. Recent insights into the molecular pathophysiology of lipid droplet formation in hepatocytes. *Progress in Lipid Research*. **54**, pp.86–112.

Saitoh, M., Endo, K., Furuya, S., Minami, M., Fukasawa, A., Imamura, T. and Miyazawa, K. 2016. STAT3 integrates cooperative Ras and TGF-β signals that induce Snail expression. *Oncogene*. **35**(8), pp.1049–1057.

Sehgal, P.B., Guo, G.G., Shah, M., Kumar, V. and Patel, K. 2002. Cytokine Signaling: Stats in Plasma Membrane Rafts. *Journal of Biological Chemistry*. **277**(14), pp.12067–12074.

Sezgin, E., Azbazdar, Y., Ng, X.W., Teh, C., Simons, K., Weidinger, G., Wohland, T., Eggeling, C. and Ozhan, G. 2017. Binding of canonical Wnt ligands to their receptor

complexes occurs in ordered plasma membrane environments. *The Febs Journal*. **284**(15), pp.2513–2526.

Shibue, T. and Weinberg, R.A. 2017. EMT, CSCs, and drug resistance: the mechanistic link and clinical implications. *Nature reviews. Clinical oncology*. **14**(10), pp.611–629.

Sikand, K., Singh, J., Ebron, J.S. and Shukla, G.C. 2012. Housekeeping Gene Selection Advisory: Glyceraldehyde-3-Phosphate Dehydrogenase (GAPDH) and β-Actin Are Targets of miR-644a. *PLoS ONE*. **7**(10), p.e47510.

Siveen, K.S., Sikka, S., Surana, R., Dai, X., Zhang, J., Kumar, A.P., Tan, B.K.H., Sethi, G. and Bishayee, A. 2014. Targeting the STAT3 signaling pathway in cancer: Role of synthetic and natural inhibitors. *Biochimica et Biophysica Acta (BBA) - Reviews on Cancer*. **1845**(2), pp.136–154.

Skarkova, V., Kralova, V., Krbal, L., Matouskova, P., Soukup, J. and Rudolf, E. 2018. Oxaliplatin and irinotecan induce heterogenous changes in the EMT markers of metastasizing colorectal carcinoma cells. *Experimental Cell Research*. **369**(2), pp.295–303.

Stemmler, M.P., Eccles, R.L., Brabletz, S. and Brabletz, T. 2019. Non-redundant functions of EMT transcription factors. *Nature Cell Biology*. **21**(1), pp.102–112.

Stintzing, S. 2014. Management of colorectal cancer. *F1000Prime Rep*. **6**(108).

Suarez-Carmona, M., Lesage, J., Cataldo, D. and Gilles, C. 2017. EMT and inflammation: inseparable actors of cancer progression. *Molecular Oncology*. **11**(7), pp.805–823.

Sullivan, N.J., Sasser, A.K., Axel, A.E., Vesuna, F., Raman, V., Ramirez, N., Oberyszyn, T.M. and Hall, B.M. 2009. Interleukin-6 induces an epithelial-mesenchymal transition phenotype in human breast cancer cells. *Oncogene*. **28**(33), pp.2940–2947.

Sung, H., Ferlay, J., Siegel, R.L., Laversanne, M., Soerjomataram, I., Jemal, A. and Bray, F. 2021. Global Cancer Statistics 2020: GLOBOCAN Estimates of Incidence and Mortality Worldwide for 36 Cancers in 185 Countries. *CA: A Cancer Journal for Clinicians*. **71**(3), pp.209–249.

Sylvester, P.W. 2011. Optimization of the tetrazolium dye (MTT) colorimetric assay for cellular growth and viability. *Methods in Molecular Biology (Clifton, N.J.)*. **716**, pp.157–168.

Taube, J.H., Herschkowitz, J.I., Komurov, K., Zhou, A.Y., Gupta, S., Yang, J., Hartwell, K., Onder, T.T., Gupta, P.B., Evans, K.W., Hollier, B.G., Ram, P.T., Lander, E.S., Rosen, J.M., Weinberg, R.A. and Mani, S.A. 2010. Core epithelial-to-mesenchymal transition interactome gene-expression signature is associated with claudin-low and metaplastic breast cancer subtypes. *Proceedings of the National Academy of Sciences of the United States of America*. **107**(35), pp.15449–15454.

Thomson, S., Petti, F., Sujka-Kwok, I., Mercado, P., Bean, J., Monaghan, M., Seymour, S.L., Argast, G.M., Epstein, D.M. and Haley, J.D. 2011. A systems view of epithelial–mesenchymal transition signaling states. *Clinical & Experimental Metastasis*. **28**(2), pp.137–155.

Tisza, M.J., Zhao, W., Fuentes, J.S.R., Prijic, S., Chen, X., Levental, I. and Chang, J.T. 2016. Motility and stem cell properties induced by the epithelial-mesenchymal transition require destabilization of lipid rafts. *Oncotarget*. **7**(32), pp.51553–51568.

Tsai, J.H., Donaher, J.L., Murphy, D.A., Chau, S. and Yang, J. 2012. Spatiotemporal Regulation of Epithelial-Mesenchymal Transition Is Essential for Squamous Cell Carcinoma Metastasis. *Cancer Cell*. **22**(6), pp.725–736.

Tsoupras, A., Lordan, R. and Zabetakis, I. 2018. Inflammation, not Cholesterol, Is a Cause of Chronic Disease. *Nutrients*. **10**(5), p.604.

Ullman, T.A. and Itzkowitz, S.H. 2011. Intestinal inflammation and cancer. *Gastroenterology*. **140**(6), pp.1807–1816.

Usman, S., Waseem, N.H., Nguyen, T.K.N., Mohsin, S., Jamal, A., Teh, M.-T. and Waseem, A. 2021. Vimentin Is at the Heart of Epithelial Mesenchymal Transition (EMT) Mediated Metastasis. *Cancers*. **13**(19), p.4985.

Vega, S., Morales, A.V., Ocaña, O.H., Valdés, F., Fabregat, I. and Nieto, M.A. 2004. Snail blocks the cell cycle and confers resistance to cell death. *Genes & Development*. **18**(10), pp.1131–1143.

Vleminckx, K., Vakaet, L., Mareel, M., Fiers, W. and van Roy, F. 1991. Genetic manipulation of E-cadherin expression by epithelial tumor cells reveals an invasion suppressor role. *Cell*. **66**(1), pp.107–119.

Vu, T. and Datta, P.K. 2017. Regulation of EMT in Colorectal Cancer: A Culprit in Metastasis. *Cancers*. **9**(12), p.E171.

Wang, N., Liu, D., Guo, J., Sun, Y., Guo, T. and Zhu, X. 2018. Molecular mechanism of Poria cocos combined with oxaliplatin on the inhibition of epithelial-mesenchymal transition in gastric cancer cells. *Biomedicine & Pharmacotherapy = Biomedecine & Pharmacotherapie*. **102**, pp.865–873.

Wang, S., Wang, L., Zhou, Z., Deng, Q., Li, L., Zhang, M., Liu, L. and Li, Y. 2017. Leucovorin Enhances the Anti-cancer Effect of Bortezomib in Colorectal Cancer Cells. *Scientific Reports*. **7**.

Wang, T., Song, P., Zhong, T., Wang, X., Xiang, X., Liu, Q., Chen, H., Xia, T., Liu, H., Niu, Y., Hu, Y., Xu, L., Shao, Y., Zhu, L., Qi, H., Shen, J., Hou, T., Fodde, R. and Shao, J. 2019. The inflammatory cytokine IL-6 induces FRA1 deacetylation promoting colorectal cancer stem-like properties. *Oncogene*. **38**(25), pp.4932–4947.

Warita, K., Ishikawa, T., Sugiura, A. Tashiro, J., Shimakura, H., Hosaka, Y., Ohta, K., Warita, T., Oltvai, Z. 2021. Concomitant attenuation of HMGCR expression and activity enhances the growth inhibitory effect of atorvastatin on TGF-β-treated epithelial cancer cells. *Sci Rep.* **11**(12763).

Warita, K., Warita, T., Beckwitt, C.H., Schurdak, M.E., Vazquez, A., Wells, A. and Oltvai, Z.N. 2014. Statin-induced mevalonate pathway inhibition attenuates the growth of mesenchymal-like cancer cells that lack functional E-cadherin mediated cell cohesion. *Scientific Reports*. **4**, p.7593.

Wei, C., Yang, C., Wang, S., Shi, D., Zhang, C., Lin, X., Liu, Q., Dou, R. and Xiong, B. 2019. Crosstalk between cancer cells and tumor associated macrophages is required for mesenchymal circulating tumor cell-mediated colorectal cancer metastasis. *Molecular Cancer*. **18**(1), p.64.

Weidenfeld, K. and Barkan, D. 2018. EMT and Stemness in Tumor Dormancy and Outgrowth: Are They Intertwined Processes? *Frontiers in Oncology*. **8**.

Welch, D.R. and Hurst, D.R. 2019. Defining the Hallmarks of Metastasis. *Cancer Research*. **79**(12), pp.3011–3027.

Wen, Y.-A., Xiong, X., Zaytseva, Y.Y., Napier, D.L., Vallee, E., Li, A.T., Wang, C., Weiss, H.L., Evers, B.M. and Gao, T. 2018. Downregulation of SREBP inhibits tumor growth and initiation by altering cellular metabolism in colon cancer. *Cell Death & Disease*. **9**(3), p.265.

Wu, S., Du, Y., Beckford, J. and Alachkar, H. 2018. Upregulation of the EMT marker vimentin is associated with poor clinical outcome in acute myeloid leukemia. *Journal of Translational Medicine*. **16**(1), p.170.

Wu, Y., Zhao, Y., He, X., He, Z., Wang, T., Wan, L., Chen, L. and Yan, N. 2020. Hydroxypropyl-β-cyclodextrin attenuates the epithelial-to-mesenchymal transition via endoplasmic reticulum stress in MDA-MB-231 breast cancer cells. *Molecular Medicine Reports*. **21**(1), pp.249–257.

Xie, Y. H., Chen, Y. X., and Fang, J. Y., 2020. Comprehensive review of targeted therapy for colorectal cancer. *Signal Transduction and Targeted Therapy*. **5**(1), pp.1–30.

Xiong, H., Hong, J., Du, W., Lin, Y., Ren, L., Wang, Y., Su, W., Wang, J., Cui, Y., Wang, Z. and Fang, J.-Y. 2012. Roles of STAT3 and ZEB1 Proteins in E-cadherin Down-regulation and Human Colorectal Cancer Epithelial-Mesenchymal Transition. *The Journal of Biological Chemistry*. **287**(8), pp.5819–5832.

Yadav, A., Kumar, B., Datta, J., Teknos, T.N. and Kumar, P. 2011. IL-6 Promotes Head and Neck Tumor Metastasis by Inducing Epithelial–Mesenchymal Transition via the JAK-STAT3-SNAIL Signaling Pathway. *Molecular Cancer Research*. **9**(12), pp.1658–1667.

Yan, A., Jia, Z., Qiao, C., Wang, M. and Ding, X. 2020. Cholesterol metabolism in drug-resistant cancer (Review). *International Journal of Oncology*. **57**(5), pp.1103–1115.

Yan, J., Du, F., Li, S., Yuan, Y., Jiang, J., Li, S., Li, X., and Du, Z. 2018. AUF1 modulates TGF-β signal in renal tubular epithelial cells via post-transcriptional regulation of Nedd4L expression. *Biochimica Et Biophysica Acta. Molecular Cell Research*. **1865**(1), pp.48–56.

Yang, F., Sun, L., Li, Q., Han, X., Lei, L., Zhang, H. and Shang, Y. 2012. SET8 promotes epithelial–mesenchymal transition and confers TWIST dual transcriptional activities. *The EMBO Journal*. **31**(1), pp.110–123.

Yu, R., Longo, J., van Leeuwen, J.E., Mullen, P.J., Ba-Alawi, W., Haibe-Kains, B. and Penn, L.Z. 2018. Statin-Induced Cancer Cell Death Can Be Mechanistically Uncoupled from Prenylation of RAS Family Proteins. *Cancer Research*. **78**(5), pp.1347–1357.

Zalba, S. and ten Hagen, T.L.M. 2017. Cell membrane modulation as adjuvant in cancer therapy. *Cancer treatment reviews*. **52**, pp.48–57.

Zhang, C., Guo, F., Xu, G., Ma, J. and Shao, F. 2015. STAT3 cooperates with Twist to mediate epithelial-mesenchymal transition in human hepatocellular carcinoma cells. *Oncology Reports*. **33**(4), pp.1872–1882.

Zhang, J.H., Chung, T.D. and Oldenburg, K.R. 1999. A Simple Statistical Parameter for Use in Evaluation and Validation of High Throughput Screening Assays. *Journal of Biomolecular Screening*. **4**(2), pp.67–73.

Zhang, N., Yin, Y., Xu, S.-J. and Chen, W. 2008. 5-Fluorouracil: Mechanisms of Resistance and Reversal Strategies. *Molecules*. **13**(8), pp.1551–1569.

Zhang, X., Zhao, X., Liu, D., Han, C., Du, L., Jing, J. and Wang, Y. 2014. Lipid levels in serum and cancerous tissues of colorectal cancer patients. *World Journal of Gastroenterology : WJG*. **20**(26), pp.8646–8652.

Zhang, X.L, Topley, N., Ito, T., Phillips, A. 2005. Interleukin-6 regulation of transforming growth factor (TGF)-beta receptor compartmentalization and turnover enhances TGF-beta1 signaling. *J Biol Chem*. **280**(13), pp.12239-45.

Zhao, L., Chen, Yaxi, Tang, R., Chen, Yao, Li, Q., Gong, J., Huang, A., Varghese, Z., Moorhead, J.F. and Ruan, X.Z. 2011. Inflammatory stress exacerbates hepatic cholesterol accumulation via increasing cholesterol uptake and de novo synthesis. *Journal of Gastroenterology and Hepatology*. **26**(5), pp.875–883.

Zhao, W., Prijic, S., Urban, B.C., Tisza, M.J., Zuo, Y., Li, L., Tan, Z., Chen, X., Mani, S.A. and Chang, J.T. 2016. Candidate Antimetastasis Drugs Suppress the Metastatic

Capacity of Breast Cancer Cells by Reducing Membrane Fluidity. *Cancer research*. **76**(7), pp.2037–2049.

Zhou, J., Kang, Y., Chen, L., Wang, H., Liu, J., Zeng, S. and Yu, L. 2020. The Drug-Resistance Mechanisms of Five Platinum-Based Antitumor Agents. *Frontiers in Pharmacology*. **11**.

Zhu, R., Ou, Z., Ruan, X. and Gong, J. 2012. Role of liver X receptors in cholesterol efflux and inflammatory signaling (Review). *Molecular Medicine Reports*. **5**(4), pp.895–900.

Zidovetzki, R. and Levitan, I. 2007. Use of cyclodextrins to manipulate plasma membrane cholesterol content: evidence, misconceptions and control strategies. *Biochimica et biophysica acta*. **1768**(6), pp.1311–1324.

Zuo, W. and Chen, Y.G. 2009. Specific Activation of Mitogen-activated Protein Kinase by Transforming Growth Factor-β Receptors in Lipid Rafts Is Required for Epithelial Cell Plasticity. *Molecular Biology of the Cell*. **20**(3), pp.1020–1029.

Appendix

An MTT assay was performed, showing the effect of 0.1, 0.2 and 0.3% DMSO on cell viability in HT-29 cells, over 48 hours. The data confirms that DMSO had no effect on cell viability, up to 0.3% DMSO. A maximum of 0.2% DMSO was used in culture.

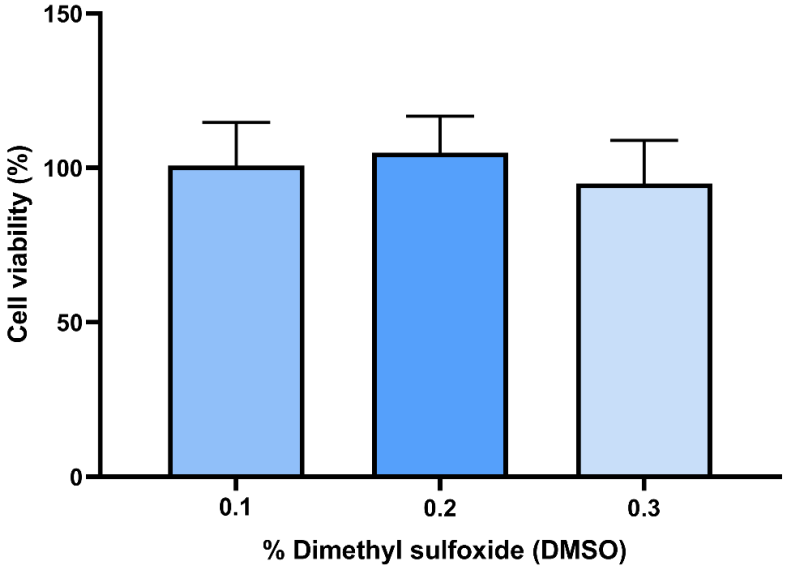


Figure A.1: The effect of DMSO on cell viability in HT-29 cells, over 48 hours. *An MTT assay was performed, serving as a DMSO-only control. HT-29 cells treated with 0.1, 0.2 and 0.3% DMSO showed 100.76%, 104.9%, and 94.9% cell viability, respectively. n=3.*

An MTT assay was performed to ascertain the effect of folinic acid on 5-FU cytotoxicity. Cells were treated with 20 µM of 5-FU and increasing concentrations of folinic acid, for 48 hours. There was no significant difference in cytotoxicity with or without folinic acid. Therefore, folinic acid was excluded from the *in vitro* FOLFOX treatments.

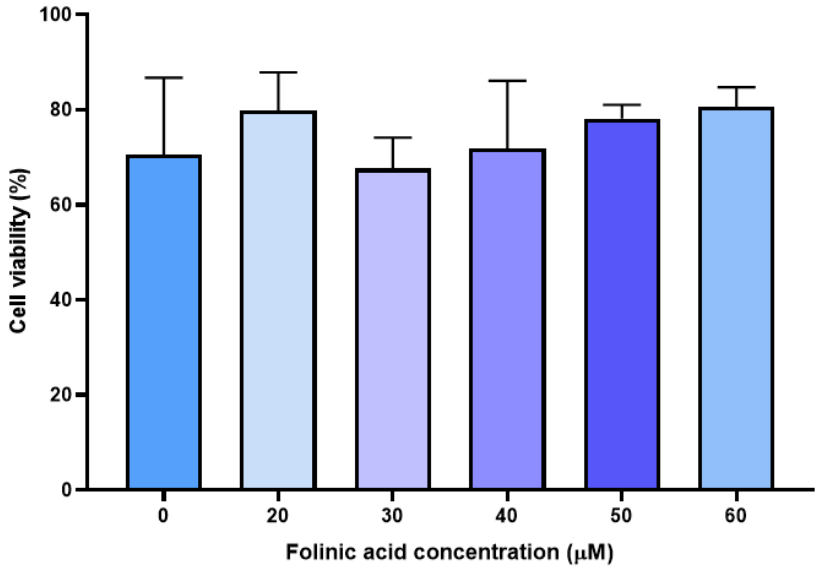


Figure A.2: The effect of increasing concentrations of folinic acid on 5-FU cytotoxicity. *Folinic acid had no significant effect on 5-FU cytotoxicity at concentrations ranging up to 60 µM, after 48 hours. A one-way ANOVA ($P < 0.05$) was performed for statistical analysis. n=3.*